Advanced Transportation

Part 1

Edited by
Shucai Li

TRANS TECH PUBLICATIONS

Advanced Transportation

Edited by:
Shucai Li

Advanced Transportation

Selected, peer reviewed papers from the
2011 International Conference on
Civil Engineering and Transportation
(ICCET 2011),
14-16 October, 2011, Jinan, China

Edited by

Shucai Li

Trans Tech Publications Ltd
Kreuzstrasse 10
CH-8635 Durnten-Zurich
Switzerland
http://www.ttp.net

Volumes 97-98 of
Applied Mechanics and Materials 2-vol.-set
ISSN 1660-9336

Full text available online at http://www.scientific.net

Distributed worldwide by

Trans Tech Publications Ltd
Kreuzstrasse 10
CH-8635 Durnten-Zuerich
Switzerland

Fax: +41 (44) 922 10 33
e-mail: sales@ttp.net

and in the Americas by

Trans Tech Publications Inc.
PO Box 699, May Street
Enfield, NH 03748
USA

Phone: +1 (603) 632-7377
Fax: +1 (603) 632-5611
e-mail: sales-usa@ttp.net

Preface

The present book includes a set of selected papers from The 2011 International Conference on Civil Engineering and Transportation (ICCET 2011), held in Jinan, China, from 14 to 16 October 2011, sponsored by School of Civil Engineering, Shandong Jianzhu University; School of Civil Engineering, Shandong University; School of Civil Engineering and Architecture, Shandong University of Science and Technology; School of Civil Engineering, Yantai University and Shandong Provincial Key Lab of Appraisal and Retrofitting in Building Structures. The conference was organized in four simultaneous tracks: “Advances in Civil Engineering”, “Advances in Structural Engineering”, “Advanced Transportation” and “Architecture and Building Materials”.

All those contributions were reviewed by the reviewers of international and domestic of China before accepted for publication. This book covers the subject areas of Road and Railway Engineering, Transportation Planning, Construction and Operation Organization, Modern Logistics System Planning and Optimization, Vehicle Engineering, Carrier Operation Engineering, ITS Theory and Applications, Traffic Control and Information Technology, Transportation and Social Economic Development, Low-carbon Transportation Technology and Urban Transportation Planning and Management.

The editors would like to thank the members of the scientific committees and invited referees for their assistance in reviewing the abstracts and full papers. Special thanks go to the authors without whom we could not have achieved the high quality.

Prof. Shucai Li
Shandong University, China

The 2011 International Conference on

Civil Engineering and Transportation

(ICCET 2011)

Organized by:

School of Civil Engineering, Shandong Jianzhu University, China

Co-organized by:

School of Civil Engineering, Shandong University

School of Civil Engineering and Architecture, Shandong University of Science and Technology

School of Civil Engineering, Yantai University

Shandong Provincial Key Lab of Appraisal and Retrofitting in Building Structures

Conference Organization

Chairman

Prof. Xiliang Liu, Tianjin University, China

International Scientific Committee

Prof. J. H. Bungey, University of Liverpool, Liverpool, UK

Prof. K. J. Bathe, Massachusetts Institute of Technology, USA

Prof. Lawrence C. Bank, University of Wisconsin-Madison, USA

Prof. Longsheng Bao, Shenyang Jianzhu University, China

Prof. Chaohe Chen, Hainan University, China

Prof. Zhihua Chen, Tianjin Universiyt, China

Prof. Jian-Fei Chen, the University of Edinburgh, UK

Prof. Feng Fan, Harbin Institute of Technology, China

Prof. Luciano Feo, University of Salerno, Italy

Prof. Han-Bin Ge, Meiju University, Japan

Prof. Haiyan Guo, Ocean University of China

Prof.Zong Woo Geem, iGlobal University, USA

Prof. Linhai Han, Tsinghua University, China

Prof. Yong Huang, Guizhou University, China

Prof. Jiping Hao,Xi'an University of Architecture and Technology,China

Prof. I. E. Harik, University of Kentucky, USA

Prof. David Hui, University of New Orleans, USA

Prof. Tan Kiang Hwee, National University of Singapore

Prof. Tim Ibell, University of Bath, UK

Dr.Tianjian Ji, The University of Manchester, UK

Prof. A. Kaveh, Iran University of Science & Technology, Iran

Prof. Guoqiang Li, Tongji University, China

Prof. Lijuan Li, Guangdong University of Technology, China

Prof. Shucai Li, Shandong University, China

Prof. Zhongxian Li, Tianjin University, China

Prof. Qiusheng Li, Hong Kong City University, Hong Kong

Prof. Kang Seok Lee, Chonnam National University, South Korea

Prof. Marcus M.K. Lee, the University of Southampton, UK

Prof. Zhengliang Li, Chongqing University, China

Prof. Zhengnong Li, Hunan University, China

Prof. Guangfan Li, Hainan University, China

Prof. Xiliang Liu, Tianjin University, China

Prof. Yew-Chaye Loo, Griffith University, Australia

Prof. Yaozhi Luo, Zhejiang University, China

Prof. Ayman Mosallam, Univ of California Irvine, USA

Prof. Aftab Mufti, University of Manitoba, Canada

Prof. Antoine E. Naaman, University of Michigan, USA

Prof. Hamid Ronagh, The University of Queensland, Australia

Prof. R. Sri Ravindra rajah, University of Technology, Australia

Prof. Yongjiu Shi, Tsinghua University, China

Prof. Xingping Shu, Hunan University, China

Prof. Ramiro Sofronie, University of Bucharest, Romania

Prof. M. N. Soutsos, University of Liverpool, Liverpool, UK

Prof. Mark G Stewart, The University of Newcastle, Australia

Prof. Dasui Wang, Shanghai Xiandai Architechural Design(Group) Co.,Ltd.

Prof. B. H. V. Topping, Heriot-Watt University, Edinburgh, UK

Prof. Tamon UEDA, Hokkaido University, Japan

Prof. Guangyue Wang, Shandong University,China

Prof. Lai Wang, Shandong University of Science and Technology, China

Prof. Yan Wang, Qingdao Technological University, China

Prof. Jinfeng Wang, Huaqiao University, China

Prof. Zhi-Shen Wu, Ibaraki University, Japan

Prof. Shi Yan, Shenyang Jianzhu University, China

Dr. Scott T. SMITH, Hong Kong University, Hong Kong

Prof. J-G. Teng, Hong Kong Polytechnic University, Hong Kong

Prof. Yan Xiao, Hunan University, China

Prof. Zhixin Yan, Lanzhou University, China

Prof. Yanzhen Yu, Jinan University, China

Prof. Qilin Zhang, Tongji University, China

Prof. Xin Zhang, Shandong Jianzhu University, China

Prof. Yigang Zhang, Beijing University of Technology, China

Prof. Jincheng Zhao, Shanghai Jiaotong University, China

Prof. Xin'gang Zhou, Yantai University, China

Prof. Xuejun Zhou, Shandong Jianzhu University

Prof. Yanpeng Zhu, Lanzhou University of Technology, China

Prof. Chaoying Zou, Harbin Institute of Technology, China

Prof. Jiru Zhang, Wuhan University of Technology, China

Prof. Chuangbin Zhou, Wuhan University, China

Local Organizing Committee

Chair

Prof. Xuejun Zhou, Shandong Jianzhu University, China

Co-Chairs

Prof. Shucai Li, Shandong University, China

Prof. Lai Wang, Shandong University of Science and Technology

Prof. Xin'gang Zhou, Yantai University, China

Table of Contents

Chapter 2: Transportation Planning, Construction and Operation Organization

Chapter 4: Vehicle Engineering

Chapter 5: Carrier Operation Engineering

Chapter 6: ITS Theory and Applications

Chapter 7: Traffic Control and Information Technology

Chapter 8: Transportation and Social Economic Development

Chapter 9: Low-Carbon Transportation Technology

Chapter 10: Urban Transportation Planning and Management

CHAPTER 1:

Road and Railway Engineering

Applied Mechanics and Materials Vols. 97-98 (2011) pp 3-9

doi:10.4028/www.scientific.net/AMM.97-98.3

The Calculation of the Supporting Stress of Track Plate in Ballastless High-speed Rail Structure

Yang Wang[1, a], Quanmei Gong[2,b] Meifang Li[3,c]

[1,2,3]Key Laboratory of Road and Traffic Engineering of the Ministry of Education, Tongji University, 4800 Caoan Road, Shanghai, 201804 China

[a]wangyang19870301@163.com, [b]gongqm@tongji.edu.cn, [c]limeifang2006@126.com

Keywords: Slab track structure; Method of composite beam; Matlab; Support stress

Abstract. The slab track is a new sort of track structure, which has been widely used in high-speed rail and special line for passenger. However, the ballastless track structure design theory is still not perfect and can not meet the requirements of current high-speed rail and passenger line ballastless track. In this paper, composite beam method is used to calculate the deflection of the track plate and in this way the vertical supporting stress distribution of the track plate can be gotten which set a basis for the follow-up study of the dynamic stress distribution in the subgrade. Slab track plate's bearing stress under moving load is analyzed through Matlab program. By calculation and analysis, it is found that the deflection of track plate and the rail in the double-point-supported finite beam model refers to the rate of spring coefficient of the fastener and the mortar.The supporting stress of the rail plate is inversely proportional to the supporting stress of the rail. The two boundary conditions of that model ,namely, setting the end of the model in the seams of the track plate or not , have little effect on the results. We can use the supporting stress of the track plates on state 1to get the distribution of the supporting stress in the track plate when bogies pass. Also, when the dynamic load magnification factor is 1.2, the track plate supporting stress of CRST I & CRST II-plate non-ballasted structure is around 40kPa.

Introduction

High-speed railway has strict requirements for subgrade settlement. In general, the settlement must be less than 15mm.The subgrade settlement generally includes filling compaction subsidence, post-construction settlement due to the foundation, subgrade cumulative subsidence caused by driving load, all of them are related to the level of dynamic stress of the subgrade. At present,there are two main ways concerning the calculation of dynamic stress of the subgrade. The first one is the finite element method, and the second is using the composite beam method to calculate the supporting stress of the track plate, and then calculate the dynamic stress of the embankment with Boussinseq method. However, the finite element method needs enormous time and energy to construct the finite element model. As for the analytical method, Chinese and foreign scholars do lots of researches mainly dealing with the track dynamics, track structure forces, but they do not show concern for the track plate supporting stress. Timoshennko [1] used a single degree-of-freedom lumped parameter track model to study displacement response and dynamic stress of the rail in the effect of sinusoidal load and wrote a new page for track dynamic analysis. Di Wanming [2] developed a vehicle - track coupling dynamics model. He made the slab track system two-beam system for analysis and mainly analysed the effect of the change of welded concave joints of long rail ,stepped irregularity , and slab track's CA mortar layer kinetic parameters not smooth of kinetic parameters on the whole system.LI Chun-Xia [3-4] constructed slab track structure analysis model on the subgrade to make an analysis of slab track force characteristics on the subgrade. She regarded the track structure as a flexible entity and calculated the force and deformation of the layers of the slab track . Liu Yuxiang[5-6] and other scholars made a contrast and analysis between the composite beam method and the finite element method and found little difference between the results of two methods. Lou Ping [7] and other

researchers made an analysis of the dynamic response of slab track under the effect of moving load by using the finite element method and studied the relationship between the speed of the moving load, types of rail and elasticity of rail fulcrum and the dynamic response of rail and the rail plate.

As for the foregoing problems, in this paper rail, track plate, rail fasteners, CA mortar layer are regarded as a system to analyze and the relevant double-point-supported finite beam model is built up. The rail is treated as infinite beam, rail plate is treated as short beam, rail and rail fastening plate are represented as discrete spring, CA mortar layer under track plate is described by the Winkler foundation. The effect that parameter values exert on the track plate deflection and track plate stress is analyzed, and the track plate supporting stress distribution of two kinds of Chinese high-speed railway track form is obtained.

The construction of computation model

The rail is regarded as infinite beam , rail plate as finite short beam. Intercepting half track from the center line, a rail and the corresponding track plate compose the double-layer beams model on elastic foundation. The model is shown in Fig. 1.

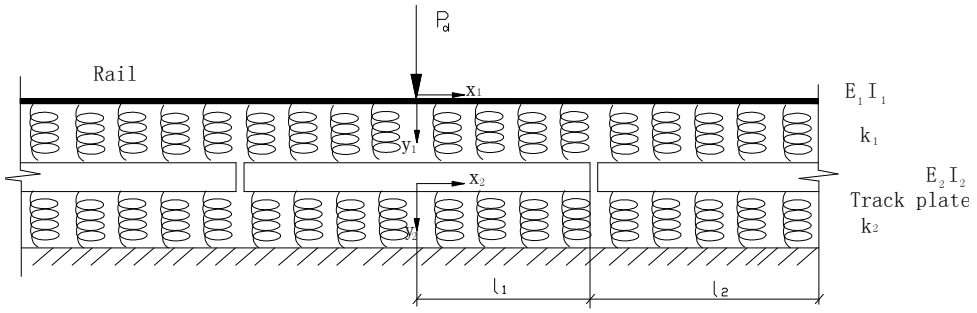

Fig.1 Double-layer point supported finite beam model

Between the upper rail track beam and the lower rail track beam is the spring, which is the simplified version of the fasteners. The spring coefficient is the result that the stiffness of a fastener divide the spacing of rail pivots. The lower beam is the track plate, the supporting is simulated as spring which is in accordance with Winkler's assumptions. The concentrated load Pd is applied on the rail.

Differential Equations. The origin of coordinate is set at the loading position, the composite beam is divided into two sections: $l_1 \& l_2$. l_1 is the distance between track plate loading position and the right edge of the plate . l_2 is the distance between the right edge of the plate to the edge of the model. According to the elasticity and mechanics knowledge and the elastic-plastic theory, the beam is regarded as Euler beams and the deflection differential equations concerning the model are listed as Eq. 1, Eq. 2, Eq. 3, Eq. 4.

$$E_1 I_1 \frac{d^4 y_{11}}{dx_{11}^4} + k_1 (y_{11} - y_{21}) = 0 \quad \text{(the subject is the rail in } l_1\text{)} \tag{1}$$

$$E_1 I_1 \frac{d^4 y_{12}}{dx_{12}^4} + k_1 (y_{12} - y_{22}) = 0 \quad \text{(the subject is the rail in } l_2\text{)} \tag{2}$$

$$E_2 I_2 \frac{d^4 y_{21}}{dx_{21}^4} + k_1 (y_{21} - y_{11}) + k_2 y_{21} = 0 \quad \text{(the subject is the track plate in } l_1\text{)} \tag{3}$$

$$E_2 I_2 \frac{d^4 y_{22}}{dx_{22}^4} + k_1 (y_{22} - y_{12}) + k_2 y_{22} = 0 \quad \text{(the subject is the track plate in } l_2\text{)} \tag{4}$$

In the equation, E_1I_1 ---- the bending stiffness of a single rail;

E_2I_2 ---- the bending stiffness of half the track plate;

y_{11}, y_{12} ---- the deflection of the rail in l_1, l_2;

y_{11}, y_{12} ---- the deflection of the track plate in l_1, l_2;

k_1, k_2 ---- the supporting spring coefficient of the rail and track plate per unit length.

Boundary conditions. At the loading position(x=0), $y'_{11}=0$ (5) $y'''_{11}=\frac{P_d}{2E_1I_1}$ (6) $y'_{21}=0$ (7) $y'''_{21}=0$ (8); At the seam of the track plate($x=l_1$),

$y_{11}=y_{12}$ (9) $y'_{11}=y'_{12}$ (10) $y''_{11}=y''_{12}$ (11) $y'''_{11}=y'''_{12}$ (12) $y''_{21}=0$ (13) $y'''_{21}=0$ (14) $y''_{22}=0$ (15) $y'''_{22}=0$ (16);

At the edge of the model($x=l_1+l_2$), $y_{12}=0$ (17) $y'_{12}=0$ (18)

when the terminal is not set in the seam of the track plate, $y_{22}=0$ (19-1) $y'_{22}=0$ (20-1)

when the terminal is set in the seam of the track plate， $y''_{22}=0$ (19-2) $y'''_{22}=0$ (20-2)

Analysis of calculation parameters

Except for the spring coefficient, the values of other parameters of point-supported finite beam model are based on the form of track plate, so the spring coefficient has a remarkable effect on the structure. The following are researches on the values of those parameters.

The simulation of the dynamic process when train passes. The dynamic load is transferred on the rail by the wheel and passed on to the track plate by the fastener. Taking a track plate as the study object, the process of the train passing can be simulated here to three states. State 1 is the load of a bogie is located at the edge of a track plate, and the other wheel load is 2.5m away from the edge of the track plate, namely, a bogie just gets full access to a track plate(Fig. 2); state 2, a bogie just arrives in the middle of a track plate, namely, the bogie passes the track plate(in Fig. 3); state 3 is that one wheel load of a bogie is in the middle of a track plate and the other wheel load is on another track plate, namely, the bogie is leaving the track plate(Fig. 4).

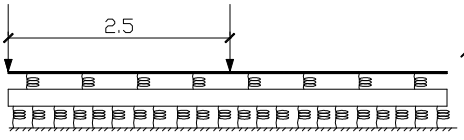

Fig.2 State1

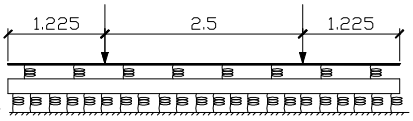

Fig.3 State2

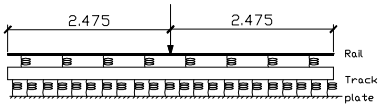

Fig.4 State3

The analysis of calculation results. Compile a Matlab program to solute the differential equations above. The coefficients of double-layer point-supporting finite beam model depend on the form of the track plate except for spring coefficient., so the criminal of spring coefficient plays an important role in the construction. Liu[5] express that Fastener stiffness 60MN/m is reasonable. So k1=60MN/m， the value of K2 is changed to analyze how it effects the result. In the Calculate of the CRTSI rail board, the stiffness of the track board is 60kg/m, the size of track board is 4.95m long, 2.4m wide and 0.19m thick. The unit fulcrum spacing of the fastener is 0.625m. The Elastic coefficient of CA mortar layer is 30~200MN/m. The Elastic modulus of the rail is 210GPa. The inertia of iron rail section is 3.22x10-5m4. The Elastic modulus of track plate is 41.2GPa. The rail vertical force is 90KN when the impact coefficient is 1.2.

In state1, the deflection and supporting stress are basically same, no matter whether the edge of model is on the juncture (Fig5, 6). So the two kinds of boundary conditions have little influence in the result. So in following analysis, we take this state that final point is not on the juncture into consideration.

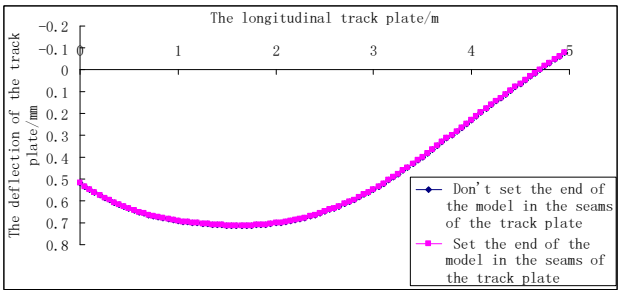

Fig.5 The longitudinal deflection distribution of the track plate

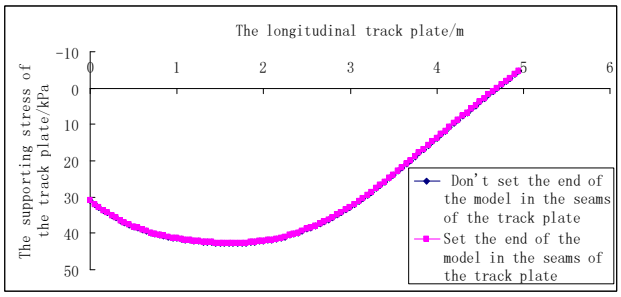

Fig.6 The longitudinal supporting stress distribution of the track plate

The results are shown in Figure 7, Figure 8, Figure 9 and Figure 10. Figure 7, Figure 8 are respectively the deflection distribution of the track plate and the rail when the spring coefficients differ. when k_2 is bigger than 60MN/m, the deflection of track plate will increase as k_2 increases. As Figure 11 shows, the deflection of track plate is relevant to the ratio of k_1 and k_2. When $k_1/k_2 <1$, the fastener stiffness is relatively larger ,the deflection of track plate will decrease as the result of k_1/k_2 increases; when $k_1/k_2> 1$, the deflection of track plate will increase as the value of k_1/k_2 increases. As Figure 8 and Figure 12 shows, the rail deflection will increase as the result of k_1/k_2 increases. As Figure 9 and Figure 10 shows, the supporting stress of the track plate is in inverse proportional to the supporting stress of the rail. The supporting stress of the rail increases as the result of k_1/k_2 increases, while the supporting stress of the track plate decreases as the result of k_1/k_2 increases.

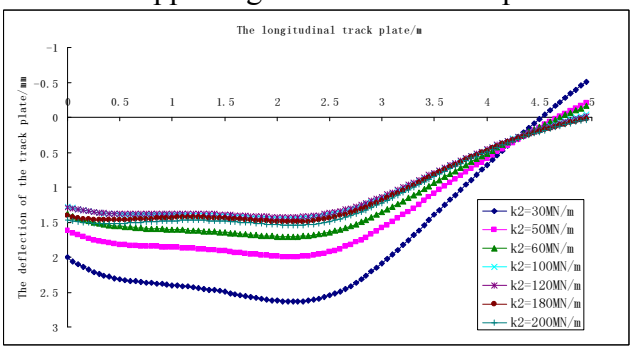

Fig.7 The deflection distribution of the track plate under different spring coefficients

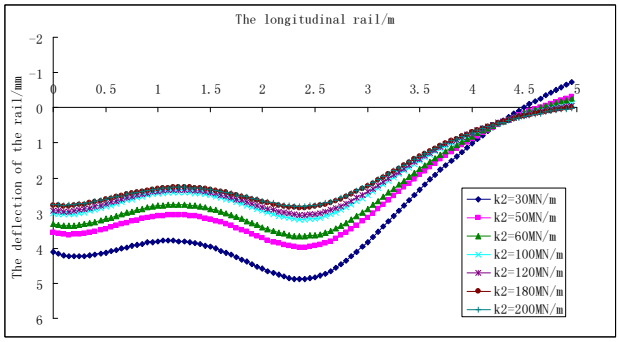

Fig.8 The deflection distribution of the rail under different spring coefficients

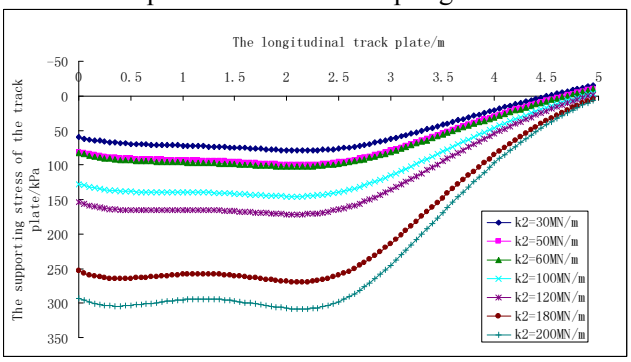

Fig.9 The supporting stress distribution of the track plate under different spring coefficients

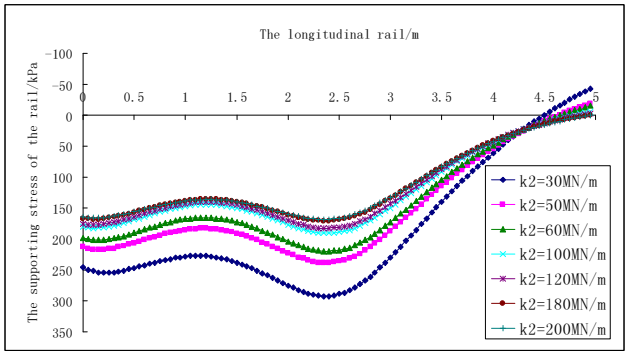

Fig.10 The supporting stress distribution of the rail under different spring coefficients

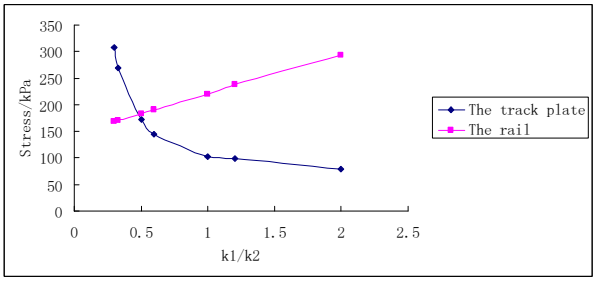

Fig.11 The curve of the track plate's supporting stress varying with k_1/k_2

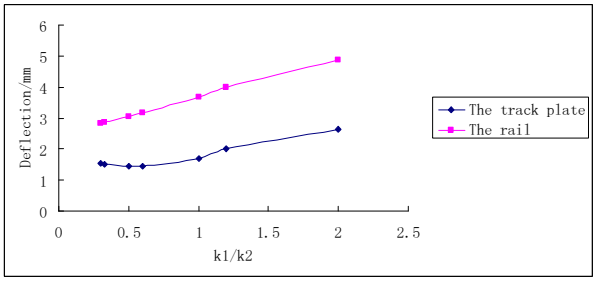

Fig.12 The curve of the track plate's deflection varying with k_1/k_2

The verification of Reliability. Chen Peng [8] from Beijing Jiaotong University conducted a corresponding dynamic test in the Suining-Chongqing comprehensive test section and got a lot of test data. The speed range of motor car in test in Suining-Chongqing line is 160 ~ 220km/h, the wheel-rail vertical force is 59.6 ~ 106.1kN, and to make a contrast to the experimental results in Suining-Chongqing line, the concentrated force P_d is changed to 106kN to verify the reliability of the results of double-layer point supported finite beam model. The calculation results is shown in Fig.13, Fig.14.

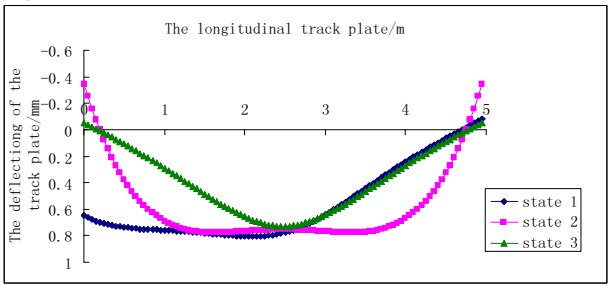

Fig.13 The longitudinal deflection distribution of the track plate

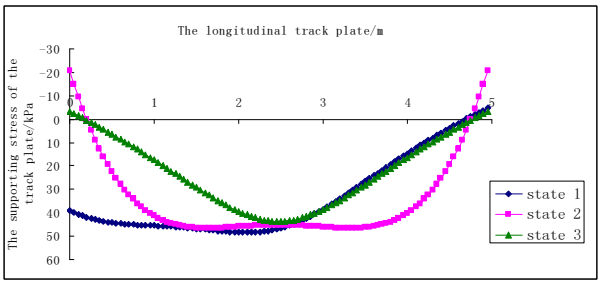

Fig.14 The longitudinal supporting stress distribution of the track plate

The contrast between the calculation results and test results is shown in Table 1. Due to the large discreteness of dynamic test and the approximate nature of dynamic calculation in this article, the test results and calculation results can not be exactly the same, but the result still has good comparability and reference value. Using double-layer point-supporting finite beam model can not get the vertical acceleration of rail and track plate, so acceleration is not involved in the contrast. In summary, the calculation results of the deflection and supporting stress of track plate is almost the same with the test results. but the calculation results of the deflection and supporting stress of rail is relatively bigger than the test results. This result is relevant to the complexity of the text site.

Table 1 The contrast between the calculation results and test results in Suining-Chongqing line

	Test results	Calculate results
the wheel-rail vertical force (kN)	59.6~106.1	106
The vertical displacement of the rail (mm)	0.30~0.88	1.73
The vertical acceleration of the rail (g)	173~926	/
The supporting force of the rail (kN)	14.4~68.5	104
The displacement of the track plate(mm)	0.01~0.87	0.805
The vertical acceleration of the track plate (g)	6.1~58.0	/
The stress in the CA mortar layer (kPa)	25.631~38.484	48
The acceleration of the subgrade(g)	0.5~9.7	/

The supporting stress of high-speed railway track plate

At present, Beijing-Shanghai high speed railway, Shanghai-Nanjing inter-city railway, Shanghai-Hangzhou inter-city railway, Wuhan-Guangzhou inter-city railway, all use CRSTI, CRST Ⅱ track plate in the ballastless track structure. The detailed dimensions of the two kinds of track plate is shown in Table 2. Applying the above method, the rail plate supporting stress of the two existing rail plate is calculated. In this way, the supporting stress of the high-speed railway track plate can be gotten to provide a basis for the follow-up study of the dynamic stress distribution in the subgrade.

Table 2 The type of slab track

	CRSTI	CRST Ⅱ
Rail	60kg/m, U71Mn(k)rail	
Fastener	WJ-7B elastic separated rail fastening	Vossloh 300-1 rail fastening
Track plate	2400mm wide,4950mm long 190mm thick	2550mm wide,6450mm long,200mm thick
Mortar Bed	50mm wide	30mm wide
concrete bed	300mm thick， 3000mm wide	207mm thick(the centre of the line),2950mm wide

The calculation parameters. The dynamic load selects CRH2 EMU, the axle load is 15t. Taking into account of dynamic effects and taking the impact factor as 1.2, the dynamic wheel weight in calculation is 90kN (axle load / 2×3.0).The calculation parameters are shown in Table 3.

Table 3 The calculation parameters

	E1/Gpa	I1/m4	k1/MN/m	E2/Gpa	I2/ m4	k2/MN/m	Pd/kN
CRSTI track plate	210	3.22e-5	60	41.2	6.8e-4	60	90
CRST Ⅱ track plate				35.5	8.5e-4		

The calculation results of CRST I track plate. By calculation, in state1, the deflection of track plate is the largest, so it can be considered the worst state. According to the distribution of the track plate supporting stress in state 1, it is easy to get the envelope map of track plate supporting stress and then get the distribution rule of track plate supporting stress. The maximum deflection of the track plate is 0.7mm and the supporting stress is 42.5kPa.

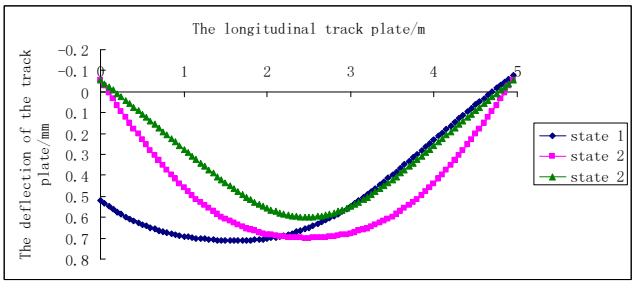

Fig.15 The longitudinal deflection distribution of the CRSTI track plate

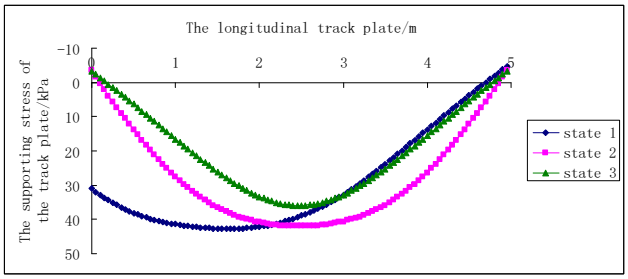

Fig.16 The longitudinal supporting stress distribution of the CRSTI track plate

The calculation results of CRST II track plate. As the length of CRST Ⅱ track plate is 6450mm, the bogie on the track plate can be represented in two states, referring to Figure 17, Figure 18. Figure 19, Figure 20are the envelope map of track plate supporting stress based on the track plate supporting stress distribution in state 1. The maximum deflection of the track plate is 0.63mm, and the maximum supporting stress is 37.7kPa.

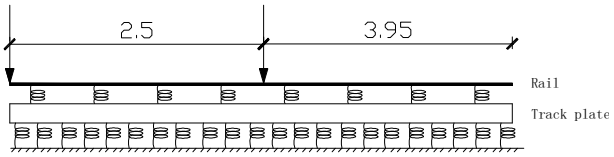

Fig.17 State1 of CRST Ⅱ track plate

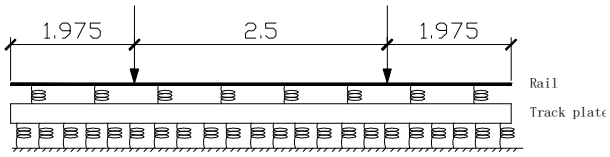

Fig.18 State2 of CRST Ⅱ track plate

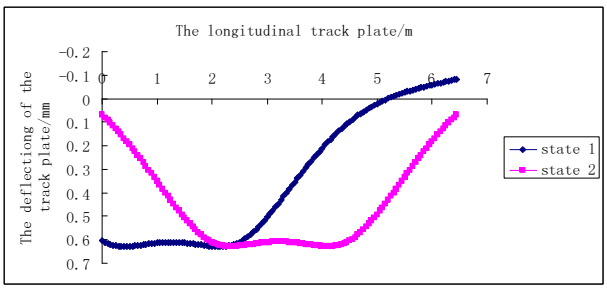

Fig.19 The longitudinal deflection distribution of the CRST Ⅱ track plate

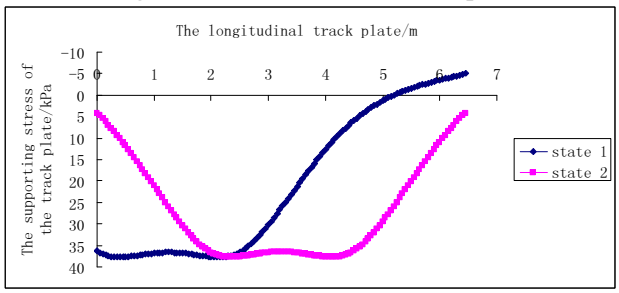

Fig.20 The longitudinal supporting stress distribution of the CRST Ⅱ track plate

Conclusions

By Matlab program, making use of double-layer point supported finite beam model, conclusions can be drawn as follows.

(1) It is found that the deflection of track plate and the rail in the double-point-supported finite beam model refers to the rate of spring coefficient of the fastener and the mortar. When k_1/k_2 <1, the deflection of track plate will decrease as the result of k_1/k_2 increases; when k_1/k_2> 1, the deflection of track plate will increase as the value of k_1/k_2 increases.The rail deflection will increase as the result of

k_1/k_2 increases. the supporting stress of the track plate is in inverse proportional to the supporting stress of the rail. The supporting stress of the rail increases as the result of k_1/k_2 increases, while the supporting stress of the track plate decreases as the result of k_1/k_2 increases.
(2) The two boundary conditions of that model ,namely, setting the end of the model in the seams of the track plate or not , have little effect on the results.
(3) Using the supporting stress of the track plates on state 1,We can get the distribution of the supporting stress in the track plate when bogies pass.
(4) when the dynamic load magnification factor is 1.2, the track plate supporting stress of CRST I & CRST II-plate non-ballasted structure is around 40kPa.

Acknowledgements

This work was financially supported by the Scientific and Technological Program of the Ministry of Railways (2010G003-A)

References

[1] Timoshennko. Vibration problems in engineering [M]. Beijing: CHINA RAILWAY PUBLISHING HOUSE, 1979.

[2] Zhai Wanming. Vehicle-Track Coupling Dynamics(Third edition) [M]. Beijing: Science Press, 2007.

[3] Li Chunxia, Li Chenghui, Kou Zhonghou. The Mechanical analysis of slab track on soft formation[J]. RAILWAY ENGINEERING, 2005(7)p:88-90.

[4] Li Chunxia. The Mechanical analysis of slab track on soft formation[D]. Cheng Du: Southwest Jiaotong University, 2005.

[5] Liu Yuxiang. Study on the method of analyzing slab track in Ballastless railway[D]. central south university, 2006:19-32.

[6] Liu Yuxiang, Chen Xiufang. The two methods of analyzing and calculating slab track structure[J]. URBAN MASS TRANSIT, 2007, 10(6): 32-34.

[7] Lou Ping, Ceng Qingyuan. Finite element analysis of slab track subjected to moving losds[J]. JOURNAL OF TRAFFIC AND TRANSPORTATION ENGINEERING, 2004, 4(1): 29-33.

[8] Chen Peng. Research on Mechanical Characteristics of Ballastless Track in High-Speed Railway[D]. Beijing:Beijing Jiaotong University, 2008.

Applied Mechanics and Materials Vols. 97-98 (2011) pp 10-16

doi:10.4028/www.scientific.net/AMM.97-98.10

The study of fatigue life of cold-recycled base material based on the fracture mechanics method

ZHANG Hai[1], ZANG Yun[2]

([1,2]Shenyang Jianzhu University,Shenyang,China,110168)

haizhang-11@163.com

Keywords: fracture mechanics; fatigue life ;parameter; life forecast equation

Abstract. The method of fracture mechanics is used to analyse the fatigue crack propagation of cold-recycled base material in this paper. The suitable fracture mechanics formula and parameters are choosen and then we deduce the fatigue life forecast equation.After that we annlyse the method of determineing parameters and give the axample.The conclusion is gained through comparing with the database obtained from the experiment .It is more reasonable to forecast the fatigue life of cold-recycled base material with crack based on the method of fracture mechanics.

Introduction

Asphalt pavement based cold-recycled technology is a relatively new city road asphalt maintained technology and it has good application prospect.In recent years, people at home and abroad have made a series of research results of asphalt pavement based cold-recycled technology[1]-[3]. But those results mainly concentrated in the aspect of road properties，and the research results of fatigued performance of old-recycled material are relatively scarce It is usually processing the fatigue experiment of cold-recycled material for forecasting fatigue life of cold-recycled material.It is to fit the fatigue forecast equation through the experiment results.But the fatigue forecast equation gained from the experiment results fitting has big differences with actual life.The mainly because the big different stress state between indoor cold-recycled material specimens[4]and actual road and the considered factors also are relatively single.

In this century 40s and early 50s , fracture mechanics have been widely used in metal materials, then open up to nonmetal material field such as rock, concrete, gypsum etc.Since the 70's, the fatigue fracture mechanics had the very big development, gradually become emollient tool for analysising and predicting the fatigue life of structure.This paper deduce fatigue life forecast equation of cold-recycled material with method of fracture mechanics and estimate fatigue life of cold-recycled material through analysisng the factors affecting the fatigue life of cold-recycled material and choosing the suitable parameters.

Basic assumption

Cold-recycled material is composed with transition zone through analysising the microcosmic composition of cold-recycled material.This is diffenent with semi-rigid base material. Transition area mainly include the new interface transition zone and old transition zone.New old interface interface transition zone is the interface which is composed with aggregate and new cement. Old interface transition zone is the interface between the regeneration of aggregates source within aggregates and the old cement (as shown in Figure 1).Interface transition zone is the weak spots of mechanical properties and durability of cold-recycled mixed material .Because the cement can produce the chemical contraction and produce heat in hydration and hardening, the aggregate can make restrict to contraction and various materials constrains different thermal expansion coefficients, the initial stress and crackle will produce between the interface. In addition, the mechanical broken and milling are used in in the recycling asphalt pavement materials, there are inevitably produce internal micro cracks and initial damage in old interface[5].

Figure 1 Cold-recycled mixture mesoscopic structure

At present, It is less to study pavement structure semi-rigid base material using fracture mechanics theory and methods.More is used to study the metal materials with ductile fracture. Usually, the pavement materials fracture all belong to brittle fracture.There has no obvious sign before fault and there also is not macro plastic area in a material.The destruction is suddenly. The linear elastic fracture mechanics is generally used for brittle fracture

Through the analysis above, we can make the assumption below：

1.All the cold-recycled base material specimens exist the micro cracks, that is only the calculation of crack extend life just do to the cold-recycled base material.

2. All the cold-recycled base material are linear elastic or alignment elastic crack body.

This paper based on the above two assume that, using the crack propagation velocity , the fatigue life of cold-recycled base material are calculated.

2. **Cold-recycled base material fatigue life equation**

The fatigue life is usually component of crack formation life and the crack propagation life two parts, crack propagation life is the main part. Fatigue crack propagation characteristics can be divided into three areas[6](As shown in figure 2), In the first Ⅰ area there is a threshold a value of ΔK_{th}, In this area circulation within the scope of stress intensity factor ΔK below the threshold value of ΔK_{th}, Fatigue crack basic is not expanded. The second Ⅱ area for medium speed expansion area, the stress intensity factor ΔK of the region is bigger than ΔK_{th} range of the fatigue crack propagation characteristics. Crack growth rate da/dN and the stress intensity factor amplitude ΔK of the relationship obey paris formula. The third Ⅲ area is the spreading area, the maximum stress intensity factor to fracture toughness of material, crack growth rate increase sharply until fracture.

Though the paris formula of crack extension has made great success in the calculation of life,, still has limitations. Because paris formula only think about the Ⅱ influence.

Then Forman [7] continue the perfect, and put forward the more reasonable formula, This paper, based on the Forman formula , deduced cold regeneration grassroots material fatigue life calculation formula.

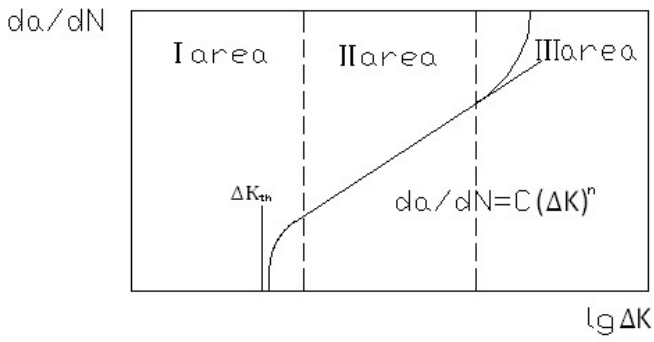

Figure 2 Fatigue crack growth rate division

Forman formula is considered the Ⅱ area, Ⅲ area and the average stress on the fatigue crack effect, The average stress on to the influence of the fatigue crack, choose as the main parameters of the stress ratio R, Forman formula [7] below:

$$\frac{da}{dN}=\frac{C\left(\Delta K\right)^{\mathrm{m}}}{\left(1-R\right)K_{IC}-\Delta K} \tag{1}$$

C,m ——Material test parameters

ΔK ——Stress intensity factor picture ($\Delta K=K_{\max}-K_{\min}$)

R ——Stress than ($R=\sigma_{\min}/\sigma_{\max}$)

K_{IC} ——Fracture toughness of material

In all the influence factors of crack propagation, Elastic modulus, propagation threshold and the fracture toughness three factors change to crack growth behavior change is the most direct reason, and other factors on the influence of the crack propagation is indirect. If do not consider the elastic modulus on crack propagation, the influence of different materials shows different extending behavior, is caused by different K_{IC} and ΔK_{th} fundamentally ,and Other factors were through the K_{IC} and ΔK_{th} value and effect to the effect the crack growth rate [8]. The influence of various factors of crack extension, in addition to the material's state and the performance, stress level of crack propagation also have great impact, on different stress and fatigue life have obvious difference. LiuHaoWen[9][10] in sheet metal research in repeated load in the process of the crack propagation deduces influence fatigue , stress change $\Delta\sigma$ process parameters was the most important stress in crack growth rate . Based on the above analysis, chooses the material for cold regeneration of KIC stress fracture toughness, R and stress amplitude $\Delta\sigma$ as main parameters to deduce the fatigue life formula.

By $\Delta\sigma$ formula to (1) the ΔK, can be expressed as:

$$\Delta K=\alpha\Delta\sigma\sqrt{\pi a} \tag{2}$$

$\Delta\sigma$ ——Stress amplitude， ($\Delta\sigma=\sigma_{\max}-\sigma_{\min}$) .

α ——Stress intensity factor coefficient, reference《stress intensity factor》manual value.

a ——Specimen of produce crack length.

Will (2) into (1) type, integral to get：

When m=3

$$N=\frac{\left(1-R\right)K_{IC}\left(a_c^{\,1-\frac{m}{2}}-a_0^{\,1-\frac{m}{2}}\right)}{\left(1-\frac{m}{2}\right)C\alpha^m\Delta\sigma^m\pi^{\frac{m}{2}}}-\frac{\ln a_c-\ln a_0}{C\alpha^{m-1}\Delta\sigma^{m-1}\pi^{\frac{m-1}{2}}} \tag{3}$$

When m≠3

$$N=\frac{\left(1-R\right)K_{IC}\left(a_c^{\,1-\frac{m}{2}}-a_0^{\,1-\frac{m}{2}}\right)}{\left(1-\frac{m}{2}\right)C\alpha^m\Delta\sigma^m\pi^{\frac{m}{2}}}-\frac{a_c^{\frac{3-m}{2}}-a_0^{\frac{3-m}{2}}}{\left(\frac{3-m}{2}\right)C\alpha^{m-1}\Delta\sigma^{m-1}\pi^{\frac{m-1}{2}}} \tag{4}$$

The a_c in the specimen of the said at fracture length of the crack. If the stress intensity factor to the fracture toughness K_{IC}, crack growth rate tendency to define fracture failure, infinite can be used to represent K_{IC} a fracture toughness of the biggest component crack length a_c (See type (6))

$$K_{IC}=\alpha\sigma_{\max}\sqrt{\pi a_c} \tag{5}$$

$$a_c = \left(\frac{K_{IC}}{\alpha \sigma_{\max}} \right)^2 \frac{1}{\pi} \tag{6}$$

Will type (6) into a type (3) (4) get type：

When m=3

$$N = \frac{(1-R) K_{IC}^{3-m}}{A_1 \Delta\sigma^m \sigma_{\max}^{2-m}} - \frac{(1-R) K_{IC} a_0^{1-\frac{m}{2}}}{A_2 \Delta\sigma^m} + \frac{\ln a_0 - \ln K_{IC}^2 + \ln \alpha^2 \sigma_{\max}^2}{A_3 \Delta\sigma^{m-1}} \tag{7}$$

When m≠3

$$N = \frac{(3-\mathrm{m})(1-R)\sigma_{\max} - (2-m)\Delta\sigma}{A_1 \Delta\sigma^m \sigma_{\max}^{3-m}} K_{IC}^{3-m} - \frac{(1-R) K_{IC} a_0^{1-\frac{m}{2}}}{A_2 (\Delta\sigma)^m} + \frac{2 a_0^{\frac{3-m}{2}}}{A_3 \Delta\sigma^{m-1}} \tag{8}$$

$$A_1 = (3\text{-m})\left(1-\frac{\mathrm{m}}{2}\right) C\pi\alpha^2 \quad A_2 = \left(1\text{-}\frac{\mathrm{m}}{2}\right) C\pi^{\frac{m}{2}} \alpha^m \quad A_3 = (3-m) C\pi^{\frac{m\text{-}1}{2}} \alpha^{m\text{-}1}$$

Type (7) and type (8) is fatigue life prediction equations, this equation with R, stress amplitude Δσ, and fracture toughness KIC to describe the fatigue life of materials.

C and m of Fatigue life prediction formula are material test parameters, and many other factors affect fatigue life of the test, such as temperature, humidity, loading frequency, and all of the implicit. At present about this aspect of the recycled material test research is little, in view of the cold regeneration materials and concrete property is similar, so this paper concrete C, m values of the value method.

[11] the elastic patch direct observation of light before concrete samples instability fracture cracks stable expansion process, to get da/dN and ΔK .Through the linear regression to get c,m in formula of paris. This method is widely used, but worthy of note, c,m in the value of the parameters of the formula of paris is different Forman, formula of c,m value. The literature with A fatigue test machine (MTS) of cement concrete fatigue test.[10]Load of pressure sensor, through BLR — 1/5000 measurement, Crack opening displacement through the mouth with homemade stretched instrument measurement, type and the dynamic strain sensor with load is X—Y recorder access. The use of such as repeated load, stress than set to 0.1. By tests with a number of fatigue crack length change law of N， From a/h—N curve obtained by the difference da/dN. According to the relative length a/h crack at this time for ΔK, Then the test data further treatment, get $\lg\left\{\frac{da}{dN}\left[(1-R)K_{IC}-\Delta K\right]\right\}\sim\Delta K$ relation curves. Linear regression get C= 6.1207×10-8， m=2.3541. The test method is adopted in this paper to obtain c,m of cold regeneration material value.

At present, the research of cold-recycled base material for fracture toughness also less, the same reference to fracture toughness of concrete material relevant material for cold fracture toughness of recycled materials. The fracture toughness of concrete research [13] suggests：Fracture toughness of concrete with size effect. For this phenomenon is also controversial. Another view is that [14][15]， Cable elastic fracture mechanics does not apply to cement slurry, mortar, the concrete kind of material, the fracture toughness K_{IC} can be used as the criterion of the fracture characteristics. And another view think [13]， Each concrete materials there is K_{IC} inherent critical stress intensity A value, Because concrete materials is random statistical properties，K_{IC} specimen size with larger than，But the change rule can be used to describe Weibull theory，And the little specimen of K_{IC} determination to derive value of K_{IC} big size component. Literature [16] consider the concrete as nonlinear object consideration the nonlinear, The rheological model,in concrete are tested by the 3 point bending test， the experimental data with the elastic theory analytical method, the energy method consider concrete creep characteristics of viscoelastic theory analysis, calculation and comparison to get fracture toughness of concrete. This paper also uses the test method to get material K_{IC} value of cold regeneration fracture toughness.

Fatigue estimate in the formula of stress intensity factor coefficient values, will be α grassroots as an infinite long attrib wattle, the limited width pull force crack under unilateral. accessliterature [17]，This paper recommend stress intensity factor coefficient values A.

Example

In this paper, using MTS810 fatigue machine of cement to fatigue test stabilized sand gravel subgrade materials and cold regeneration of the material results trabecular [5]，By using the method of test to data fitting to get the fatigue equation estimate. In order to compare the test results and calculation using the same stress level. The fracture toughness reference [13] and [16] test data (Test specimen size and fatigue test specimen size close, avoid the influence of size effect).We make $K_{IC} = 71.1 KN / cm^{\frac{3}{2}}$ in this paper.

Usually crack width of concrete material with 0.05 mm as boundary，Crack width of concrete less than 0.05 mm for "no cracks of concrete", that is, the invisible cracks, and the other for crack concrete [18].Because there are new old interface transition region in cold regeneration material, the initial cracks of concrete is much bigger than concrete. Combine the type (6)，for security reasons. The initial crack length were taken 0.05mm, 0.75mm, 0.1mm to calculate.The calculation results is shown in table 1.The tendency of material life N changes with the initial cracks is shown in figure 3 below.The tendency of material life N changes with Δσchanging of stress amplitude shown as shown in figure 4.

Table 1 The computational results of fatigue life

Pure cold recycled materials	stress		R	Δσ	K_C	a_0	N (10^5)
	σ_{max}	σ_{min}					
1#	1.010	0.101	0.1	0.909	71.1	0.05	8.26
						0.075	3.23
						0.1	1.22
2#	0.968	0.097	0.1	0.871		0.05	13.6
						0.075	7.41
						0.1	4.73
3#	0.803	0.080	0.1	0.723		0.05	28.2
						0.075	16.6
						0.12	9.88

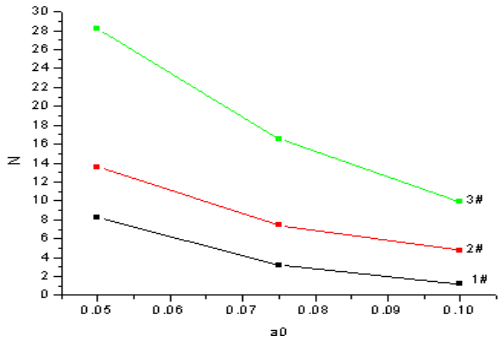

Figure 3 With initial crack a0 life change trend of the N map

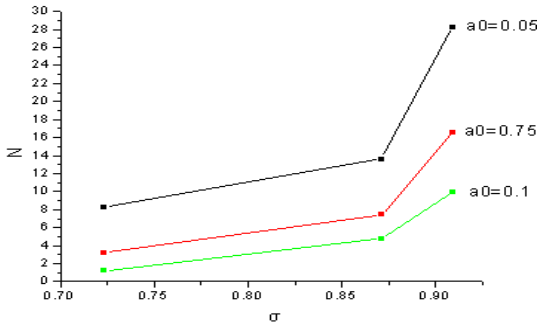

Figure 4 Stress amplitude with Δσ life change trend of the N map

In figure 3 can see clearly, with the increase of the initial cracks, life decreased and gradually reduce to a larger extent. It is explained that the initial cracks has a very big effect on fatigue life. So in order to improve the fatigue life, we should try to minimize the initial crack width. When the initial crack is the certain value, along with the increase of stress intensity maximum, the l life of material is decreasing. When the initial crack is smaller,it is especially remarkable.

In figure 4 can get, stress amplitude also have a greater impact on fatigue life , with stress amplitude decreases, the fatigue life increased significantly, this is consistent with paper before analyzed the theory. Stress amplitude can be used as a main parameters of stress level , reaction to the influence of stress level to fatigue life.

The literature [5] analysis with the test data to calculated for the fatigue life of 1.9 x 106， which is much bigger than the fracture mechanics method to calculate the fatigue life of the. From the actual situation of road early destruction, the method of fracture mechanics to forecast crack at the cold regeneration fatigue life is more reasonable， and the literature[5] of fatigue life prediction equations by test method without considering the initial crack, stress amplitude and the fracture toughness, and other important parameters.

Because in this paper calculating the fracture toughness and parameters of c,m value is according to the relevant data of the concrete, so the results are still exist errors. So the cold regeneration will in future fracture toughness of material parameters and the value of c,m should be further studied, so as to get more accurate estimate material fatigue life of cold regeneration.

Conclusion

1. Based on the theory of fracture mechanics, derived the cold regeneration fatigue life prediction equations. Equation with the fracture toughness, KIC main stress than R and stress amplitude $\Delta\sigma$ as main parameters.

2. The initial cracks have obvious influence on fatigue life .the fatigue life will increase with the initial cracks decreases. So we should try to minimize the initial cracks.

3. The change of stress amplitude has a significant influence on fatigue life, stress amplitude increase, life was decreased. Stress amplitude is thought as stress level parameter to analyze the fatigue life.

References

[1] Zhang Weijun ,Ge Zhesheng.Study on performance evaluation of cold recycled mixture. Journal of Central South Highway Engineering Vol.3(2007),p.124-126.

[2] Chen Zhaoxia,Song Changbo,Wei Lianyu.Indoor Experimental Study on Performances in Highway Application of Cement Stabilized Recycled Asphalt Mixture. Journal of Hebei University of Technology Vol.3(2004),p.108-112.

[3] Wang Li.Research on Asphalt Pavement Cold In-Place Recycling Technique Using Cement as Additive.HeBei: He bei university of technology,2003.

[4] Yue fuqing,Yang chunfeng. Application of Fracture Mechanics on the Prediction of Pavement s Fatigue Life. Application of Fracture Mechanics on the Prediction of Pavement s Fatigue Life Vol.28(2003),p.87-90.

[5] Ma jing. Cold regeneration of the cement stable asphalt road surface fatigue life study.ShenYang:Shen yang jian zhu university .2011.

[6] Yi Cheng,Shen Shizhao.The fatigue crack propagation laws and their application in the research on fatigue property of concrete. Journal of hatbin Uniwetsty of ciwil engineeting and architecture.Vol.5(2000),p.20-24.

[7] Cheng Yuren,Miu Longxiu,Hou Binglin. Fatigue strength. China railway publishing house.1990.

[8] Jia Kan.Study on the Fatigue Performance of Semi-rigid Base Course Materials.XiAn: Changan University.2008.

[9] LIU H W.Crack Prupagation in Thin Metal sheet under Repeated Loading.ph.D Dissertation,Univesity of Illinois,1959.

[10] LIU H W.Crack Propagation in Thin Metal Sheet under Repeated Loading. ASME Trans. J. of Basic Engineering,(1961),p.23-32.

[11] Lu Xijing. Study on fatigue fracture and size effect ofconcrete. Dalian: Dalian University of Technology,2004.

[12] Wu Zhimin,Zhao Guofan,Huang chengkui. Inwestigation of fatigue ftacture properties of concrete. China Civil Engineering Journal of DalianLigong University Vol.28(1995),p.59-65.

[13] Xu Shiliang. The fracture toughness of concrete test and analysis. Journal of Hydraulic Engineering of Dalian Engineering college Vol.6(1982),p.61-66.

[14] Strange，P.C.et al. J .of the Engg.Meeh.Div. ASCE. Vol. 105(1979), p.337-343.

[15] Tian Minglun,Huang Songmei,Liu enxi. Fracture Toughness of Concrete. Journal of Hydraulic Engineering of Shanxi Mechanical Engineering Institute,Vol.6(1981).

[16] Jiang Guobin.Research on Experiments of Concrete Plane-strain Fracture Toughness.Journal of Chongqing Jiaotong University Vol.3(1986),p.105-113.

[17] China aviation research institute, Stress intensity factor manual. Science press,1981.

[18] Xiong Wenyong. Cause of early crack of mass concrete and its prevention measures. Shanxi Architecture Vol.12(2006),p.135-136.

Applied Mechanics and Materials Vols. 97-98 (2011) pp 17-22

doi:10.4028/www.scientific.net/AMM.97-98.17

Experimental study on stresses Distribution under Embankment

Hongbing XIAO [1,2,a], Guanlu JIANG [1,b]

[1]Key Laboratory of High-speed Railway Engineering, Ministry of Education, Southwest Jiaotong Universsity, Chengdu, 610031, China.

[2]Department of Traffic Engineering, Southwest Universsity of Science and Technology, Mianyang, 621010, China.

[a]xiaohongbing2004@126.com, [b]wgljiang@yahoo.com.cn

Keywords: Embankment, Stresses Distribution, Settlement, Centrifuge Model Test, High-speed Railway

Abstract. For high-speed railway subgrade settlement, there was usually a big difference between calculated and measured value. Studying the stresses distribution under embankment, giving more accurate simplified method，was a approach to improve the accuracy of calculated settlement. The stresses distribution under embankment were studied through tests on experimental embankment segment, geotechnical centrifuge model tests, and numerical analysis and calculation. Studies showed that the measured stresses distribution was curve, the stresses under the embankment centre were highest, under the vicinity of shoulder the stresses changed smoothly, the stresses was above zero at toe of the side slope.

Introduction

Predicting and controlling of subgrade settlement is a topic that engineers care much. The stresses under the embankment are usually simplified as two similar kinds of stress shown in figure.1. In current development of high-speed railway and free-way in China, the subgrade settlement values calculated by this two simplified method are very different from the measured value[1], the accuracy of the calculated value is not so high to meet the practical demands of the subgrade engineering.

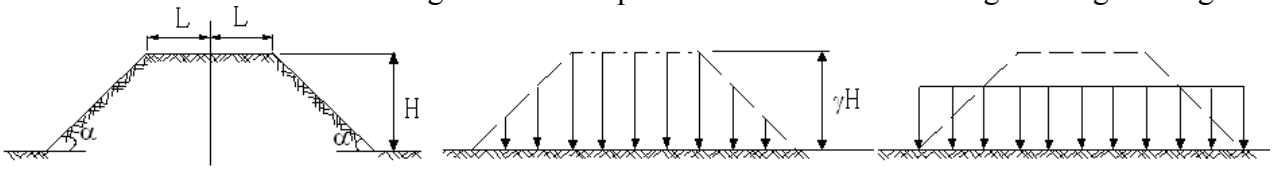

(a)actual embankment form (b)proportional load form (c) uniform load form

Fig.1 The simplified forms of stresses under the embankment

The stresses distribution under rigid foundation has gained much in-depth research. But the stresses distribution within and under flexible foundation, such as embankment, has not maken much more In-depth study[2,3].

Grasping the law of stresses distribution under embankment is a key to accurately calculate the embankment settlement[4,5]. Combined with tests on experimental embankment segment, geotechnical centrifuge model tests, and numerical analysis and calculation, we studied the stresses distribution under embankment. On this basis, combined with measured value of embankment settlement, we can summary a more accurate simplified form of stresses distribution under foundation, which can improve the calculation accuracy of embankment settlement. This is the meaning of this study.

Background of Project

The experimental embankment segment of Hainan east high-speed railway line is from wavy mounds micro slope to slight slope. Experimental embankment sections were section DK67+620, DK67+630, DK67+666, DK67+680, DK79+065 and DK79+399.6. The prototypical sections of the centrifuge model test was section DK67+630 and section DK67+666.

In the typical section DK67+630, for example, The physical and mechanical parameters of the soil are shown in Table 1.

Table 1 Physical and mechanics parameters of soil

Soil	Densiy ρ/[g.cm^{-3}]	Natural moisture content w/[%]	Liquid limit w_L/[%]	Plastic limit w_P/[%]	Void ratio e	Natural quickt-shear strength		Vertical compression	
						Cohesion c/[kPa]	Friction angle φ/[°]	Compression modulus E_s/[MPa]	Compressibility factor $a_{1\text{-}2}$/[MPa^{-1}]
(4)	1.99	12.8	21.1	12.6	0.49	12.6	27.7	8.24	0.18
(6-w4)	1.90	49.0	64.7	32.1	1.26	33.8	17.4	7.5	0.67
(6-1-w4)	1.85	32.3	36.2	21.4	0.96	23.1	22.5	6.03	0.31
(6-w3)	2.30	/	/	/	/	/	35.0	10.00	/

The route goes across each section in the form of embankment. The ground of section DK67+620, DK67+630 , DK79+399.6 was not treated. The ground of section DK67+666 and DK67+680 was treated by cement-mixed piles, which of section DK79+065 was cement-flyash-gravel piles. The geology of the topical test section and layout of the observation instrument were shown in figure 2.

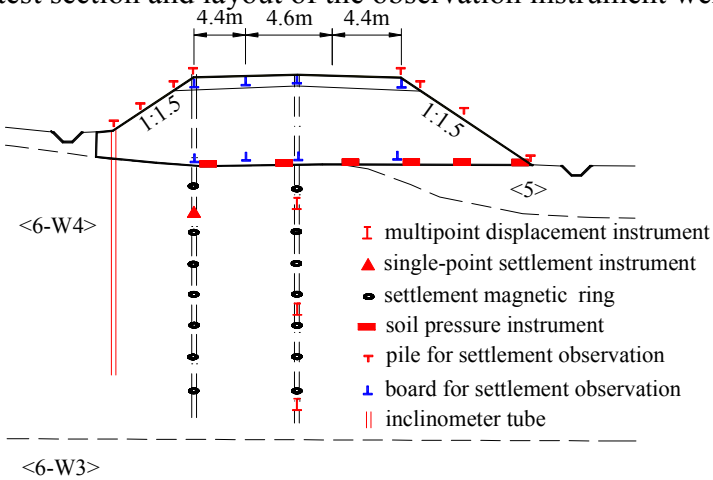

Fig. 2 The geology of the topical test section and layout of the observation instrument

A simulation is made for the single-track railway embankment and deep completely decomposed granitical foundation soil in the centrifugal model test. The surface width of the subgrade bed is 8.2m, the central height of these two embankment cross-sections is 5m for DK67+630 and 3.99m for DK67+666, and the slope ratio is 1:1.5. The vertical distance from ground surface to the point where the ratio of additional stress to self-weight reaches less than 10% is the influenced scope of compressive soil. The width of the influenced zone of the additional stress in the foundation is 46.6 m at section DK67+630, and 40 m at section DK67+666.The depth of the influenced region is 20.4 m at section DK67+630, and 20.1 m at section DK67+666. Combined with the centrifuge model box size and boundary conditions, the test model scale n is determined to be 60.

In the similar theory[6,7], the time scale n^2 for test model is chosen as 3600. The load is exerted in three phases (i.e., the self-consolidation of foundation soil, the embankment construction, and long-term use of embankment) on the model to simulate the characteristics of subgrade settlement and the stress distribution between the embankment and foundation. The test equipment used is the TLJ-2 geotechnical centrifuge of Southwest Jiaotong University, China.

The height of simulated embankment is 5m in model I, II and III, and 3.99 m in model IV. In model I the embankment is filled in four layers. Afer each filling, it will be put in centrifugal field to work in pertinent time. Then we stop to fill the next layer and put it in the centrifugal field.The

acceleration keeps 60g in the whole filling. The embankment is filled once only in model II, III and IV, then it is posted in centrifugal field to work in relevant time in stages with the value of acceleration varing form 0 to 60g and no stopping.

The model size is converted from the prototype size with the equivalent value of 60, as shown in Fig.3.

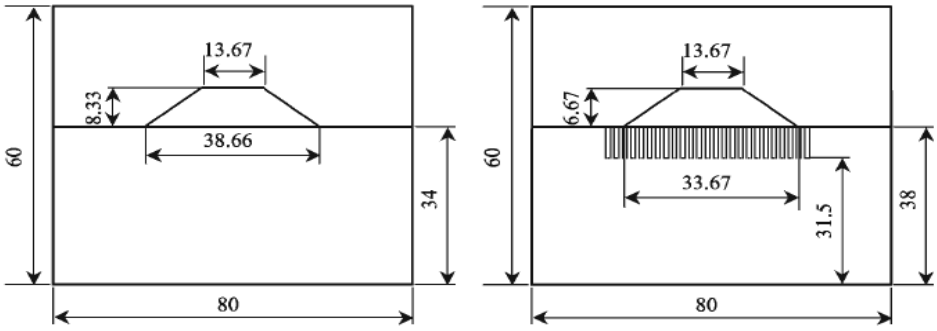

(a) Models Ⅰ, Ⅱ and Ⅲ (b) Model Ⅳ

Fig.3 Dimensions of models(unit:cm)

Results and Analyses

The stresses of the four centrifugal models tests was shown in Fig. 4, including the stresses under the shoulder and under the centre the embankment.

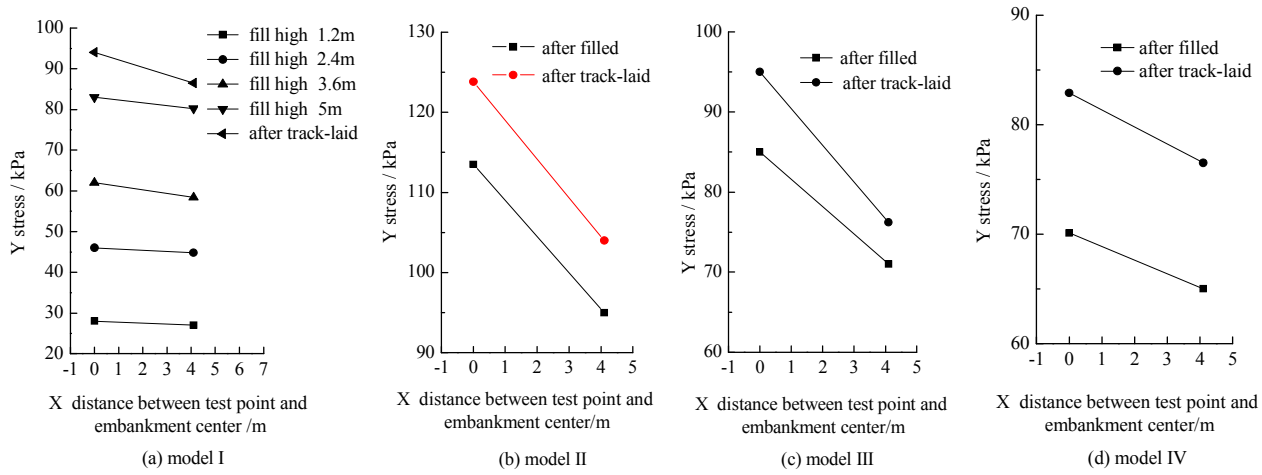

Fig.4 Tested stresses of the four centrifugal model tests

Whenever during or after the filling, as shown in fig.4, the stresses are deifferent, the stresses under the embankment centre are always higher than that under the shoulder. By comparision and analysis, we knew that the measured stresses are quite different from the stresses calculated by proportional load method or uniform load method. For the five-metres-high embankment, the caculated stresses are 20.5% higher than the stresses calculated by proportional load method. The difference is about 17KPa and can't be ignored in embankment settlement calculation.

The embankment of section DK67+620, DK67+630, DK79+399.6 were not treated. The measured stresses of each section and the stresses calculated by propotional load form and uniform load form were shown in fig.5.

As shown in fig.5, within the bounds of left and right shoulder, the measured stresses were lower than the stresses calculated by propotional load form and higher than which by uniform load form. Morever, the measured stresses distribution was curve, the stresses under the embankment centre were highest and which decreased nonlinearly as it approached the left or right shoulder. Within the bounds of shoulder and toe of side slope, the measured stresses distribution was also curve.

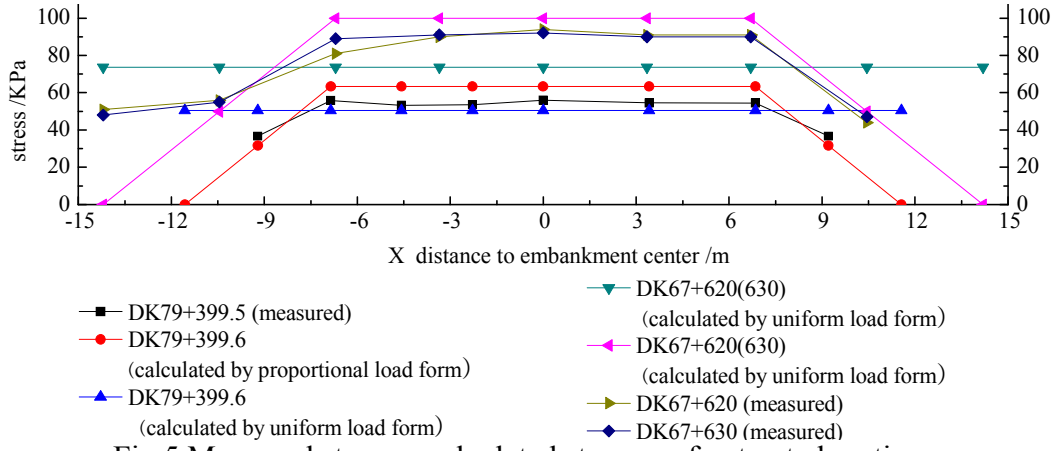

Fig.5 Measured stresses calculated stresses of untreated sections

Within the bounds of shoulder and up one-third of slope, the measured stresses is lower than the stresses calculated by propotional load form and higher than which by uniform load form. Under the other range of the slope, the measured stresses is higher than the stresses calculated by propotional load form and lower than which by uniform load form.

Section DK67+666 and DK67+680 wers treated by cement-mixed piles, which of section DK79+065 was cement-flyash-gravel piles. In relivation with the stress of un-treated ground, The average stresses under the embankment were calculated by the formula shown below：

$$\bar{p} = \frac{p_p \cdot A_p + p_s \cdot A_s}{A_p + A_s} \tag{1}$$

Where, $\bar{p}, p_p, p_s$ —average stresses, stresses above the pile bolck, ground stress of a pile treatment range，KPa.

A_p, A_s —cross section area of pile, area of a pile treatment range.

Measured stresses of each section and the stresses calculated by proportional load form and uniform load form were shown in fig.6.

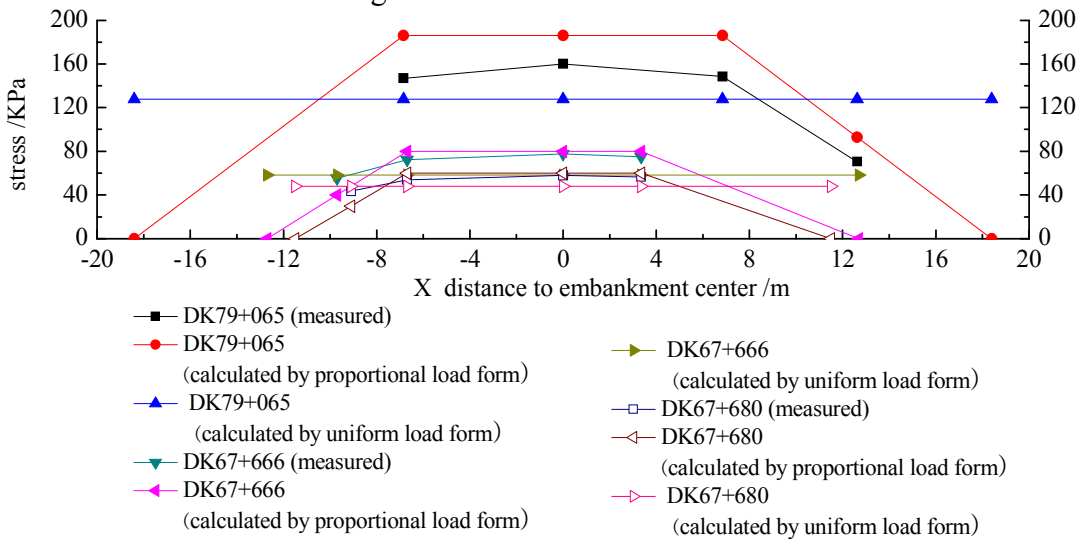

Fig.6 Soil pressure tranverse of embankment in treated sections

We could see from fig.6 that measured stresses of treated ground had the same rule of untreated ground.

When the ratio of width and height was small, from fig. 5 and fig.6, we knew that the measured stresses had a big difference from which calculated by propotional load form, but the difference became smaller while the ratio of height and width of embankmet went up.

Numerical Analysis

By use of compute program FLAC^{3D}V3.0, section DK67+630 for example, the computational model of embankment and ground was shown in fig.7.

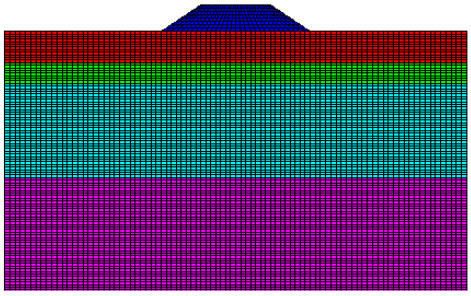

Fig.7 Computational model of section DK67+630

For example, soil parameters of section DK67+630 in the model were listed in table 2. The constitutive model of embankment was set as ELAS, and which of ground was set as MOHR. The analysis of interaction between flow and solid was seepage model, it is set as CONFIG fluid in calculation.

Table 2. Soil parameters of section DK67+630 in the model

part	soil layer thickness [m]	density [kg/m^3]	Compression modulus [MPa]	poisson's ratio	cohesion [kPa]	Friction angle [°]
embankment	5	2000	60	0.3	70	36
ground	0-6	1900	6.4	0.33	10	34.7
ground W4	6-10	1900	11.15	0.33	18	29.0
ground	10-28	1900	11.15	0.33	70	24
ground W3	Under 28	1900	35.65	0.33	70	24

The stresses distribution under embankment of 6 sections calculated through numerical analysis was shown in fig.8. The stresses distribution were curves and equilivant to the measured stresses. Under the vicinity of shoulder the stresses changed smoothly. The stresses was above zero at toe of the side slope.

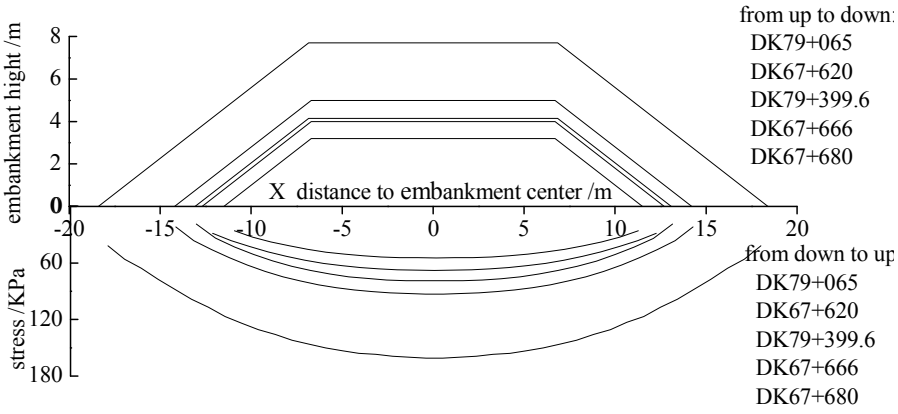

Fig.8 Numerical analysis results

The stressess under the center of embankment gained in different way were shown in table 3 .

Table3 The stressess under the center of embankment (unit:KPa)

section	measured stresse	calculated by numerical analysis	calculated by propotional load form	calculated by propotional load form
DK67+630	92.0	92.9	100.0	73.6
DK67+666	77.7	68.0	80.0	60.9
DK67+680	57.9	54.8	64.0	50.8
DK79+065	160.2	161.0	186.3	127.9
DK79+399.6	56．5	59.1	63.3	50.4

By comparison these stresses value, it was clear that stresses from numerical analysis was close to measured stresses, and the distribution law of measured stresses was similar to the numerical analysis one.

Conclusion

The stresses distribution under embankment had a big difference from simplified method we commonly used, which are propotional load form and propotional load form.

The measured stresses distribution was curve within the bounds of left and right shoulder. The stresses under the embankment centre were highest and which decreased nonlinearly as it approached the left or right shoulder. The measured stresses were lower than the stresses calculated by propotional load form and higher than which calculated by uniform load form.

Within the bounds of shoulder and toe of side slope, the stresses distribution was also curve. Within the bounds of shoulder and up one-third of slope, the measured stresses is lower than the stresses calculated by propotional load form and higher than which by uniform load form. Under the other range of the slope, the measured stresses is higher than the stresses calculated by propotional load form and lower than which by uniform load form.

Under the vicinity of shoulder the stresses changed smoothly. The stresses was above zero at toe of the side slope.

When the ratio of width and height was small, the measured stresses had a big difference from γH, but the difference became smaller while the ratio of height and width of embankmet went up.

References

[1] JIANG Guan-lu, WANG Hai-long, LI An-hong. Study on the base stresses calculation methods of high-speed railway subgrade. *Railway Engineering*, 2009, (4): 65-69(in Chinese).

[2] N. Hasebe, X.F. Wang. Irregular elastic half-plane gravity problem. *International Journal of Rock Mechanics & Mining Sciences*, 2003, 40: 863–875. (in Chinese).

[3] Perloff, W.H., Baladi, G.Y.. Stress distribution within and under long elastic embankments. *Highway Research Record*, 1967, No.181, 12-40.

[4]XIAO Hong-bing, JIANG Guan-lu ,WANG Jing-zhi , LI An-hong.Centrifugal Model Tests on the Settlement of Railway Embankment on Deep,Completely Decomposed Granite Soil.*Journal of Southwest Jiaotong University(English Edition)*, 2010,Vol.18, No.3, 189-195.

[5] XIAO Hong-bing, JIANG Guan-lu ,WANG Jing-zhi , LI An-hong. Experimental Research on Settlement of Railway Embankment on Deep Layer Completely Decomposed Granite Foundation Based on Centrifugal Model Test. *Journal of Highway and Transportation Research and Development*, 2010, Vol.27,No.8,40-44. (in Chinese).

[6] Geo-Institute of Nanjing Science and Technology Institute of Water Conservancy. *Soil Test Technical Manua*. China Communications Press，Beijing 2003.

[7] ZHANG Zhong-yun, JIANG Guan-lu. Research on centrifugal model test of improved red mudstone embankment for unallasted truck. *Journal of Railway Science and Engineering*, 2010, Vol.7,No.5,41-46. (in Chinese).

Applied Mechanics and Materials Vols. 97-98 (2011) pp 23-27

doi:10.4028/www.scientific.net/AMM.97-98.23

Research on Designing Optimum Asphalt Content of Asphalt Mixture by Calculation and Experimental Method

Wenfang Liu [1,a], Hongmei Li[1,b] ,Beiping Tian[1,c]

[1]Department of Architectural Engineering, Sichuan University of Science and Engineering, Zigong 643000, China

[a]16437023@qq.com, [b]lihongmei8229@163.com, [c]tianbeiping@126.com

Key words: asphalt mixture; optimum asphalt content; calculation method; experimental method

Abstract. In this paper, the initial asphalt content is estimated by the hot-mixed asphalt mixture rapid calculation method in condition that we have no information about the similar project, and five asphalt content are selected with regarding the estimated asphalt content as the middle value, then carries on the Marshall test. The optimuml asphalt content is very accurate by the calculation and experimental method, the method greatly improved the test efficiency.

Introduction

The optimum asphalt content is one of the most important design parameters among the asphalt mixture design parameters. The asphalt content has important influence on road usage performance. If the asphalt content is too much, the road will appear the weeping and rutting phenomenon; If the asphalt content is too little, the road will occur the durability problems. Therefore, it is necessary to research on designing optimum asphalt content so that the road performance can be improved. In the asphalt mixture design process, the Marshall method are usually used to determine the optimum asphalt content, but the Marshall design method has some limitations[1], its result is dispersed relatively great and is apt to be interfered by the human factor. So the author estimates the initial asphalt content by the hot-mixed asphalt mixture rapid calculation method[2] before Marshall experiment, then selects five asphalt content with regarding the estimated asphalt content as the middle value, finally carries on the Marshall test to design the optimum asphalt content. In the central laboratory of Zhashui-Xiaohe highway, the author used the calculation and experimental method in designing optimum asphalt content.of the middle surface layer AC-25 asphalt mixture.

Analysis of the raw materials' technical properties and the plan of the gradation design

Asphalt. The asphalt is called SK SBS modified asphalt produced in Korean, its main technical indicators are shown in table 1.

Table1 The main technical indicators of this kind of asphalt

test item		the test result	request of the criteria
penetration (25℃,5s,100g)/0.1mm		82	60～80
penetration index PI		-0.03	≥－0.8
softening point（ring and ball method）/℃		78.9	≥70
135℃ kinematic viscosity /Pa·s		1.3	≤3
ductility（5℃，5cm/min）/cm		47.9	≥40
elastic recovery（25℃）/%		95	≥80
flash point（℃）		284	≥230
solubility /%		99.7	≥99
density（15℃）/g.cm^{-3}		1.030	actual measurement
hull heat test	mass loss /%	-0.08	≤1.0
	penetration ratio /%	62.5	≥60
	residual ductility（5℃）/cm	22.0	≥20

Mineral aggregate. The aggregate is diorite rock in Zhashui country of Shanxi province，its main technical indicators are shown in table 2.

Table2 The main technical indicators of the aggregate

aggregate	test item		unit	technical requirement	the test result
coarse aggregate	apparent relative density	2.36~4.75mm	/	≮2.6	2.707
		4.75~9.5mm	/	≮2.6	2.666
		9.5~19mm	/	≮2.6	2.722
		19~31.5mm	/	≮2.6	2.704
	absorption rate	2.36~4.75mm	%	≯2	1.2
		4.75~9.5mm	%	≯2	0.47
		9.5~19mm	%	≯2	0.36
		19~31.5mm	%	≯2	0.24
	crush value		%	≯26	10.6
	Adhesiveness with asphalt		grade	≮4	4
fine aggregate (mechanism sand)	apparent relative density		/	≮2.5	2.741
	sand equivalent		%	≮60	77
	arris property（flowing time）		s	≮30	31
breeze	hydrophile coefficient		/	＜1	0.8

The plan of the gradation design. The design gradation of the AC-25 asphalt mixture is ultimately determined through propriety adjusting the screen hole passing percent of the initial gradation according to JTG F40-2004 gradation and AC-25 gradation service condition home and abroad, the passing percent of synthesize gradation is shown in table 3.

Table3 The passing percent of synthesize gradation

gradation	quality percentage of passing the follow screen hole											
	26.5	19	16	13.2	9.5	4.75	2.36	1.18	0.6	0.3	0.15	0.075
design gradation	95	81	72	62	50	35	23	17	13	8	7	4.5
upper limit	100	90	83	76	65	52	42	33	24	17	13	7
lower limit	90	75	65	57	45	24	16	12	8	5	4	3

Predicting the initial asphalt content by calculation method

Validity asphalt content Q_{be} **.**The validity asphalt volume V_{be} equal to aggregate clearance ratio VMA subtract design requirement void volume VV.

That is: $V_{be} = VMA - VV$, whereas $VMA = (1 - G_{mw}/G_{sb}) \times 100(\%)$

$$\therefore G_{mw} = (1 - 0.01VMA) \times G_{sb}$$

The validity asphalt content $Q_{be} = \dfrac{V_{be} \times G_b}{G_{mw}} = \dfrac{VMA - VV}{1 - 0.01VMA} \times \dfrac{G_b}{G_{sb}} (\%)$ (1)

If only we have bulk volume relative density of the synthesize aggregate G_{sb} and relative density of the asphalt G_b, we can figure out validity asphalt content Q_{be} according to the required VV and VMA.

Asphalt content absorbed by aggregate. The asphalt volume absorbed by aggregate

$$V_{ba} = G_{mw}(\frac{1}{G_{sb}} - \frac{1}{G_{se}}) \tag{2}$$

The asphalt content absorbed by aggregate $Q_{ba} = \frac{V_{ba} \times G_b}{G_{mw}} \times 100 = (\frac{1}{G_{sb}} - \frac{1}{G_{se}}) \times G_b \times 100(\%)$ (3)

In reference documentation[3], the computing formula is deduced according to plenty of measured results of the validity relative density.

$$G_{se} = G_{sb} + C(G_{sa} - G_{sb}) \tag{4}$$

While C—the asphalt volume coefficient absorbed by aggregate

$(1/G_{sb} - 1/G_{se})$ —the asphalt volume absorbed by unit mass' aggregate

$(1/G_{sb} - 1/G_{sa})$ —unit mass surface absorption volume

$$(\frac{1}{G_{sb}} - \frac{1}{G_{se}}) \div (\frac{1}{G_{sb}} - \frac{1}{G_{sa}}) = \frac{G_{se} - G_{sb}}{G_{sa} - G_{sb}} \times \frac{G_{sa}}{G_{se}}$$

We can see from the formula (4) $C = \frac{G_{se} - G_{sb}}{G_{sa} - G_{sb}}$

If consider the water density as 1, then $(1/G_{sb} - 1/G_{sa}) \times 100 = W(\%)$

$\therefore \frac{1}{G_{sb}} - \frac{1}{G_{se}} = C \times W \times \frac{G_{sa}}{G_{se}}$ $\quad\quad$ $\therefore Q_{ba} = C \times W \times G_b \times \frac{G_{sa}}{G_{se}}$

the value of G_{sa} and G_{se} is contiguous, if $G_{sa}/G_{se} = 1$, Q_{ba} only reduces 0.005%～0.007%, so we can proximity deduce $Q_{ba} = C \times W \times G_b$. From the above we can see that Q_{ba} absolutely depends on aggregate surface absorption rate, that is G_{sb} and G_{sa}.

The optimum asphalt content of asphalt mixture Q_b.

$$Q_b = Q_{be} + Q_{ba} = \frac{VMA - V}{1 - 0.01VMA} \times \frac{G_b}{G_{sb}} + C \times W \times G_b \tag{5}$$

the requirement void volume of Zhashui-Xiaohe highway' bidding documents is 3%～6%, we take the middle value 4.5%, VMA is taken 12.5%, SBS modified asphalt relative density is 1.026 at 25℃, the synthesize bulk volume relative density of the aggregate is 2.676, C=0.840, W=0.332, put the above parameters in the formula (5), we can derive Q_b=3.79%, so the initial asphalt content is estimated 3.8%.

Determining the optimum asphalt content by Experimental method

Take the asphalt content 3.8% for the middle value, determine five asphalt content 3.2%，3.5%，3.8%，4.1%，4.4% with 0.3% interval. Mixing temperature is 185℃, compaction temperature is 175℃. The Marshall sample is compacted 75 times both sides with the standard Marshall compaction device. The bulk volume relative density is measured by superficial drying method, and measure stability degree and flow value of the sample, then work out VV, VMA, VFA. The results are shown in table 4.

Table4 The results of the Marshall test

asphalt content （%）	bulk volume relative density γ_f	theoretic maximal relative density γ_t	void volume VV(%)	VMA （%）	VFA (%)	stability degree （kN）	flow value (mm)
3.2	2.422	2.567	5.6	12.4	54.4	15.03	26.8
3.5	2.424	2.556	5.2	12.5	58.5	15.66	32.8
3.8	2.431	2.545	4.5	12.5	64.1	15.44	33.6
4.1	2.429	2.534	4.1	12.8	67.7	14.37	35.3
4.4	2.426	2.523	3.8	13.2	70.9	13.76	38.8

According to the above data from table 4， we draw the relational graph between asphalt content and each physical index. Take the asphalt content as horizontal coordinates and each physical index as vertical coordinates, draw the smooth curve as figure1, the optimum asphalt content is determined according to figure 1[4].

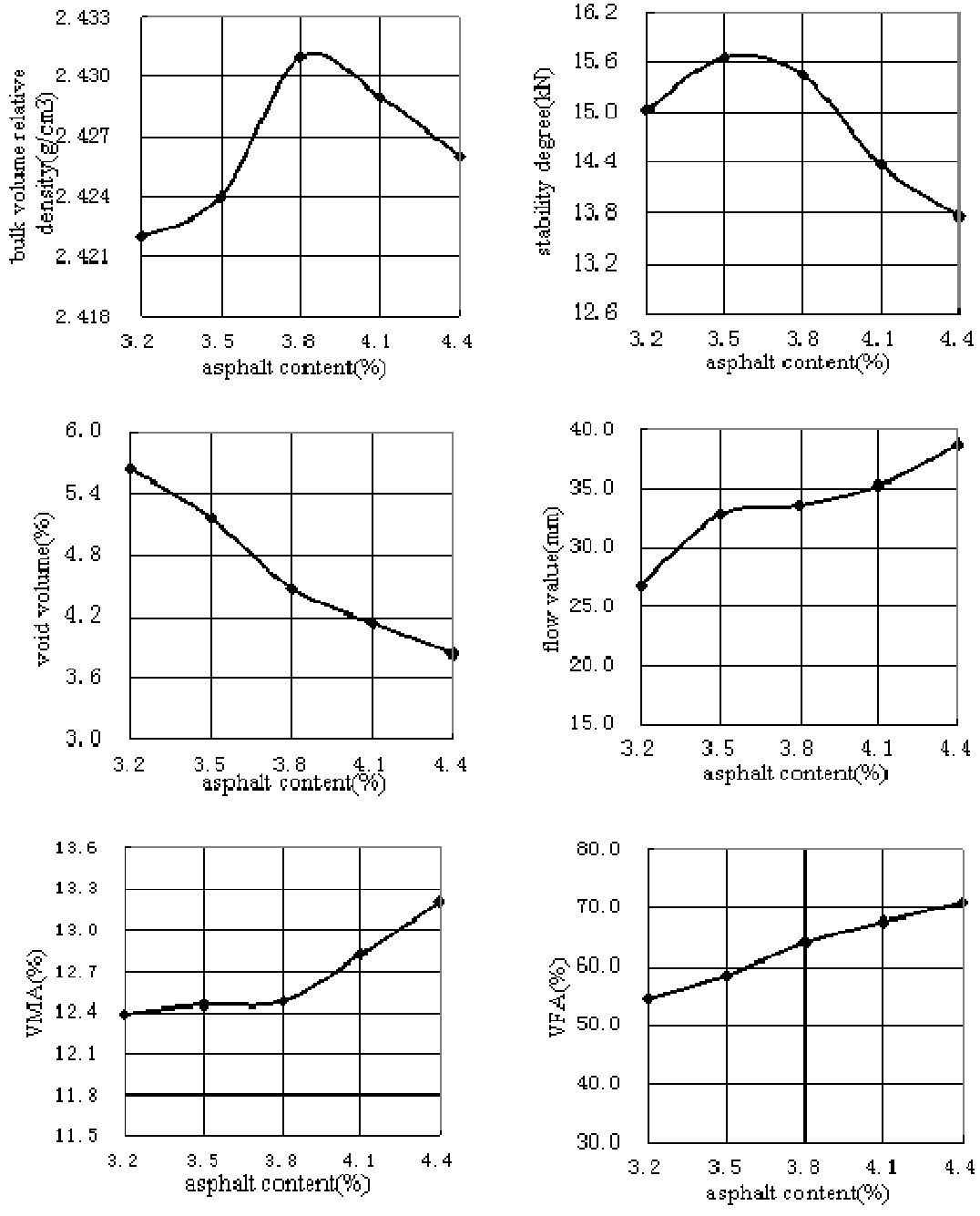

Figure1 Relationship between asphalt content and each physical index

The author's study subject is AC-25 asphalt concret middle surface layer, the climate subzone of Zhashui-xiaohe highway belongs to 1-2 section, and the road belongs to heavy transportation pavement, the range of the criteria required void volume is 4%～6%, but void volume of middle surface layer is not suitable to too big, so the range of the bidding documents required void volume is 3%～6%, we can take 4.5% as goal void volume. We can known from figure 1, OAC1= (a1+a2+a3+a4)/4 = (3.80%+3.60%+3.79%+3.71%)/4 = 3.73%. According to asphalt content mutual range that satisfied each physical index, OAC2 = (OACmin+OACmax)/2＝3.78%, so the ultimately optimum asphalt content OAC = (OAC1 +OAC2)/2 ＝3.75%. Then we do the test samples at the optimum asphalt content 3.75%, each indicator of the samples is shown in table 5. We can see from table 5, the road performance satisfy the requirement of engineering techniques criteria, and well exceed the requirement of the bidding documents.

Table5 Indicators of the optimum asphalt content

optimum asphalt content （%）	void volume VV(%)	VMA （%）	VFA (%)	stability degree （kN）	flow value (mm)	rut test DS(time s/mm)	freeze-thaw splitting test TSR(%)	flexural -tensile strain (με)
3.75	4.56	12.5	63.5	15.56	33.2	11123.1	83.2	3777
request of the criteria	3～6	≥12.5	55～70	≥8	20～40	≥2400	≥80	≥2800

Conclusions

In condition that we have no information about the similar project, we can determine the optimum asphalt content by the calculation and experimental method. The above method can estimate the initial asphalt content in short time, and the performance of the determined optimum asphalt content satisfy the requirement of engineering techniques criteria through experimental verification. Thus construction enterprise can finish the design of asphalt mixture in short time, fasten the project schedule and improve project efficiency. Therefore, the author suggests construction enterprise first estimate the initial asphalt content by the hot-mixed asphalt mixture rapid calculation method, and determine five asphalt content classify, thus tester has a specific goal before doing the test, thereby supervise practical engineering better. Then carries on the Marshall test according to the five asphalt content classify so that we can ensure the performance of the asphalt mixture. the calculation and experimental method greatly improved the test efficiency, at the same time it ensure engineering quality.

Acknowledgements

This work was financially supported by the Sichuan University of Science & Engineering Foundation (2009XJKYL003)

References

[1] Huaxin Chen, Xing Jiang: The Abnormal Phenomena Analyses of the Marshall Design, Journal of China & Foreign Highway (2006), in Chinese.

[2] Xiuxian Lin: The Optimuml Asphalt Content Rapid Calculation Method of HMA&SMA, East China Highway (2003), in Chinese.

[3] Qin Wang, Guolan You: Research on theAggregate Validity Relative Density of the Asphalt Mixture by Experimental and Calculation Method, East China Highway (2001), in Chinese.

[4] Engineering Techniques Criteria of Highway Asphalt Pavement[S], JTG F40- 2004.

[5] Information on http://www.cncivil.com

Applied Mechanics and Materials Vols. 97-98 (2011) pp 28-31

doi:10.4028/www.scientific.net/AMM.97-98.28

Impact of Subgrade Resilience Modulus on Heavy Load Asphalt Pavement Mechanical Properties

Tian Xiao[1,a], Hui ran Pi[2,b] and Can zhang Jin[1]

[1] Tianjin Municipal Engineering Design & Research Institute, No. 239 Yingkou Street, Hexi District, Tianjin, 300051, China

[2] School of Civil Engineering, Hebei University of Technology, No. 29 Guangrong Road, Hongqiao District, Tianjin, 300130, China

[a]xiaotian95@126.com, [b]pihuiran@126.com

Keywords: Road engineering, Subgrade resilience modulus, Asphalt pavement, Heavy load, Mechanical properties

Abstract. Subgrade resilience modulus is an important mechanical parameter in pavement design. It will directly influence the design result of pavement structure. Using BISAR3 of SHELL design method, the impacts of subgrade resilience modulus on pavement surface deflection, base and subbase bottom tensile stress, surface layer bottom tensile stress of the heavy load asphalt pavement structure were analyzed. And the influencing laws were analyzed, too. The results show that the mechanical and deforming characteristics of heavy load asphalt pavement were influnced significantly by subgrade resilience modulus. With the increasing of subgrade resilience modulus, the pavement surface deflection, base bottom tensile stress would significantly decrease, and fatigue life would be improved.

Introduction

With the rapid development of national economy, the road traffic increased rapidly in China. Large transport vehicles increase sharply, and vehicle overloading is widespread [1]. Overloading of vehicles had led to serious damage during the initial period of pavement structure. In order to reduce the early destruction caused by overloading and heavy traffic, the domestic and foreign experts carried out a lot of useful researches [2] [3]. Major initiatives include: increasing the thickness of asphalt concrete surface layer, selecting high-quality medium-grained asphalt concrete, improving the strength and stiffness of asphalt concrete surface layer.

Subgrade is the foundation of pavement structure, and its quality will directly affect the quality of the whole highway projects. Improving the strength of sub-grade to some extent can raise the life of the pavement structure [4], and then solve the heavy traffic problems. In this paper applied the BISAR3 program of SHELL design method, systematically analysis the effect of sub-grade modulus changing to asphalt pavement surface deflection, base layer bottom tensile stress, and compressive strain on the top of sub-grade and pavement structure fatigue life under heavy traffic, which has significance in enriching asphalt pavement design options, reducing early destruction caused by overloading and heavy traffic.

Calculation Parameters and Pavement Structure

Calculation parameters. The action type of load formulated in "Specifications for Design of Highway Asphalt Pavement" in China is single axle double circle, two-round load pattern [5]. Standard axle load is BZZ-100, when the axle load is excessive, consider the center distance of two-round 3δ stay the same, and the contact pressure and area are variable. Due to the lack of the relation between axle load, pressure and the contact area in domestic, here quote Belgium empirical relation as followed [6]:

$$A = (0.008P + 152) \pm 70 \quad (1)$$

Where A is tire contact area, cm2; P is the load of each tire, N; ±70 is the deviation range.

The relationship between equivalent radius δ and tire contact pressure can be discribed as follow:

$$\delta = \sqrt{\frac{P}{\pi \cdot p}} \tag{2}$$

Where P is the load acting on the wheels, KN; p is tire contact pressure, KPa; δ is equivalent radius, m.

Refer with Eq.(1) and Eq.(2), the specific values of equivalent radius and wheel pressure are shown in Table 1.

Table 1 Axle Load, Wheel Pressure and Tire Contact Area

Axle Load [KN]	100	130	150	170
Tire Contact Area[cm2]	352	412	452	492
Equivalent Radius[cm]	10.59	11.45	11.99	12.51
Wheel Pressure[MPa]	0.71	0.79	0.83	0.86

Pavement structure. In this paper, take the typical semi-rigid base pavement for an example. The pavement structural parameters used in calculation are shown in Table 2.

Table 2 Pavement Structural and Parameters

Layer	**Material Name**	**Thickness** [cm]	**Compressive Modulus** [MPa]	**Poisson Ratio**
1	Asphalt concrete	18	1200	0.25
2	Cement stabilized crushed stone	40	1500	0.25
3	Lime-fly ash-soil	20	750	0.25
4	Foundation	---	40	0.35

Results and Analysis

Impact of Subgrade Resilience Modulus on Surface Deflection. The pavement surface deflection values of different subgrade resilience modulus under the different axle loads of 100KN, 130KN, 150KN, and 170KN were calculated respectively. The results were shown in Figure 1.

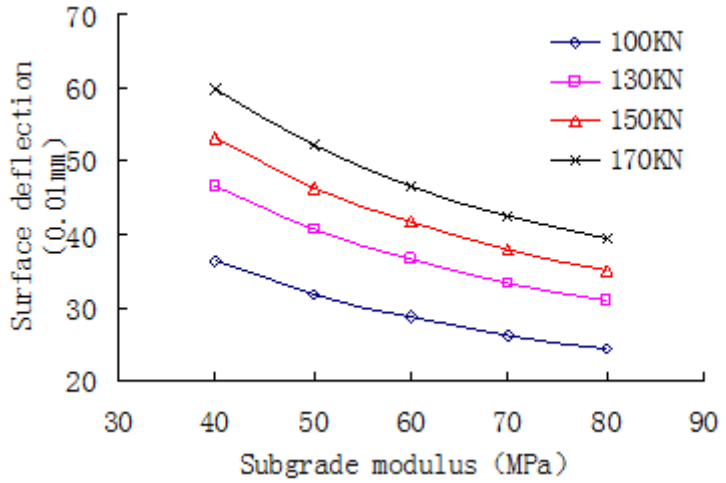

Fig.1 Surface deflection of different subgrade modulus

The Figure 1 indicates that, with the increasing of subgrade resilience modulus, surface deflection decreased. When the axle load is 100KN, the surface deflection decreased 4.49(0.01mm) while the subgrade resilience modulus changed from 40MPa to 50MPa. With the increasing of axle load, the

effect of subgrade modulus changing on surface deflection become more obvious: when the sub-grade modulus raised from 40MPa to 80MPa, the surface deflection reduced 12.02(0.01mm) under 100KN, while decreased 20.39(0.01mm) under 170KN.

Impact of Subgrade Resilience Modulus on Asphalt Layer Stress. The Asphalt layer bottom tensile stress of different subgrade resilience modulus under the different axle loads of 100KN, 130KN, 150KN, and 170KN were calculated respectively. The results were shown in Figure 2.

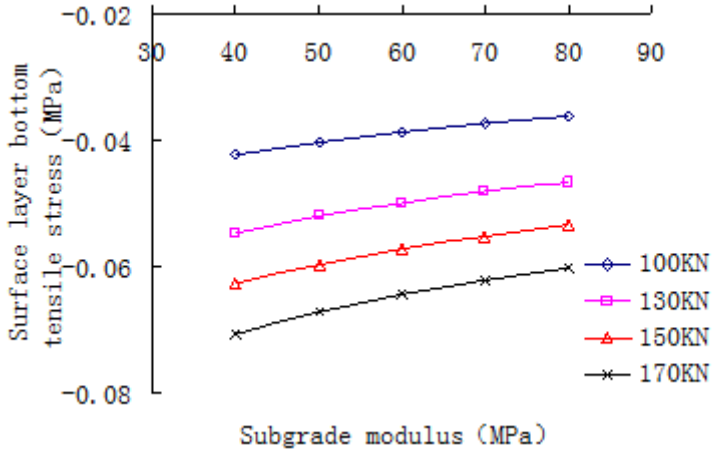

Fig.2 Surface Layer Bottom Tensile Stress of Different Subgrade Modulus

The maximum of tensile occurred on the center of two wheels. Under the different axle load in this paper, the surface layer withstands compressive stress, and the pressure reduced with the increasing of sub-grade modulus.

Impact of Subgrade Resilience Modulus on Base Layer Tensile Stress. The base layer bottom tensile stress of different subgrade resilience modulus under the different axle loads of 100KN, 130KN, 150KN, and 170KN were calculated respectively. The results were shown in Figure 3.

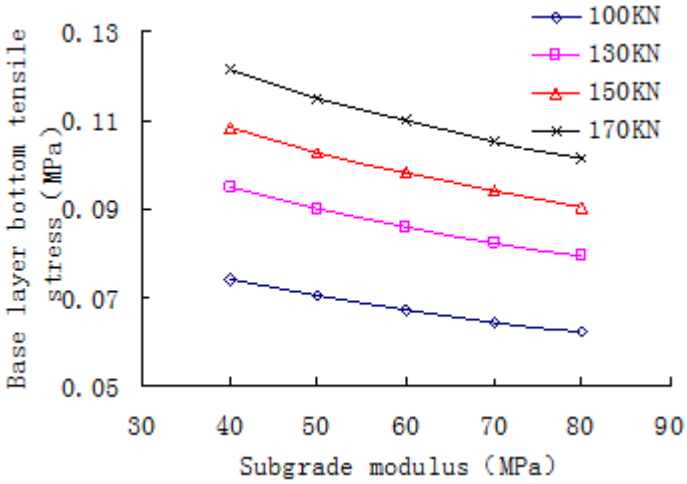

Fig.3 Base Layer Bottom Tensile Stress of Different Subgrade Modulus

The Figure 3 indicates that, the base layer bottom tensile stress will decrease with the increasing of subgrade resilience modulus. When the axle load is 100KN, the base layer bottom tensile stress decreased 16.1% while the subgrade resilience modulus changed from 40MPa to 80MPa. Stronger subgrade can improve the properties of asphalt pavement.

Impact of Subgrade Resilience Modulus on Subbase Layer Tensile Stress. The subbase layer bottom tensile stress of different subgrade resilience modulus under the different axle loads of 100KN, 130KN, 150KN, and 170KN were calculated respectively. The results were shown in Figure 4.

The Figure 4 indicates that, the subbase layer bottom tensile stress will decrease with the increasing of subgrade resilience modulus. And the effect of subgrade resilience modulus on subbase tensile stress was more serious than on that of base layer. When the axle load is 170KN, the base layer

bottom tensile stress decreased 21.8% while the subgrade resilience modulus changed from 40MPa to 80MPa. While the decreased extent is 21.6% under the axle load of 100KN. The effect of subgrade modulus changing on subbase layer bottom tensile stress become more obvious under heavy load asphalt pavement.

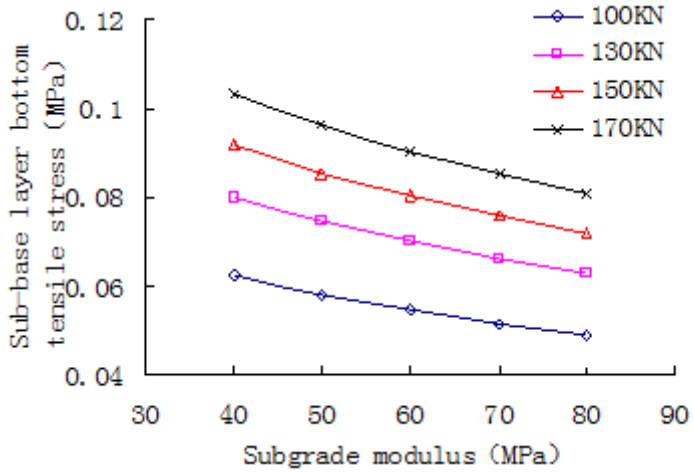

Fig.4 Subbase Layer Bottom Tensile Stress of Different Subgrade Modulus

Conclusions

(1) The subgrade resilience modulus has a significant impact on asphalt pavement mechanical properties, include surface deflection, base layer tensile stress and subbase layer tensile stress.

(2) Surface deflection will decrease with the increasing of subgrade resilience modulus. And with the increasing of axle load, the effect of subgrade modulus changing on surface deflection become more obvious.

(3) Under the different axle load in this paper, the surface layer withstands compressive stress, and the pressure reduced with the increasing of sub-grade modulus.

(4) The bottom tensile stress of base and subbase layer will both decrease with the increasing of subgrade resilience modulus. The effect of subgrade modulus changing on subbase layer bottom tensile stress become more obvious under heavy load asphalt pavement.

(5) The mechanical properties of heavy load asphalt pavement can be improved through increasing the subgrade resilience modulus

References

[1] Hong duo Zhao. “Determination of Conversion Factor of Equivalent Axle Load Based on Axle Load Spectrum Measured”, *Chinese Journal of Highway,* Vol.4 (2004):p1-6 (in Chinese).

[2] Xin zhong Wang. Heavy Traffic Asphalt Pavement Design Method [D]. *A Master's Degree Thesis of Chang’an University*, 2005 (in Chinese).

[3] Ministry of Communications Highway Research Institute. Heavy Traffic Asphalt Pavement Design Report[R]. 2003 (in Chinese).

[4] Shan qi Du, etc. “Effect Analysis of Subgrade Modulus to Asphalt Pavement Performance”, *Chinese Journal of Transportation Science,* Vol.2 (2009):p15-9 (in Chinese).

[5] Ministry of *Communications*. “Specification for Design of Highway Asphalt Pavement”. *China Communication Press,* 2007 (in Chinese).

[6] Ying Liu. “Pavement Design of Overloading Road”, *A Master's Degree Thesis of Chang’an University*, 2000 (in Chinese).

Applied Mechanics and Materials Vols. 97-98 (2011) pp 32-35

doi:10.4028/www.scientific.net/AMM.97-98.32

Contrast Study on Prediction Models of the Post-construction Settlement of Embankment in Saline Soil Area

Tianwen lai[1,2,a], Qiyun Zhou[3,b]

[1] School of Civil Engineering and mechanics, Lanzhou University, Lanzhou, Gansu, 730000, China

[2] School of Civil Engineering, Lanzhou Jiaotong University, Lanzhou, Gansu, 730070, China

[3] lan-xin Railway Ganqing limited company, Lanzhou, Gansu, 730000, China

[a]laitianwen@mail.lzjtu.cn, [b]Zqiyun551105@163.com

Keywords: Saline soil, Embankment, Post-construction settlement, Prediction model, new model, standard hyperbolic model, modified hyperbolic model, exponential model.

Abstract. Post-construction settlement is one of the main issues in high grade railway construction in saline areas. The efective solution to the problem is to find the post-construction settlement law for the guidance to the design and construction based on the field monitored data. After analyzing the large quantities of monitored data from the second double line of Lanzhou-Xinjiang Railway in saline areas, a new model is put forward. The standard hyperbolic model, the modified hyperbolic model and exponential model were applied to the forecasting settlements based on the same monitored data to test the presented new model. By comparing fitting, forecasting accuracy and stability of different methods, show that the new model has a high prediction accuracy and good stability, and the forecasting data agree well with the monitored data. The new model presents a new method for analysis and prediction of settlement, and it is found to be a good reference to post-construction settlement of embankment in saline areas.

Introduction

Before 80s to 90s in the 20th century, the main purpose of the chinese railway embankment design is to control the intensity. The control standard of post-construction settlement of embankment is 30 ~ 50 cm. In recent years, it becomes more stringent. The current, that of high standard railway's subgrade paving no-residue track is not more than 15 mm (or 30 mm), shows it has changed dramatically. Subgrade design changes by the strength control design to the deformation control design. So how to effectively analyze and forecast the post-construction settlement of embankment becomes a very important issue of subgrade engineering.

Beause of the complexity of subgrade constitute and its deformed diversity, the variation of the post-construction settlement of subgrade with time is hard to accurately expressed by a theoretical formula. More practical used methods determining post-construction settlement of subgrade is by analysis of on-site measured settlement data, inversively determine parameters of settlement - time model, and then predict the later settlement. Commonly used such methods have the standard hyperbolic model[1 ~ 3], the modified hyperbolic model[4] and exponential model[5,6], etc.

After analyzing the large quantities of monitored data from the second double line DK821 + 863 of Lanzhou-Xinjiang Railway in saline areas, a new model is put forward. To test it, the standard hyperbolic model, the modified hyperbolic model and exponential model were applied to fit and forecast settlements based on the same monitored data. By comparing fitting and forecasting accuracy and stability of different methods, to obtain the ideal prediction models of the post-construction settlement of embankment in saline soil area, so as to reference for the future construction of a high standard railway in similar areas.

Forecasting methods of settlement from the measured data

The standard hyperbolic method. Standard hyperbolic method assumes that the average speed and time of settlement was by the law of hyperbolic diminishing changes, be expressed as

$$s_t = s_0 + \frac{t}{a + bt} . \tag{1}$$

Where s_t is the settlement for t; s_0 is the settlement for t_0; a , b is undetermined coefficients, with the graphical method or the least squares obtained.

The modified hyperbolic method. The modified hyperbolic method basis standard hyperbolic method is introduced the concept of load factor. The settlement increment is usually considered proportional load increment, be expressed as

$$s_t = \frac{t}{a + b * t} * \xi \tag{2}$$

Where s_t is the settlement for t ; t is the time; a , b is undetermined coefficients, with the graphical method or the least squares obtained; $\xi = \frac{\sigma}{\sigma_{\max}}$, σ is the load for t, $\sigma_{\max}$ is maximum design load.

The exponential method. Exponential method assumes that the settlement of embankment changes with time exponentially, be expressed as

$$s_t = s_\infty (1 - a\mathrm{e}^{-bt}) \tag{3}$$

Where s_t is the settlement for t; s_∞ is final settlement; a , b is undetermined coefficients.

New method

The process of analyzing the data presents a new model, which is expressed as

$$S_t = a - \frac{b}{t+1} . \tag{4}$$

Where s_t is the settlement for t; t is the time; a , b is undetermined coefficients.

The new model has the following characteristics: (1) Monotonicity. With the increasment of t , this function monotonically increasing, can reflect the general law of settlement; (2) Boundedness. When $t \to \infty$, $S_t \to a$.

Analysis of Engineering example

Project overview. The second double line of Lanzhou-Xinjiang Railway is a national I-class railway, the design speed of 200 km / h. DK821 + 600 ~ DK821 + 900 is the test embankment of the saline soil areas, its foundation using CFG pile composite foundation. In the test interval, set 3 settlement observation section. From November 15, 2010 subgrade settlement observation began, to June 2, 2011 total observations 199 days, 30 times. DK821 + 863 secatin settlement observation data in Table 1. The observations are divided into 2 groups. Group 1 for the measured data within 147 d, used to fit; group 2 within 148 d ~199 d , used to forecast.

Table 1 Observed settlement data of the DK821 + 863

Cumulative time / d	0	2	8	11	13	15	18	21	27	31	38	50	57	67	71
Cumulative settlement /mm	0	0.79	0.79	0.79	1.82	2.01	2.83	2.83	2.83	3.46	3.46	3.46	3.46	3.16	3.55
Cumulative time / d	86	95	100	106	113	121	129	135	147	156	167	180	188	194	199
Cumulative settlement /mm	3.55	3.55	3.55	3.55	3.55	3.55	3.32	3.57	3.87	3.74	4.63	4.98	4.96	4.96	4.45

The forecasting result of different methods. According to principle of the different forecasting methods, the use of standardized hyperbolic method, modified hyperbolic method, exponential method and the new model to fit and forecast the DK821 + 863 settlement data. The mathematical expression of the 4 kinds of model is

$$S_t = \frac{t}{2.373 + 0.26t} . \tag{5}$$

$$S_t = \frac{0.133t}{0.554 + 0.0323t} . \tag{6}$$

$$S_t = 3.9513 - 3.1899e^{-0.0195t}) . \tag{7}$$

$$S_t = 4.5885 - \frac{20.5715}{1+t} . \tag{8}$$

According to the above four models, calculating the settlement value at different times in Table 2, the s - t curve are shown in Figure 1.

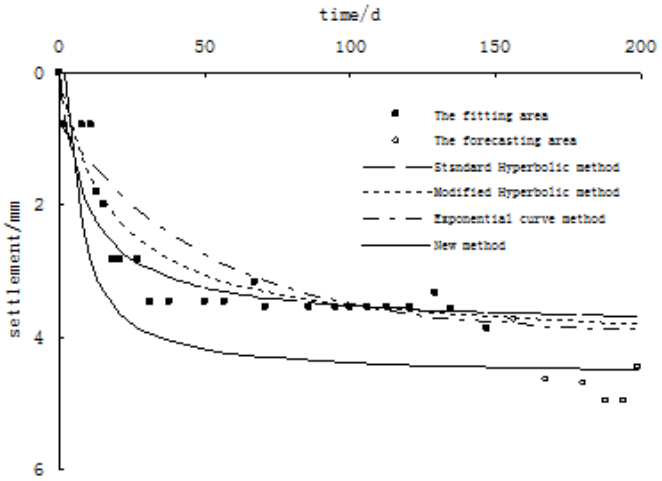

Fig.1 Fitting settlement-curves of 4 kinds of prediction models

Table2 The prediction data of different models

Cumulative time / d	0	2	8	11	13	15	18	21	27	31	38	50	57	67	71
SH Method / mm	0	0.69	1.80	2.10	2.26	2.39	2.55	2.68	2.87	2.97	3.10	3.25	3.32	3.39	3.41
MH Method / mm	0	0.43	1.31	1.61	1.78	1.92	2.11	2.27	2.52	2.65	2.84	3.07	3.17	3.28	3.32
E Method / mm	0.76	0.88	1.22	1.38	1.48	1.57	1.71	1.83	2.07	2.21	2.43	2.75	2.90	3.09	3.15
New Method / mm	0	0	2.30	2.87	3.12	3.30	3.51	3.65	3.85	3.95	4.06	4.19	4.23	4.29	4.30
Cumulative time / d	86	95	100	106	113	121	129	135	147	156	167	180	188	194	199
SH Method / mm	3.48	3.51	3.52	3.54	3.56	3.58	3.59	3.60	3.62	3.63	3.65	3.66	3.67	3.67	3.38
MH Method / mm	3.43	3.49	3.52	3.54	3.58	3.61	3.64	3.65	3.69	3.71	3.73	3.76	3.77	3.78	3.79
E Method / mm	3.35	3.45	3.50	3.55	3.60	3.65	3.69	3.72	3.77	3.80	3.83	3.86	3.87	3.88	3.89
New Method / mm	4.35	4.37	4.38	4.40	4.41	4.42	4.43	4.44	4.45	4.46	4.47	4.47	4.48	4.48	4.49

Predictive the final settlement in Table 3.The mean and the standard deviation of fitting accuracy and forecasting accuracy of 4 kinds of model are calculated. The results in Table 4. In general, the greater the mean, indicating the higher accuracy of the method; the standard deviation smaller that the precision of the method more stable.

Table3 The predictive final settlement

method	Standardized Hyperbolic Method	Modified Hyperbolic Method	Exponential Method	New Method
The final settlement / mm	3.68	3.79	3.89	4.49

Table 4 Settlement prediction of the DK821+863 section

Standardized Hyperbolic Method				Modified Hyperbolic Method				Exponential Method				New Method			
Fitting Precision		Forecasting Precision		Fitting Precision		Forecasting Precision		Fitting Precision		Forecasting Precision		Fitting Precision		Forecasting Precision	
M	SD	M	SD	M	SD	M	SD	M	SD	M	SD	M	SD	M	SD
0.85	0.28	0.43	0.43	0.84	0.25	0.45	0.45	0.73	0.36	0.76	0.25	0.63	0.78	0.86	0.17

Note: M representatives of mean; SD representatives of standard deviation.

Conclusions

Form Fig.1, Table 2, Table 3 and Table 4 can be seen:

(1) The high fitting precision does not mean high forecasting precision, and good stability of fitting precision does not mean good stability of forecasting precision.

(2) The standardized hyperbolic method, the modified hyperbolic and the exponential method have higher fitting precision, better fitting stability, but their forecastingprecision is lower and unstable; the exponential method has higher fitting precision and forecasting precision, and relatively stable; the new method' preliminary data deviate from the measured settlement is large, causing the fitting precision is not high and unstable, but its forecasting precision is the highest and stability is the best in the four kinds of method. This shows that there is the bigber error by the standardized hyperbolic method and the modified hyperbolic method to predict post-construction settlement of embankment in saline soil area, but the forecasting settlement, by the exponential method and new method, closes to the field monitored data.

(3) From the final settlement of four kinds of methods view, the forecasting settlement predicted by the new model is the closest actual value, followed by the exponential model. It indicats that these two methods is the most suitable for forecasting post-construction settlement of embankment in saline soil area, and can meet the actual requirments, using post-construction settlement to determine the appropriate time laying track. Can provide a reference for similar projects.

References

[1] T.L. YANG, G.W. YANG and Q. Wei: Rock and Soil Mechanics, Vol. 25 (2004), in Chinese, pp. 1551-1554

[2] L.J. JIA: Communications Standardization, Vol. 6 (2006), in Chinese, pp. 102-104

[3] X.J. LV, Zh.Q. WANG: Railway Engineering, Vol. 9 (2008), in Chinese, pp. 61-63

[4] W. K. FENG, H. CH. LIU: Journal of Geological Hazards and Environment Preservation, Vol. 12 (2001), in Chinese, pp. 60-63

[5] G. LI, F.Sh. WANG and X.X. HE: Subgrade Engineering, Vol. 125 (2006), in Chinese, pp. 71-73

[6] T. YANG, J.Q. DAI and G.W. LI: China Civil Engineering Journal, Vol. 38 (2005), in Chinese, pp. 92-95

Applied Mechanics and Materials Vols. 97-98 (2011) pp 36-39

doi:10.4028/www.scientific.net/AMM.97-98.36

Research on Prediction Method of Soft Soil Foundation Settlement

Xiaoma Dong

Zhengzhou Institute Of Aeronautical Industry Management, Zhengzhou, China

njddmark@163.com

Keywords: settlement prediction, soft soil foundation, LS-SVM, neural networks

Abstract. The current prediction methods of foundation settlement have biggish error under the condition of lesser foundation settlement observational datum. Aim at the localization of present prediction methods and the virtues of Support Vector Machine arithmetic, the method of predicting soft soil foundation settlement based on Least Square Support Vector Machine (LS-SVM) was proposed in this paper and compared with the neural network method and curve fitting method. The research results show that this proposed method is feasible and effective for predicting soft soil foundation settlement. Least Square Support Vector Machine provides a more advanced method than these conventional methods for predicting foundation settlement.

Introduction

Many highways are build in the coastal provinces. There are the problems of soft soil in the construction. In view of the current construction status of highway, in order to meet the design requirements of engineering and extend service life, In addition, in order to control and guide post-construction organization and arrangements in the process of highway construction schedule, it is required to predict foundation settlement at different times and the final settlement. Therefore, it is necessary to study the soft soil subgrade settlement prediction of highway. The soft ground subsidence problems are mostly three-dimensional subjects, and the actual soil conditions are very complex. Therefore, it is great significance for utilizing the measured settlement data to calculate post-settlement. Some domestic and foreign scholars have done a lot of analysis and research for the settlement forecasting method. Such as, the literature [1] proposed the method of foundation settlement prediction based on numerical analysis. In the literature [2] the gray theory was introduced to the prediction of foundation settlement. The literature [3] proposed the method of foundation settlement prediction based on the neural networks. Because the current settlement prediction methods exists some shortcomings, for example the parameters of networks are not determined and the fitting results are not satisfactory. Especially in the case of monitoring data less, there exists a certain degree of bias between the prediction forecasts and the actual settlement. So it is necessary to find a accurate settlement prediction technique. This paper attempts to introduce the support vector machine into the prediction of foundation settlement.

Support Vector Machine is a new machine learn arithmetic that was advanced based on statistics theory by Vapnik[4]. In order to settle machine learn problem under small samples condition it sets up a new theory system. And it is becoming a new study hotspot in machine learn domain because of its predominant learn ability and good generalizing capability. Support Vector Machine arithmetic belongs to the optimizing problem which assures that the final result is the optimizing result in full range. It avoids those disadvantages of ANN, for example network structure is decided hardly, network learn is overdo or lacking[5,6]. Due to Support Vector Machine is realized venture minimum through structure risk minimum principle replacing experience risk minimum principle, which enhances meshwork generalizing capability. This characteristic is very obvious under the condition of small samples[7]. Therefore, at present Support Vector Machine is a perfect network model in mode identification and nonlinearity regression domain. Aiming at the limitations of settlement prediction in small samples and the advantages of Least Square Support Vector Machine arithmetic, this paper proposes to use least squares support vector machine algorithm to predict the settlement of soft ground.

Least Square Support Vector Machine Regression Theory

Suppose that regression sample datum:

$$s=\{(x_i,y_i),i=1,2,\cdots,l\} \tag{1}$$

where $x_i\in R^n$, $y_i\in R$. LS-SVM regression use quadric castigatory function, and its optimizing problem is as follows:

$$\min_{a,b,\xi}\|\omega\|^2/2+(C/2)\sum_{i=1}^{n}\xi_i^2 \tag{2}$$

$$\text{s.t. } y_i=\omega^T\phi(x_i)+b+\xi_i \quad i=1,\cdots,n \tag{3}$$

where $\xi_i\geq 0$ is a relaxation gene, and $C>0$ is a castigatory parameter.

The constructed Lagrange function is as follows:

$$L=\|\omega\|^2/2+(C/2)\sum_{i=1}^{n}\xi_i^2-\sum_{i=1}^{n}\alpha_i(\phi(x_i)\omega+b+\xi_i-y_i) \tag{4}$$

According to KKT condition:

$$\begin{cases}\partial L/\partial w=0\\ \partial L/\partial b=0\\ \partial L/\partial \xi=0\\ \partial L/\partial \alpha=0\end{cases} \tag{5}$$

The solution are as follows:

$$\begin{cases}\omega=\sum_{i=1}^{n}\alpha_i\varphi(x_i)\\ \sum_{i=1}^{n}\alpha_i=0\\ \alpha_i=C\xi_i\\ \varphi(x_i)\omega+b+\xi_i-y_i=0\end{cases} \tag{6}$$

Expurging ω and ξ, get:

$$\begin{bmatrix}0 & e^T\\ e & GG^T+C^{-1}\end{bmatrix}_{(n+1)\times(n+1)}\begin{Bmatrix}b\\ \alpha\end{Bmatrix}=\begin{Bmatrix}0\\ y\end{Bmatrix} \tag{7}$$

Where e is a $n\times 1$ vector whose element is 1, I is a $n\times n$ matrix whose element is 1; $\alpha=(\alpha_1,\alpha_2,\cdots,\alpha_n)^T$, $y=(y_1,\cdots,y_n)^T$, $G=\left(\phi(x_1)^T,\phi(x_2)^T,\cdots,\phi(x_n)^T\right)^T$.

According to Mercer condition, defining the kernel function $K(x_i,x_j)=\phi(x_i)\phi(x_j)$, finally LS-SVM regression model is as follows:

$$f(x)=\sum_{i=1}^{n}\alpha_iK(x,x_i)+b \tag{8}$$

In practical applications RBF kernel function is frequently chosen for kernel function, its expression is as follows:

$$K(x_i,x_j)=\exp\left(-\|x_i-x_j\|/2\sigma^2\right) \tag{9}$$

Prediction of Soft soil Ground Settlement Based on LS-SVM

Project Overview. A reconstruction of Old Highway Road is located in Nansha Development Zone of Guangzhou. The original roadbed in this region is mainly composed of plastic, soft plastic clay. There are the high liquid soil and soft clay including plastic, soft plastic clay from top soil to bottom soil. The high liquid soil is difficult to control optimum moisture content. So it is difficult to be compacted and meet the design standards. In addition, the soft soil possess visible rheological characteristics. These factors easily bring to large settlement deformation induce pavement damage. Therefore, how to monitor the soft soil foundation deformation and control embankment settlement problems are necessary to be focused in the design and construction. Through the real-time monitoring of settlement plate 3 in one section, the embankment settlement observation data shown in table 1 were obtained. The first six data sets were selected as learning samples of the original LS-SVM, and the back six data sets were selected as the test data.

Tab.1 Settlement monitoring data

time（d）	10	17	26	37	49	62	87	103	120	133	148	158
settlement（cm）	2.41	4.17	5.54	6.35	7.04	7.60	7.84	7.89	7.94	7.97	7.98	7.99

Fitness Function and Results Analysis. Here, RBF kernel function was chosen for LS-SVM network kernel function. GA was adopted to optimize LS-SVM regression parameters—(C,σ^2). Therefore, the identification error function was set up, as follows:

$$w(s)=\frac{\sum_{i=1}^{m}\left|s-\overline{s_i}\right|}{m\cdot T} \tag{10}$$

Where s_i was network practical outputs, $\overline{s_i}$ was network ideality outputs, m was the measure sample number, and T was the time range. The reciprocal of formula (10) was used to be qua GA fitness function $f(s)$. GA was applied to optimize LS-SVM regression parameters. Finally $(C,\sigma^2)=(8254,36)$. At this point the maximum value of fitness function was 769.2, and its corresponding identification error $w(F,x,y)=0.24\%$ was minimal. LS-SVM network measure results were shown in table 2.

Seeing from table 2, the prediction precision of proposed method in this paper was better than the curve fitting and neural network for predicting soft soil foundation settlement. The identification maximum absolute error value of LS-SVM was 0.14cm, and that the identification maximum absolute errors value of curve fitting and neural network were 1.62cm and 0.56cm which were 11.6 times and 4 times of frontal value. It shows that LS-SVM identification precision is much better than curve fitting and neural network, and LS-SVM can be used to be the more advanced method for predicting soft soil foundation settlement.

Tab.2 settlement results

Prediction method	time（d）											
	10	17	26	37	49	62	87	103	120	133	148	158
Measured settlement	2.41	4.17	5.54	6.35	7.04	7.60	7.84	7.89	7.94	7.97	7.98	7.99
Curve fitting value	2.44	4.12	5.52	6.45	6.97	7.62	8.03	8.17	8.32	8.61	9.10	9.61
Neural network predictive value	2.41	4.16	5.54	6.36	7.06	7.58	7.89	7.96	8.00	8.16	8.31	8.55
LS-SVM predictive value	2.41	4.17	5.53	6.35	7.05	7.61	7.86	7.92	7.96	8.01	8.08	8.13

Conclusions

Support Vector Machine is a sort of rising machine learn method. Its outstanding characteristics are good generalizing capability, and it is especially fit for high dimension and small sample learning problem. Therefore, the method of predicting soft soil foundation settlement based on Least Square Support Vector Machine was proposed in this paper. Through the real-time monitoring of settlement plate 3 in one section, LS-SVM was trained and studied the nonlinearity relation between foundation settlement and effect gene. Accordingly, LS-SVM had the prediction ability of foundation settlement. The experiment results show that the proposed method is much better than curve fitting and neural network, and LS-SVM can be used to be the more advanced method for predicting soft soil foundation settlement.

References

[1] PAN Lin-you, XIE Xin-yu. Observational settlement prediction by curve fitting methods. Rock and Soil Mechanics. 2004, 25(7): 1054~1058.

[2] Zhao Junming. Application of Grey Theory in Soft Clay Ground Settlement Prediction for Expressway. Journal of Highway and Transportation Research and Development, 2005, 22 (5): 56~58.

[3] LI Chang-dong, TANG Hui-ming, HU Bin, et al. Research on application of wavelet analysis and RBF neural network to prediction of foundation settlement. Rock and Soil Mechanics, 2008, 29(7): 1917~1922.

[4] Vapnik V N. Estimation of dependences based on empirical data[M]. Berlin: Spring-Verlag, 1982.

[5] Marcel O E, Johan A KS, Bart DM. Least squares support vector machines and primal space estimation[C]. Proceedings of the 42nd IEEE Conference on Decision and Control. Maui, Hawaii USA, 2003.

[6] Suykens J A K. Nonlinear modeling and support vector machines[C]. IEEE Instrumentation and Measurement, 2001: 120~123.

[7] Shawe-Taylor J, and Cristianini N. Kernel Methods for pattern analysis[M]. Cambridge University Press, 2004.

Applied Mechanics and Materials Vols. 97-98 (2011) pp 40-44

doi:10.4028/www.scientific.net/AMM.97-98.40

Dynamic Response in ALF Aggregate Base Asphalt Pavement

Zhuang Chuan-yi[1,2,a], Shen Ai-qin[2,b],Wang Lin[3,c]

[1]Department of Civil Engineering, Shandong Jiaotong University, Jinan250023, Shandong, China

[2]Key Laboratory of Special Area Highway Engineering of Ministry of Education ,Chang'an University, Xi'an 710064, China;

[3] Key Laboratory of Expressway Maintenance Technology of Ministry of Transport (Jinan)，Jinan 250031,China

[a]jcc1717@sina.com,[b]saq6305@163.com,[c]sddot@163.com

Keywords：road engineering, pavement dynamic response, vertical compressive stress, horizontal longitudinal strain, ALF, axle load, vehicle speed

Abstract: In order to evaluate pavement dynamic responses accurately under truck loading, the full-scale asphalt pavement accelerated loading facility (ALF) was used. 10 strain gauges and 2 soil pressure cells were installed; temperature sensors were also installed in the different depth of the HMA layer. Pavement response was measured under real traffic load with ALF. The measured pavement responses are compared between the pavement sections to evaluate the effects of various experimental factors, such as axle load, speed, et al. Dynamic strain at the bottom of HMA layer and vertical compressive stress on the top of the subgrade were examined in the full-scale testing road, the regression models between dynamic response and axle load, dynamic response and speed were put forward respectively. Studies show that there is not only tensile strain but also compressive strain in the dynamic response, and the strain response is in the station of tension and compression alternation. Under the intermediate temperature, the strain response at the bottom of the asphalt layer is increased linearly with the increase of axle load and the vertical compressive stresses at the top of the subgrade is also increased with the increase of axle load. Speed has a great effect on strain response at the bottom of HMA layer, and has little effect on vertical compressive stress, it affects the loading duration of stress only. The destroy for the pavement by low speed and heavy load is more serious than that is normal.

Introduction

Great changes have been in expressway in China, it shows over loading, low speed and higher tire pressure. But the current pavement design theory and technical standard were mostly based on the traditional low traffic volume class highway [1], without considering overload, high tire pressure and low speed driving sufficiently, so pavement was damaged severely ahead of time, long-term pavement performance (LTPP) is clearly insufficient. Currently, single axle load was from rated 100kN to 180kN, tire inflation pressure from rated 0.7MPa to 1.0MPa even higher, which is more than the standard design axle load. Operating speed of overloading vehicles is lower than that is normal, the destructive effects of the pavement is much larger than the standard axle load [2]. Thus, they have already become a major problem for highway researchers. Researches in this area have carried out related research work, Zhong-hong Dong [3] established viscoelastic layered system dynamics model under moving axle load, studied the effect of heavy vehicle dynamic response of asphalt pavement, and conducted the dynamic response of full-scale test study, pavement response by pavement temperature and offset was analyzed, but he has not studied axle load, slow speed and tire pressure on pavement dynamic response in-depth. Hong-chao Zhang, Li-jun Sun [4] established

finite element model for pavement response by numerical analysis. Siddharthan [5], who adopted elastic, layered system established the dynamic model under the moving load, but the method is based on elastic constitutive model, at high temperature, it is used the complex modulus to replace young's modulus simply, it has not been detected and verified by test road.

Full-scale Asphalt Pavement by ALF

Accelerated pavement testing has already become one of the main evaluation means to pavement structure design method and results [6]. ALF consists of testing facility and data acquisition system, shown in figure 1. Testing facility exerted loads on the pavement [7], and data acquisition system measured the parameters and pavement condition synchronously, which included surface deflection, pavement dynamic response of the pavement structure, rutting and cracking.

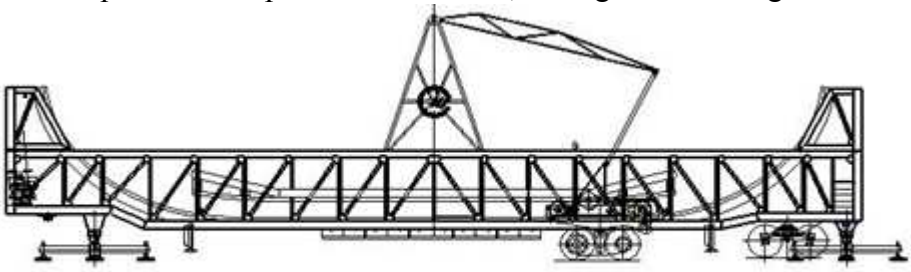

Fig. 1 Accelerated loading facility

Layout of Pavement Sensors

Strain sensors were embedded at the bottom of the asphalt layer in each of the two sections in order to measure dynamic strain responses under wheel load and environment conditions. Soil compressive cell were embedded on the top the subgrade of clay in order to measure vertical compressive, which will provide scientific basis for triaxial test and theory analysis. Thermocouples were installed in the asphalt layers in different depths from the top of the surface. In test track, 4 thermocouple sensors were installed from the surface to the bottom of the asphalt layer, which was located at surface, 2cm, 5cm and 9cm depth. The device of pavement temperature acquisition system can monitor pavement temperatures and air temperature real time, and automatically record data per 15 minutes; Asphalt strain sensors separately installed horizontal longitudinal and transverse, in order to compare different direction strain response.

Pavement Response Testing

Accelerated pavement loading test was carried out under normal temperature conditions to study the dynamic response of pavement structure with axle load.

Effect of Axle Load on Measured Strains and Stresses under HMA

We selected dynamic strain response at the bottom of the asphalt layer and vertical compressive stress as indexes [8], and analyze axle load on the dynamic pavement response. 23km/h operating speed was selected, axle load was changed by the hydraulic cylinder, at the same time it was calibrated with portable axle load weighting instrument. Dynamic response was measured under three axle load level, which is 100KN, 130KN and 165KN. At the meantime, the temperature of the middle depth of the HMA layer is measured of 26.3℃[9], figure 2 was time history plot of horizontal longitudinal tensile strain response under 100KN axle load.

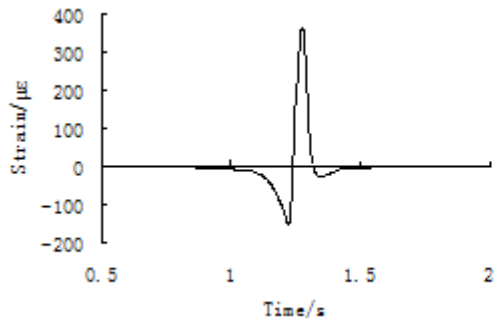

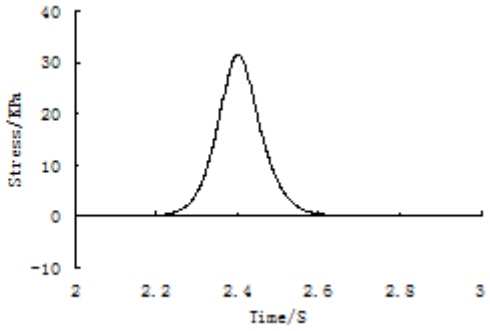

Fig. 2 Time history plot of strain *Fig. 3 Vertical compressive stress*

As is shown in fig.2, under moving vehicle loads, there is not only tensile strain but also compressive strain in the dynamic response, and the strain response is in the station of tension and compression alternation. Alternating tensile and compressive strain state of the trabecular bending fatigue test results by MTS-810 test machine, it was showed that the fatigue life under tensile strain with only the conventional fatigue test results were significantly differences within tensile and compressive strain, The alternating structure of fatigue damage affecting the pavement of the most important factor. Therefore, the fatigue life of asphalt pavement considers not only the role of tensile strain, but consider compressive strain. So the strain amplitude (i.e., the maximum strain subtract the minimum compressive strain) as control indexes.

Figure 3 shows the vertical compressive stress time history curve. It can be observed from Figure 3, only vertical compressive stress exert on the top of the subgrade, and it appears unidirectional stress state; the residual stress is 0, it indicate that under intermediate temperatures, the vertical stress on the top subgrade is nearly not affected by viscosity of the asphalt mixture.

Figure 4 shows the maximum longitudinal strain response at the bottom of asphalt layer versus axle load. It can be seen in different axle load levels, strain are still showing alternative tensile and compressive strain state, the maximum tensile strain and compressive strain and value of amplitude are increased with the axle load increasing, and the longitudinal value of amplitude can be referred as one of the indexes for evaluating mechanical properties. In the test temperature (26.3℃), the dynamic response of asphalt pavement appears linear relationship with the axle load, linear elasticity theory can be used to calculate dynamic characteristics and fatigue life of flexible pavement structure.

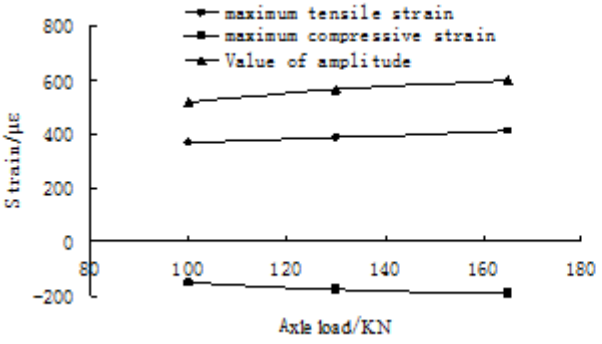

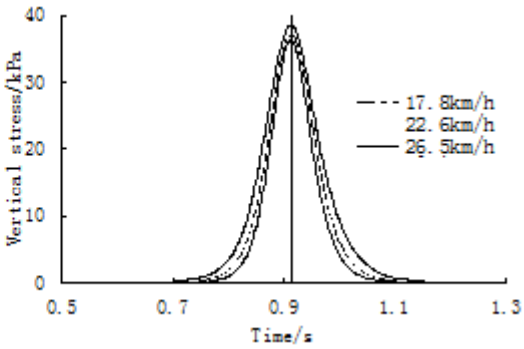

Fig. 4 Strain versus axle load *Fig. 5 Vertical stress versus vehicle speed*

Stress Pulse Lasting Time

In order to examine the vehicle speed effect on the graded gravel flexible asphalt pavement dynamic response, three speed levels were applied to the dynamic response of ALF test track, the vehicle speed was17.8km/h, 22.6km/h and 26.5km/h separately. Axle load was set at 130KN, tire pressure was set at 0.8MPa.

Asphalt mixture is one of the viscous-elastic materials; its dynamic modulus is a function of loading frequency and temperature. Determination to actual pulse time of stress and strain is very important, which will help to study the characteristics of pavement dynamic response and guide road material test. In this study, based on full-scale asphalt pavement by ALF, vertical stress pulse under 3 speeds was measured, shown in figure 5. Obviously, speed has little effected on vertical stress; it only affected lasting time of vertical stress.

Figure 6 was vertical stress pulse lasting time versus speed, we can see pulse time reduced with the increasing speed, but it was not reduced linearly, the rate of reduction of pulse time became slow down with the increase of vehicle speed.

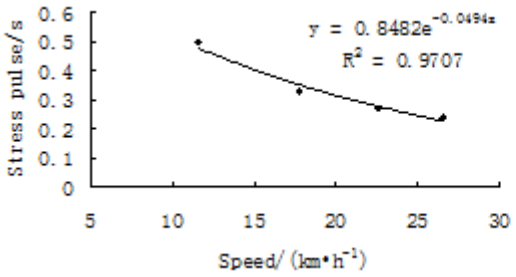

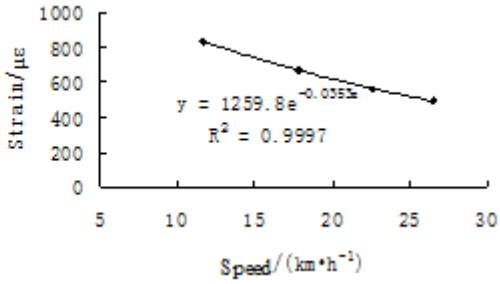

Fig. 6 Stress pulse lasting time versus speed *Fig. 7 Strain response versus speed*

Regression analysis shows that there is good relationship between stress pulse time and speed, shown as Eq.1. But pulse time is greatly affected by pavement structure and thickness, this model does not take into account pavement thickness, and the sample size is limited, so we need further calibrate and revise the formula with more data of ALF and LTPP.

$$t = 0.8482e^{-0.0494V} \quad (1)$$

Where t is the time of stress pulse with s, V is vehicle speed with km/h.

Effect of Speed on Pavement Response

Vehicle speed is directly related to not only the role of time, but stress-strain response pulse time. The modulus of viscoelastic material influenced by the speed, usually the greater the speed, the greater the modulus, while the smaller the pavement response.

Pavement response under low vehicle speed were measured by means of ALF, figure 7 was the measured strain response versus speed. Figure 8 was the measured vertical compressive stress on the top of the subgrade versus speed. It can be seen that speed significantly affect strain response at the bottom of asphalt layer, but less affect vertical compressive stress on the top of subgrade, and with the speed increases, the strain and stress response changes slowed down.

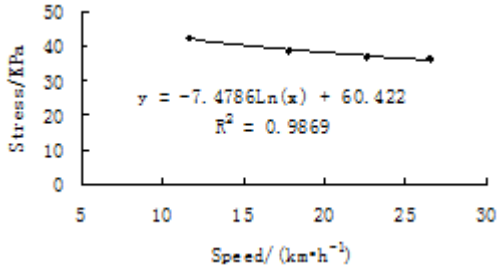

Fig. 8 Vertical compressive stress versus speed

Regression analysis shows that the maximum strain is good related with speed in exponential; the model of the maximum strain amplitude and speed is shown in Eq.2.

$$\varepsilon = 1259.8e^{-0.0353V} \quad (2)$$

Where ε is the maximum strain amplitude of microstrain.

Conclusion

(1) Under moving vehicle loads, there is not only tensile strain but also compressive strain in the dynamic response, and the strain response is in the station of tension and compression alternation.
(2)There is only compressive stress on the top of the subgrade.
(3) Vehicle speed has little effect on the maximum vertical compressive stress. The higher the vehicle speed, the longer stress pulse lasting time.
(4)The maximum tensile strain and compressive strain and value of amplitude are increased with the axle load increasing; the value strain of amplitude should be as the design indexes.
(5) The model of stress pulse lasting time and strain response with speed were put forward separately, but it needs more data to validate.

Acknowledgements

The project was supported by Western Communications Construction Scientific and Technological Project (No.200831800099) and Scientific Research Foundation of Shandong Jiaotong University (No. Z200916).

References

[1] JTG D50-2006, *Highway Asphalt Pavement Design Criterion* (In Chinese).
[2] Da-wei Liu, Jing Chen, Wei Huo and Bing-cong Chen:*Effect of Vehicle Speed on Damage of Pavement*. Transactions of the Chinese Society of Agricultural Machinery, 34(1): 11-13(2003, In Chinese)
[3] Zhong-hong Dond, Peng-min Lv: *Theoretical Research of the Dynamic Response of Asphalt Pavement Structure under Traffic Loads*, Journal of Zhengzhou University(Engineering Science), 28(4):88-91,95(2007, In Chinese)
[4] Hong-chao Zhang, Li-jun Sun: *Development and Analysis of Premature Failures of the Asphalt Pavements*. Journal of Tongji University(Natual Science) , 34(3):33l-334 (2006, In Chinese)
[5] Siddharthan Raj V, Sebaaly Peter E, EL-Desouky Maqdy, Strand Dan, Huft David: *Heavy Off-road Vehicle Tire-pavement Interactions and Response, Journal of transportation engineering*, 131(3):239-247(2005)
[6] Nan-xiang Zheng, Si-sheng Niu and Xin-quan Xu:*Temperature, Axle Load and Axle Load Frequency Model of Rutting Prediction of Heavy-duty Asphalt Pavement*.China Journal of Highway and Transport, 22(3): 7-13(2009, In Chinese)
[7] Zhi-guang Guan, Ming-xing Lin and Xu-guang Wang: *Design on Highway Accelerated Loading Testing Facility*. Proceedings of the 2009 IEEE International Conference on Automation and Logistics,253-257(2009, In Chinese)
[8] Peng Cui, Min-hua Shao and Li-jun Sun. *Research on Design Indices of Perpetual Asphalt Pavement*. Journal of Traffic and Transportation Engineering, 8(3):37-42(2008, In Chinese)
[9] Yong-shun Yang, Lin Wang, Jin-cheng Wei and Shi-jie Ma: *Typical Pavement Structure Dynamic Response Data Collection and Analysis under Heavy Vehicle Loading*. Journal of Highway and Transportation Research and Development, 27(5):11-16(2010)

Applied Mechanics and Materials Vols. 97-98 (2011) pp 45-48

doi:10.4028/www.scientific.net/AMM.97-98.45

Two-parameter Weibull Distribution Theory Testing Analysis in Fatigue Life of Asphalt Mixture

Sun jie[1, a], Jiangmiao Yu[2,b] and Haisheng Zhao[1,c]

[1]Key Laboratory of Highway Maintenance of Ministry of Transport, Jinan, Shandong, 250031, China

[2] South China University of Technology, Guangzhou, Guangdong, 510640, China

[a]sunjie602@163.com, [b]yujiangmiao@scut.edu.cn, [c]zhaohaisheng@163.com

Keywords: Asphalt Mixture, Fatigue Life, Weibull Distribution, Failure Probability.

Abstract: It has been commonly used normal distribution to describe the fatigue life of asphalt concrete. Because of the variability of the material itself and environmental conditions for test, experimental fatigue life datas obtained show a large discrete. Through a large number of laboratory tests and optimization of the strong representation of the data source, this paper verified distribution of the fatigue life of asphalt concrete in statistical in the use of two-parameter Weibull distribution theory and obtained fatigue life equation by regression under different failure probability.The results showed that: Weibull distribution theory can be used to describe asphalt concrete fatigue life distribution under the complicated conditions in a multi-factor.

Introduction

Because the variability of the material itself and the external environment, the fatigue life data of difference magnitude can not be simply described using the average statisticalion.Most of the early fatigue life test have be statisticed analysis by the lognormal distribution, but this distribution is only for the convenience of the mathematical analysis[1]. Gumbel has pointed out that the failure function of normal distribution reduced with service life or time[2] and this is contrary with the natural physical phenomena that the fatigue life of engineering materials will gradually decline with fatigue process. this paper will try to verify distribution features of the fatigue life of asphalt concrete in statistical in the use of two-parameter Weibull distribution theory.

Experimental Design

In order to research the fatigue characteristic of asphalt mixture in bigger range, the utility software UD4.0 version which was developed by Chinese Mathematical Society was used in this test plan for uniform experiment design [3]. This method could apply to multi-factor and multi-level test plan, and could make the selected testing point uniform distribution in multi-dimension test space which makes the infinite testing point has fine representativeness on whole.This test plan is shown in Table.1.

Table.1 Testing design of fatigue based on stress control

Test Parameters	Test Program
Asphalt type	3 levels (base asphalt 50 #, 70 # and 90 #)
Grading type	9 levels (3 mixture structures of the SMA \ AC \ AK × 3 maximum sizes of 26.5 \ 16 \ 9.5)
Aggregate type	1 level (granite)
Asphalt content	3 levels (4.0%, 5.0% and 6.0%)
Void	3 levels (2.0%, 4.0% and 7.0%)
Stress level	3 levels (750,1000 and 1500 micro-stress)
Test temperature/frequency/load waveform	15℃/10Hz/partial sine wave
Test level/the total number of tests	27/108

Test data collecting. The stiffness modulus in the 100th loading cycle of fatigue test was read and recognized as the initial stiffness modulus. The recoded test data read by computer controlling system should contain loading times, stress value, strain value, stiffness modulus, modulus percentage, lag angle, dissipation energy etc. The test will automatically stop when the testing stiffness modulus is less than 10% of initial stiffness modulus. The parallel test results would be treated by abandon differentials according to the dispersing degree of test results, the standard of abandon differentials is that if the difference value between one data in a group of parallel test results and the average value is larger than k(n=4, k=1.46) times of corrected standard deviation, the test data should be abandoned.

The Overview of Double-parameter Weibull Distribution Theory

The Sweden research engineer Weibull presented one kind of failure probability density distribution function to describe fatigue data in 1949[4]. Then this kind of failure distribution was applied into other areas. Weibull distribution is also named as minimum value Fisher-Tipper III type asymptotic distribution and could be educed from Limit Theory [5].

The formula of the probability density function of Weibull distribution f(n) and cumulative distribution function sum $P_f(n)$ show as follow:

$$f(n)=\frac{\alpha}{u-n_0}\left(\frac{n-n_0}{u-n_0}\right)^{\alpha-1}\exp\left[-\left(\frac{n-n_0}{u-n_0}\right)\right]^{\alpha} \qquad P_f(n)=1-\exp\left[-\left(\frac{n-n_0}{u-n_0}\right)\right]^{\alpha} \tag{1}$$

Which: n---the characteristic value of random variable N; α ---shape function; u ---scale parameter; n_0 ----location parameter or the minimum test life.

The minimum life n_0 could be set as 0 for convenience in analyzing, so the probability of failure $P_f(n)$ shows as follow:

$$P_f(n)=1-\exp\left[-\left(\frac{n}{u}\right)\right]^{\alpha} \tag{2}$$

There are two unknown parameters which should be calculated out in double-parameter Weibull failure probability distribution and build the matchup between failure probability and fatigue life[6].

The both side of formula (2) were calculated by logarithm for two times, the result as follow:

$$\ln\ln\frac{1}{1-P_f(n)}=\alpha\ln(n)-\alpha\ln(u) \tag{3}$$

If $Y=\ln\ln\frac{1}{1-\mathrm{P_f}(n)}, X=\ln(n), \beta=\alpha\ln(u)$, we can get $Y=\alpha X-\beta$ (4)

If formula (3) and (4) are both established and the R2 value is very high, the test results comply with double-parameter Weibull distribution , if not, it does not comply.

The Check of Double-parameter Weibull Failure Probability Distribution on Fatigue Life

We listed the fatigue life of the same group of specimens under every stress level respectively from small to large, and selected 4 group data for each kind of AC-25, AK-25 and SMA-25 mixture from 108 times effective fatigue test data, the parameter X and Y were calculated by formula (1) to (4) under stress level of 1.5, 1.0 and 0.75 MPa. Its failure probability $P_f(n)$ formula shows as follow:

$$P_f(n)=\frac{i}{1+k} \tag{5}$$

Which: i----the number of specimen in this group, i=1,2,3,…,k, k is the total number of this group of specimen.

The calculating result is shown in Table.2 and the curve relationship between $\ln\ln\frac{1}{1-P_f(n)}$ and $\ln(n)$ of different mixtures under different stress level is shown in Fig.1, Fig.2 and Fig.3.

Table.2 Weibull distribution checking on fatigue life N

Mixture type	Stress level σ （MP）	$P_f(n)$	N	$\ln(N)$	$\ln\ln\frac{1}{1-P_f(n)}$
SMA-25	0.75	1/5	166712	12.0240	-1.49994
	0.75	2/5	577213	13.2660	-0.671727
	0.75	3/5	709712	13.4726	-0.087422
	0.75	4/5	1318503	14.0920	0.475885
AK-25	1.0	1/5	46383	10.7447	-1.49994
	1.0	2/5	58732	10.9807	-0.671727
	1.0	3/5	119923	11.6946	-0.087422
	1.0	4/5	157113	11.9647	0.475885
AC-25	1.5	1/5	6072	8.7114	-1.49994
	1.5	2/5	128262	11.7618	-0.671727
	1.5	3/5	250613	12.4317	-0.087422
	1.5	4/5	417412	12.9418	0.475885

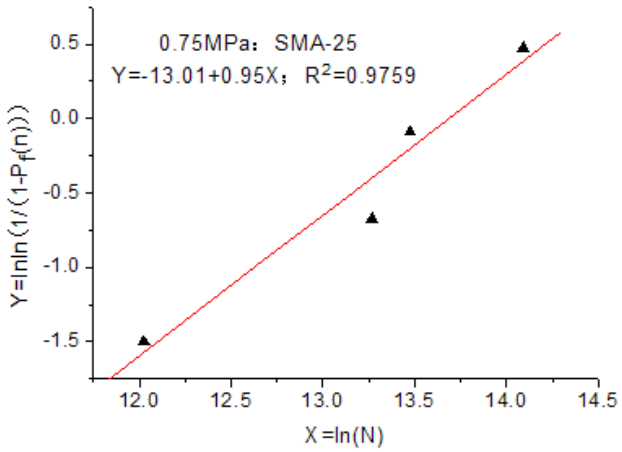

Fig.1 Fitted curve of fatigue life and failure probability of mixture SMA-25

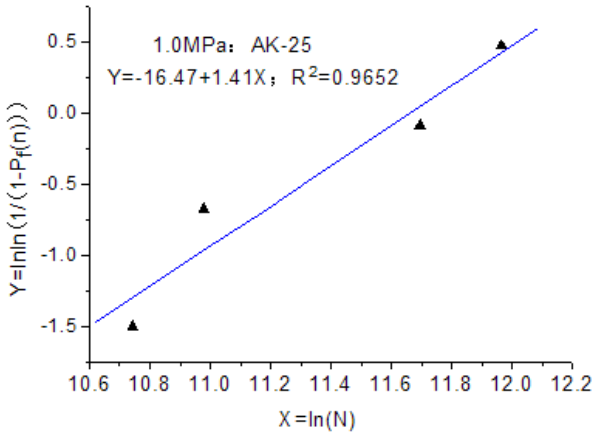

Fig.2 Fitted curve of fatigue life and failure probability of mixture AK-25

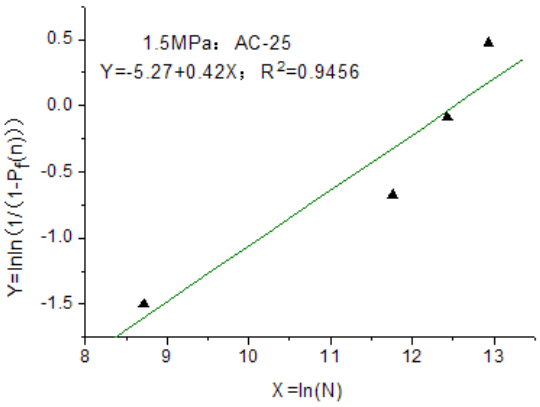

Fig.3 Fitted curve of fatigue life and failure probability of mixture AC-25

From data of Fig.1-3 we can get that the related coefficients of regression equation of three kind of mixtures' fatigue life and failure probability curve are all larger than 0.9, which can prove the fine linear relation between $\ln\ln\frac{1}{1-P_f(n)}$ and $\ln(n)$, so the fatigue life of three kind of mixtures met double-parameter Weibull distribution. The double-parameter Weibull distribution of fatigue life could clearly reflect the characteristic probability fatigue life of asphalt mixture and could be used to analyze fatigue life of asphalt mixture.

Conclusion

According to a large number of laboratory test data, this paper used double-parameter Weibull distribution theory to verify the failure probability distribution of asphalt mixture fatigue life, in other words, we can use double-parameter Weibull distribution theory to describe the failure probability distribution of fatigue life obtained from different mixture material and outer testing environment. The results of failure probability distribution statistics regression analyzing on fatigue life data of different types of asphalt mixture show that the fatigue life of asphalt mixture and failure probability have fine linear relation and we can regression parameter equation.

References

[1]X.P.Shi,T.F.Fwa,S.A.Tan.Flexural Fatigue Strength of Plain Concrete[J].ACI Materials Journal,Vol.90,No.5,September-October 1993.

[2]Gumble,E.J.,Parameters in the Distribution of Fatigue Life[M],Joumal of Engineering Machanics,ASCE,OCT,1963.

[3]Kaitai Fang, Changxing Ma. orthogonality and uniformity experimental design. Science Pulication,2001.

[4]Weibull,W.,A statistical Theory of Strength of Materials,Proc[M].Royal Academy Engry Science,15,1939.

[5]J.W.PROVAN probability cracking mechanism and rliability[M], Aerospace industry publication,1989.

[6] Byung Hwan Oh.Fatigue-Life Distribution of Concrete for Various Stress Level,ACI[J].Materials Journal,March-April 1991.

Applied Mechanics and Materials Vols. 97-98 (2011) pp 49-54
© (2011) Trans Tech Publications, Switzerland
doi:10.4028/www.scientific.net/AMM.97-98.49

The Seismic Stability Numerical Analysis of Embankment High Slope with Different Filling

Jinliang Wu[1,2,a] Yong-xing Zhang[1,b] Nian Peng[2,c]

[1]Chongqing University ,Chongqing,400045,China,

[2] Chongqing Jiaotong University, Chongqing, 400074,China

[a] jinliangwu@126.com, [b] cqyzzhang@163.com, [c] 24868227@qq.com

Keywords：earthquake； embankment high slope；filling；numerical analysis；stability safety coefficient

Abstract：In recent years, frequent earthquakes had happenned everywhere in the world.Through establishing soil dynamic constitutive model and boundary conditions, implement finite element numerical analysis of embankment high slope of different filling, using large geotechnical software GEO–SLOPE, inputting El Centro wave, Taft wave and artificially wave according to requirements specification fitting respectively in this article.Results show that different degree earthquake will reduce the stability safety coefficient of embankment slope, the properties of embankment high slope of different filling is worse,the range of reduction is larger.

Introduction

Our country is located between two most active seismic zone, the east Pacific seismic belt and the west Himalayan-Mediterranean seismic belt. Earthquake widely distributed, destructive earthquake is found almost all ovre the provinces, Among them , western region has complicated geological conditions, topography changes, and seismic activity, strong and high frequency. Therefore, ultra-high embankment slope under earthquake stability analysis is more urgent and important. Seismic slope stability problem is a hot topic of the current geotechnical earthquake engineering and earthquake engineering study. Since the composition of materials and geotechnical constitutive complexity, coupled with the particularity of seismic random loads in seismic shaking ,cause slope stability under earthquake research has become very complicated.

In this paper, large geotechnical software GEO-SLOPE was adopted to study ultra-high embankment slope stability under different conditions, analysis of the inputted seismic waves and seismic intensity, combined with changes in the parameters of embankment to explore the rules of high embankment slope stability coefficient.

Soil dynamic constitutive model and boundary conditions

2.1 Soil constitutive model

Using equivalent linear model in the dynamic analysis of soil constitutive model[1~4] ,As shown in figure 1. Shear modulus take cut line modulus: $G = \frac{\tau_c}{\gamma_c}$;damping ratio: $\eta = \frac{S}{\pi S_{ABC}}$. The relations between stress and strain such as formula (1) shows:

$$\begin{Bmatrix} \sigma_x \\ \sigma_y \\ \sigma_z \\ \tau_{xy} \end{Bmatrix} = \frac{E}{(1+\nu)(1-2\nu)} \begin{bmatrix} 1-\nu & \nu & \nu & 0 \\ \nu & 1-\nu & \nu & 0 \\ \nu & \nu & 1-\nu & 0 \\ 0 & 0 & 0 & \frac{1-2\nu}{2} \end{bmatrix} \begin{Bmatrix} \varepsilon_x \\ \varepsilon_y \\ \varepsilon_z \\ \gamma_{xy} \end{Bmatrix} \quad (1)$$

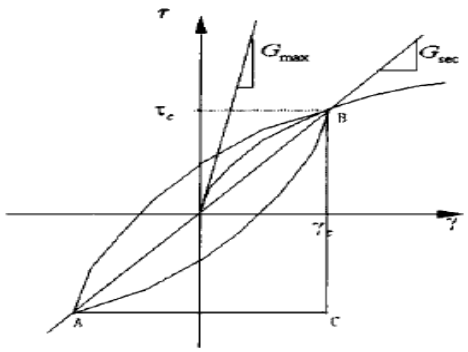

Fig1 Schematic diagram of soil constitutive model

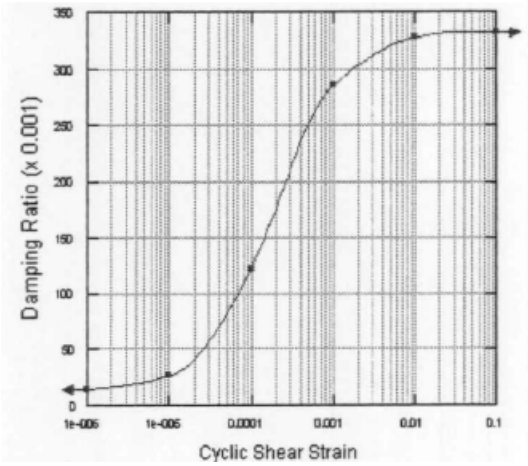

Fig2 Shear modulus and shear strain diagram

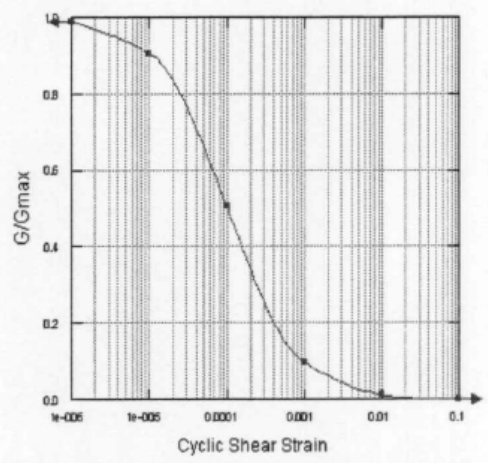

Fig3 Damping ratio and shear strain diagram

With earthquake cyclic loading, shear modulus G and damping ratio change with shear strain simultaneously. Curve of shear modulus changing with shear strain is shown in figure 2. Curve of damping ratio changing with shear strain is shown in figure 3.

2.2 The dynamic boundary conditions

When using finite element method for calculating soil seismic response, involved disposing the artificial boundary problem.The widely used artificial boundaries are dynamic viscous boundary[5], viscous boundary[6], transmitting boundary[7], etc.

The concept of viscous boundary is clear and simple and is widely used, but its accuracy is not high and low-frequency instability. In contrast, the viscoelastic boundary can constrain the zero frequency component in dynamic problems , owning good stability and high accuracy, and can simulate properties of elastic recovery of medium at the artificial boundary. The paper takes two-dimensional viscous-spring dynamic boundary.

The spring stiffness coefficient and damper coefficient parameters of two-dimensional viscoelastic dynamic artificial boundary is in [8~11]:

Boundary: $K=\frac{1}{1+a}\times\frac{\lambda+2G}{2\mathrm{r}}\times A$ (2)

$$C=\beta\rho c_{\rho} A \tag{3}$$

Tangential border: $K=\frac{1}{1+a}\times\frac{G}{2\mathrm{r}}\times A$ (4)

$$C=\beta\rho c_{\mathrm{s}} A \tag{5}$$

In the formula:

Parameter a represents the content proportion of the amplitude between the plane wave and scattered wave, and reflects the propagation characteristic of outward transmission wave of artificially boundary. Parameter b represents the relationship between physical wave velocity and apparent wave velocity, and reflects average wave velocity characteristic of multiple wavelet in different point of view. The better valuation of a and b is 0.8 and 1.1. Lame constant:

$\lambda = \frac{Ev}{(1+v)(1-2v)}$;Shear modulus: $G = \frac{E}{2(1+v)}$; the represent area within A boundary nodes; $C_P = \sqrt{(\lambda + 2G)/\rho_C}$ and $C_S = \sqrt{G/\rho}$ are P wave and S wave velocity respectively; Length r can simply take form the near field structure geometric center to the artificial boundary point in the boundary or distance.

Counting parameters choosing and model creation

3.1 Counting parameters choosing

In the process of analysis, the typical four group physics mechanical test status in embankment filling test are used as the earth parameters. The paper defined them as I, II, III, and IV shown in table 1.

Table 1 The calculation results of safety factor with load located on the top of slop

Filling type	Volume weight γ（kN/m^3）	Sticky gathered force C（kPa）	angle of internal friction Φ（°′）	Elasticity modulus **E(Mpa)**	Poisson ratio v	Subsidence ratio ξ
IType	19	33	28	60	0.3	0.15
IIType	19	26	25	60	0.3	0.15
IIIType	19	24	22	60	0.3	0.15
IVType	17	20	20	60	0.3	0.15
Base	20	120	50	10000	0.2	0.05

3.2 Model creation

Assume embankment height is 30 meters, road width is 26 meters, top-down points respectively platform height is 8 meters, 10 meters and 12 meters, the corresponding gradient value is 1.5, 1.75, 2.0, points for 2 meters platform width. The finite element grid partition is shown in figure 4 .

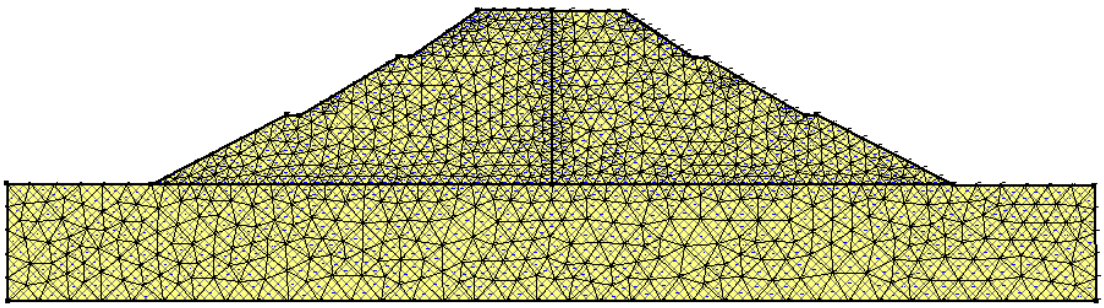

Fig4 Relation curve of dry density versus water content

Calculation result analysis

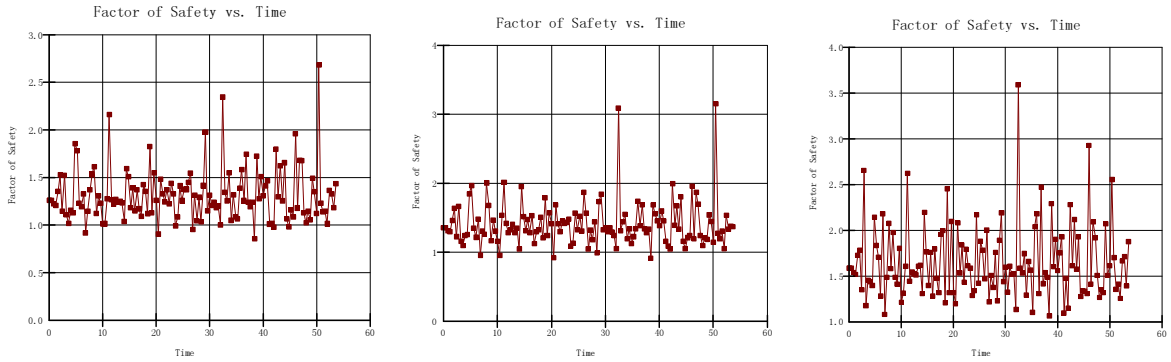

Fig5 El centro seismic，filling materials of type I，large，medium and small earthquake slope factor of safety vs. time curve

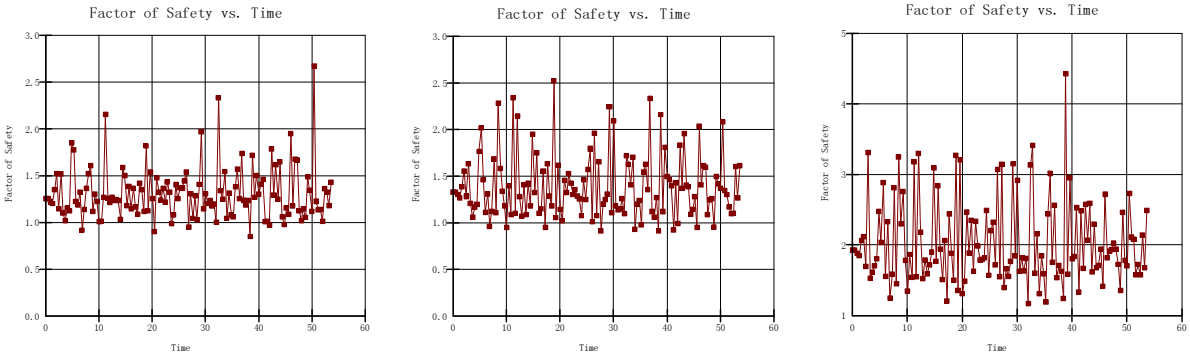

Fig6 El centro seismic，filling materials of type II，large，medium and small earthquake slope factor of safety vs. time curve

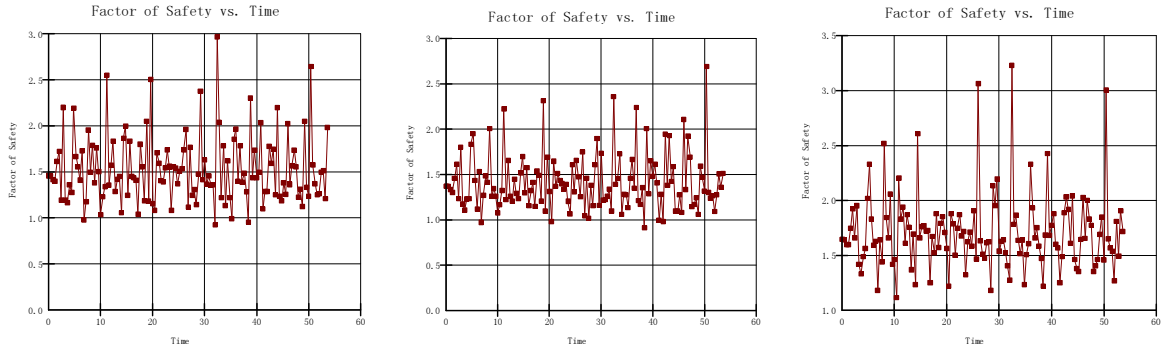

Fig7 El centro seismic，filling materials of type III，large，medium and small earthquake slope factor of safety vs. time curve

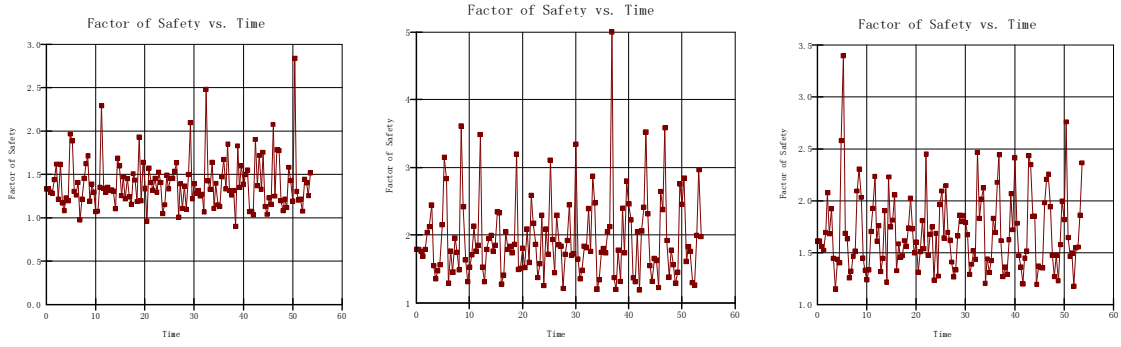

Fig8 El centro seismic，filling materials of type IV，large，medium and small earthquake slope factor of safety vs. time curve

AS the same analysis, slope stability safety coefficient can be obtained when the El centro wave was inputted , as shown in table 2:

Table 2 Enter El centro seismic, with the dynamic finite element method to calculate the stability of the safety factor summary tables

Filling	Without seismic damage	Safety factor K			Safety coefficient reducing rates （%）		
	0.0g	0.1g	0.2g	0.4g	0.1g	0.2g	0.4g
I	1.307	1.191	1.067	0.989	8.882	18.342	24.351
II	1.278	1.147	0.971	0.884	10.281	24.049	30.829
III	1.267	1.127	0.945	0.856	11.065	25.386	32.403
IV	1.15	0.995	0.823	0.700	13.514	28.435	39.105

Also analysis availably obtain safety coefficient of slope stability when the Taft wave and artificially wave input was inputted,it is as shown in table 3, in table 4.

Table 3 Enter Taft seismic, with the dynamic finite element method to calculate the stability of the safety factor summary tables

Filling	Without seismic damage	Safety factor K			Safety coefficient reducing rates （%）		
	0.0g	0.1g	0.2g	0.4g	0.1g	0.2g	0.4g
I	1.307	1.219	1.125	1.042	6.696	13.913	20.304
II	1.278	1.177	1.066	0.952	7.868	16.561	25.473
III	1.267	1.165	1.040	0.930	8.024	17.942	26.571
IV	1.15	1.021	0.889	0.799	11.25	22.736	30.482

Table 4 Enter artificial seismic, with the dynamic finite element method to calculate the stability of the safety factor summary tables

Filling	Without seismic damage	Safety factor K			Safety coefficient reducing rates （%）		
	0.0g	0.1g	0.2g	0.4g	0.1g	0.2g	0.4g
I	1.307	1.217	1.122	1.040	6.919	14.120	20.393
II	1.278	1.176	1.069	0.935	7.963	16.375	26.821
III	1.267	1.163	1.055	0.913	8.214	16.758	27.923
IV	1.15	1.015	0.906	0.768	11.698	21.188	33.259

From Table 2～Table 4 can be drawn:the relationship between stability safety coefficient of slope is I-type> II-type> III-type> IV type.Static conditions in the original stable slope,due to the effect of seismic waves,the safety coefficient of its stability will decreased in varying degrees.The drop degree when inputting El centro wave is larger than inputting Taft wave and artificial wave.The worse of the physical and mechanical properties of filling,the larger the level of the safety coefficient decreased. Such as,I, II, III, IV-type Filling slope when inputting El centro wave, Taft wave and artificial wave,the average coefficient of stability decreased 21.683%, 27.703%, 28.966 %, 34.282%.In small earthquake case, the slope is stable (safety coefficient is larger than 1); in moderate earthquake case, I, II, III type paddking slope was stable, IV-type Filling slope has the potential instability (safety coefficient is smaller than 1);in Severe earthquake situation, II, III, IV-type filling slope may be unstable, I-type filling slope is the critical security status (safety coefficient is close to 1).

Conclusion

Using the Geo - slope software, according to the dynamic finite element analysis of high slopes with different filling , we can get these conclusions:

(1) Using the application of soil constitutive model and dynamic boundary conditions for high slope seismic stability analysis is suitable.

(2) Under seismic action, no matter small, large or medium-sized earthquake, the reduction of slope stability and the extent of reducing is related to physical and mechanical properties of the filling for embankment slope, the worse the physical and mechanical properties are, the larger the safety coefficient decreases, and vice versa.

(3) Through changing the physical and mechanical properties of the filling for embankment slope to improve the anti-seismic stability of the slopes is feasible. For new embankment high slopes, using filling of the better physical and mechanical properties; for completed slope, we can improve the physical and mechanical properties by methods like slip casting.

(4) Considering the action time of the seismic forces is short duration and direction changes instantaneously, so will the slope with the safety coefficient calculated in the dynamic analysis less than 1 doesn't necessarily have to be completely destroyed, so it’s also unnecessary to take measures to improve physical and mechanical properties of the filling to excessively increase seismic stability safety coefficient, to avoid causing too much waste.

This embankment high slope anti-seismic stability analysis using in this paper can be used to guide the designing and constructing of slopes in this type, and it also has certain reference value for the designing and constructing of slopes in other types.

References:

[1] ShaoLongtan etc. Random seismic action of dam slope stability analysis for the direct-shear. Journal of hydraulic engineering, 1999 (11), 66-71.

[2] BoJingShan, xu guodong and JingLiPing. Soil slope, the dynamic stability analysis of seismic response and [J].journal of earthquake engineering and engineering vibration. 2001，2 (2)

[3] LiuChunLing, QiShengWen TongLiJiang, zhao method, FLAC3D analysis. Using a lock slope stability earthquake [J]. Journal of rock mechanics and engineering. 2004,23 (16) : 2730 ~ 2733

[4] party hair ning, hu again the strong, thanks definition. Deep cover layer of high earth-rock DAMS on the dynamic stability analysis of rock mechanics [J].journal of engineering journal; 2005，24 (12).

[5] Lysmer J，Kulemeyer RL.Finite dynamic model for infinite media [J].Journal of Engineering Mechanies，ASCE，1969，95:759-877

[6] Deeks AJ，Randolph MF.Axisymmetric time-domain transmitting boundaries [J].Journal of Engineering Mechanics，1994，120(1):25-42

[7]. Engineering wave theory LiaoZhenPeng introduction (second edition) [M]. Beijing: science press, 2002

[8] ZhaoJianFeng DuXiuLi, HanJiang, LiLiYun. Exogenous fluctuation, numerical simulation of a kind of realization [J]. Engineering mechanics. 2007,24 (4) : 52-58

[9] LiuHanLong, FeiKang, GaoYuFeng seismic stability. Slope time-history method [J] geomechanics. 2003，24 (4) : 553-556

[10]. MaFangFang seismic dynamic time-history based on the slope stability analysis of a finite element [j].journal of dalian university of technology, master's degree thesis. 2005:18-51

[11] BoJingShan WuZhaoYing, LiuGongShuai, DingRenJie, JiWenHao, LiuDeDong. Slope rock mass, the seismic stability dynamic safety factor analysis method [J]. Journal of disaster prevention project. 2004，24 (3) : 237-241

Applied Mechanics and Materials Vols. 97-98 (2011) pp 55-59

doi:10.4028/www.scientific.net/AMM.97-98.55

Numerical Analysis of Highmay under the Traffic Load

Yanmei Zhang[1, a], Zhenhua Pan[1,b]

[1]College of Architecture & Storage Engineering, China University of Petroleum (Huadong)

Qing dao,China

[a]zhangym@upc.edu.cn, [b]731687189@qq.com

Keywords: highway, traffic load, numerical analysis, geometric irregularities.

Abstract. Based on the geometry irregularity of pavement, an expression of the traffic load was put forward. The influence law of design parameters of each part of highway and geometry irregularity of pavement on dynamic response of highway was discussed by the developed two-dimension finite element numerical analysis procedure. The research shows that the vertical maximum vibration acceleration of pavement and subgrade attenuates according to certain trend along depth direction in different work conditions; with the foundation stiffness increasing, the vertical maximum vibration acceleration of base course and cushion increases gradually, and that of pavement surface, subgrade and foundation decreases, and the decreasing amplitude increases gradually along the depth direction; the size of the influence of subgrade on dynamic response of highway is relevant to itself stiffness; the rational matching of all parts of highway can effectively reduce the vibration response; with the increase of geometric irregularity index, the vertical maximum vibration acceleration and maximum dynamic stress of pavement and subgrade increases significantly.

Introduction

With China's highway system being built, how to realize the safety and comfort in high-speed operation causes the attention of people increasingly. A mass of research indicate that pavement geometry irregularity is one of the important reasons for causing vehicle vibration and influencing its comfort. The pavement, subgrade and foundation of highway will produce deformation and vibration under the traffic load. Whether deformation or vibration if too much, which may result in the premature failure of pavement, and increase the road surface irregularities which will make the vehicle load and vibration response increase further. In this paper, the influencing law of design parameters of each part of highway and pavement geometry irregularity on dynamic response of highway will be discussed by numerical simulation.

Traffic Load

In the process of research of highway dynamic problems, the determination of vehicle load is vital, and at the same time very difficult. At present, the design method of pavement and subgrade used in domestic is only limited to experience correction on the basis of static calculations when considering dynamic function. In addition, an automobile loading Fourier expression was put forward [1]; according to the randomness of pavement planeness, a concept of the power spectrum PSD was put forward to express car load [2]; based on the theory of random, a power spectral density of the unplaneness was got and used to analysis the random dynamic pressure which vehicles act on the road [3,4], etc.

In fact, traffic load relates to vehicle structure, pavement performance, driving speed, vehicle weight and so on, it is very difficulty to simulate accurately. Based on the consideration of geometric irregularity influence and combining with literature [5,6], a traffic load expression is presented.

$$F(t) = (p_0 + m_0 \alpha \omega^2)\left|\sin(\omega t)\right| \tag{1}$$

where p_0 is the vehicle weight which is different for different vehicle type, it is 20kN in this paper analysis process, m_0 is spring next quality, taking $m_0 = 120N \cdot s^2 / m$ during calculation process; α is geometric irregularity vector height, ω is vibration circular frequencies , $\omega = 2\pi v / l$,in which v is driving speed, l is wavelength (taking vehicle body long, taking 6m during analysis process).

Calculation Parameters and Finite Element Model

In this paper, based on elastic-plastic constitutive model, linked to the flow rule, a two-dimensional finite element dynamic analysis procedure was developed. Later this program will be used to numerical analysis.

Motion Equation. The motion equation based on virtual work principle is given below.

$$[M]\{\ddot{v}\} + [C]\{\dot{v}\} + [K]\{v\} = \{F(t)\} \tag{2}$$

where $[M]$ and $[K]$ are respectively the total quality matrix and the total stiffness matrix, $[C]$ is the total damping matrix, $\{\ddot{v}\}$, $\{\dot{v}\}$ and $\{v\}$ are respectively the acceleration, speed and displacement vector of nodes.

Damping matrix is determined by rayleigh linear group method as given below.

$$[C] = \alpha[M] + \beta[K] \tag{3}$$

here normally according to experience: $\alpha = 0.04, \beta = 0.01$ [7,8] .

The motion equation is solved by Newmark implicit time direct integral method. In order to speed up the solving process and guarantee calculation precision, the predicted correction method is adopted in this paper. Integral step adopts 0.004s in the process of solution. The permissible error of displacement incremental convergence is 1%. In order to guarantee the time integral unconditional stability, Newmark parameter gamma is 0.5, and delta is 0.25.

The Finite Element Model. This problem is plane strain problem, structure is symmetrical, and so half cross-section of the route is analyzed only. Fig. 1 gives the diagrammatic sketch of finite element mesh.

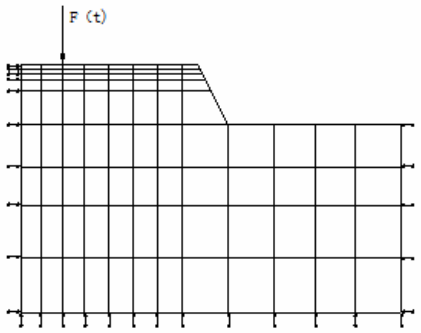

Fig. 1 The diagrammatic sketch of finite element mesh

Calculation Parameters. Table 1 gives the main calculation parameters such as thickness, elastic modulus, poisson's ratio, internal friction angle and so on.

Calculation Results and Analysis

The Influence of Foundation Stiffness on the Dynamic Response of Highway. The influence of foundation stiffness on the vertical maximum vibration acceleration of highway is shown in Fig. 2. The vertical maximum vibration acceleration of highway attenuates according to certain trend along depth direction in different work conditions; the affected depth is about 6m. With the foundation stiffness increasing, the vertical maximum vibration acceleration of base course and cushion

increases gradually, and that of pavement surface, subgrade and foundation decreases, and the decreasing amplitude increases gradually along the depth direction. Calculation results also show that when foundation stiffness increases from 30MPa to 45MPa, the vertical maximum acceleration of surface reduces about 1.5 percent, that of foundation reduces about 20.5 percent.

Table 1 Calculation Parameters

Structure layer	Thickness[m]	E[MPa]	Poisson's ratio	φ[°]	c [kPa]	ρ[t·m^{-3}]
surface	0.18	1000 1200	0.35	60	350	2.3
base course surface	0.1	700 1000 1200 1400	0.35	40	250	2.2
base course bottom	0.3	700 1000 1200 1400	0.35	40	250	2.2
cushion	0.3	260 340	0.40	35	80	1.75
subgrade	1.5	45 60 80 100	0.40	22	55	1.9
foundation	10.0	30 35 40 45	0.40	16	30	1.8

without special instructions, the stiffness from surface to foundation is respectively1000MPa,700 MPa,700MPa,260 MPa,45MPa and 35MPa。

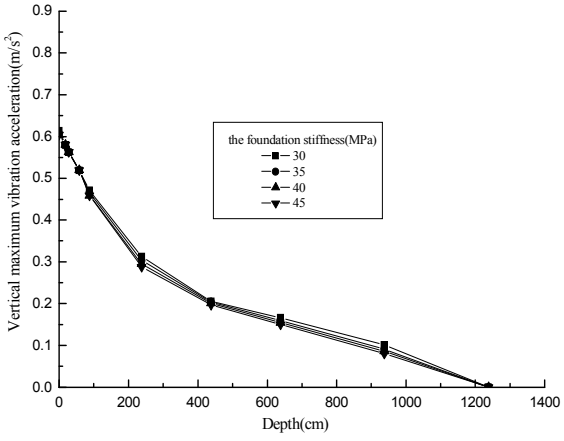

Fig. 2 The vertical maximum vibration acceleration in different foundation stiffness

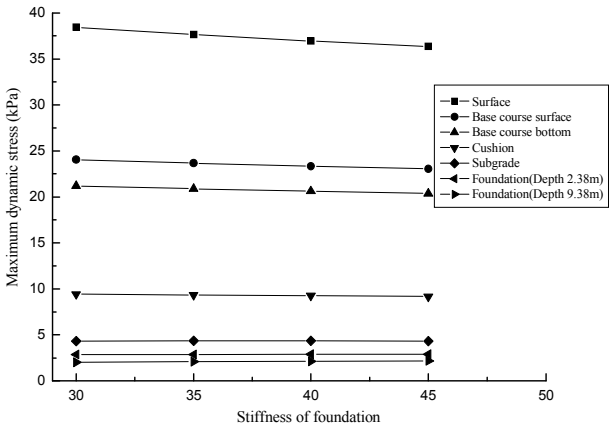

Fig. 3 The maximum dynamic stress in different foundation stiffness

Fig.3 compares the change of the maximum dynamic stress of each part of highway in different foundation stiffness conditions. Except for foundation, with the foundation stiffnes increasing, the maximum dynamic stress of other parts decreases and the decreasing amplitude reduces gradually along the depth direction.

The Influence of Subgrade Stiffness on the Dynamic Response of Highway. Fig. 4 reflects the influence of subgrade stiffness on the vertical maximum vibration acceleration. When other conditions remain unchanged, the influence of subgrade stiffness on each part is different. Calculation results show that the acceleration in surface and 2.38m depth of the foundation is the largest when the subgrade stiffness is 80MPa, the acceleration of the rest decreases gradually with the increase of subgrade stiffness. When the subgrade stiffness is 60MPa, the acceleration of surface is the minimum.

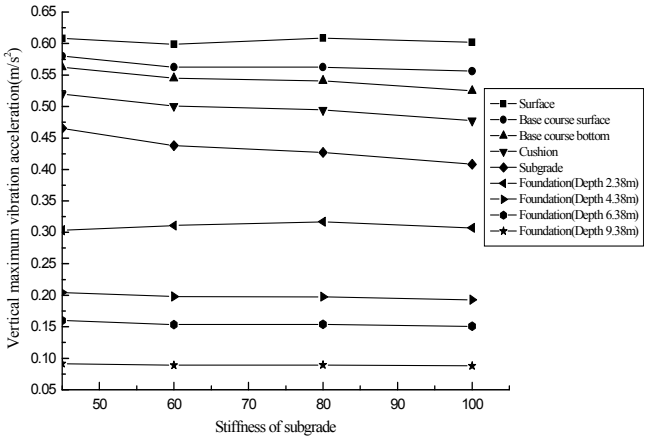

Fig. 4 The vertical maximum vibration acceleration in different subgrade stiffness

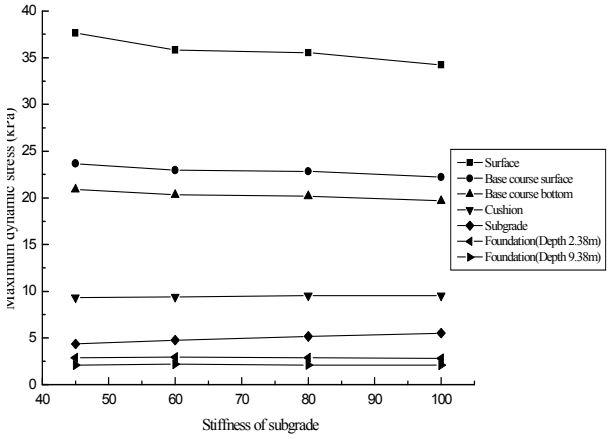

Fig. 5 The maximum dynamic stress in different subgrade stiffness

Fig. 5 shows that the maximum dynamic stress of surface and subgrade reduces with the increase of the subgrade stiffness, but that of cushion and subgrade increases, and that of foundation increases at first then decreases.

The Influence of Stiffness Matching of All Parts. Fig. 6 compares the influence of different stiffness matching on the vertical maximum acceleration. Among them, the calculated surface acceleration is the maximum which is about 0.6081m/s^2 by the first kind of stiffness matching way, and it is the minimum the seventh way. Therefore, the rational matching of all parts of highway can effectively reduce the acceleration. In addition, by comparing the first,the second and the third matching way, it can see that the maximum acceleration decreases with the base course stiffness increasing. The influence of stiffness matching on the maximum dynamic stress has similar law.

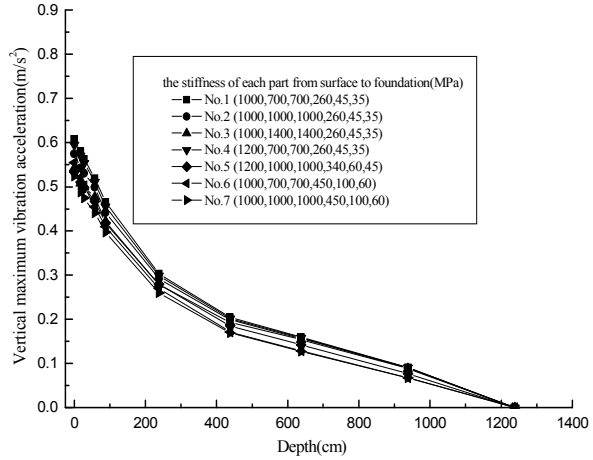

Fig. 6 The vertical maximum vibration acceleration in different stiffness matching

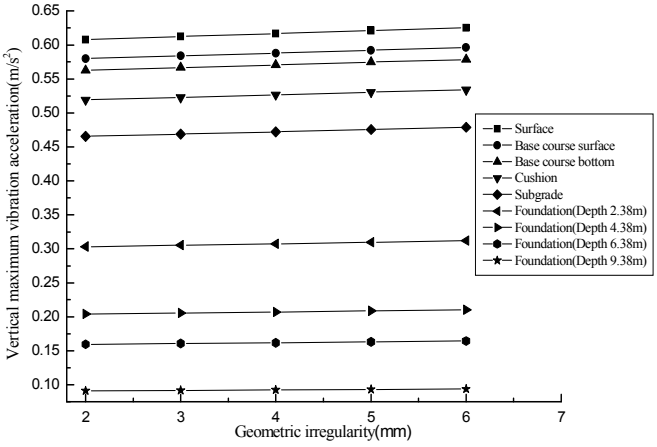

Fig. 7 The vertical maximum vibration acceleration in different geometry irregularities

The Influence of Geometry Irregularities. With geometric irregularities or planeness index increasing, the vertical maximum acceleration and the maximum dynamic stress increases as shown in Fig. 7 and Fig. 8. The calculation results show that the acceleration will increase about $0.01m/s^2$ when the planeness index increase 1mm. For highway, because the driving speed and bearing capacity increase, it more should strictly control the planeness.

The Horizontal Distribution of Dynamic Response. Fig. 9 shows that with the increase of horizontal distance to point of load application, the vertical maximum acceleration attenuate quickly, and vehicle loading has a certain influence range.

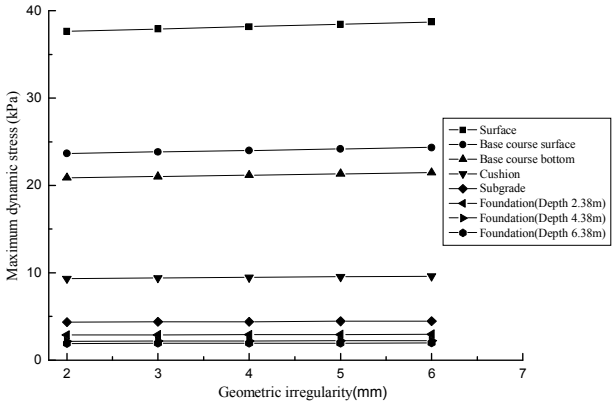

Fig. 8 The maximum dynamic stress in different geometry irregularities

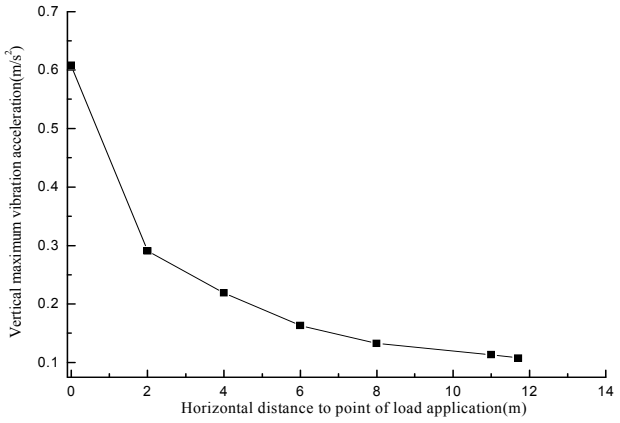

Fig. 9 The horizontal distribution of the vertical maximum vibration acceleration

Conclusions

Through numerical analysis, the vibration response of highway is discussed under traffic load. It is concluded that design parameters of each part of highway will influence the size of the dynamic response, reasonable matching parameters is very important. At present, the international highway planeness index is 2mm, but it is difficult to achieve in practical engineering, many highway engineering workers are researching from construction technology and theory, and many problems still don't get the fundamental solution.

References

[1] Toshlkazu Hanazato.J.of.Gev.Eng.ASCE. Vol.117 (1991), p.1133

[2] Lu Sun, Xuejun Deng. J. of southeast university. Vol. 26 (1996), p.143, in Chinses.

[3] Yan Zhong, Zheren Wang. China Journal of Highway and Transport. Vol. 5 (1992), p.40, in Chinses.

[4] Jingjie Zheng, Yaojun Li. Central South Highway Engineering. Vol. 24 (1999), p.8, in Chinses.

[5] Wenha Zha, Baoning Hong. J. of Wuhan University of Technology,Vol. 33(2009), p.600, in Chinses.

[6] Hui Lu, Lijun Sun. Sahnghai highway, No.1 (2009), p. 6, in Chinses.

[7] Changshi Pan: *Tunnel mechanics mumerrical method* (China Railway Publishing House, China 1955).

[8] Hongqing Wu, Xia Ren: *The Steuctural Finite Eelement Analysis* (China Railway Publishing House. China 2000).

Applied Mechanics and Materials Vols. 97-98 (2011) pp 60-68

doi:10.4028/www.scientific.net/AMM.97-98.60

Research on Load Transfer of Continuously Reinforced Concrete Pavement with Hollow Foundation

Xiaobing Chen[1,a], Xiaoming Huang[1,b] and Jinhu Tong[1,c]

[1]School of Transportation, Southeast University, 2 Si Pai Lou, Nanjing, Jiangsu 210096, P.R. China

[a]xbchen@seu.edu.cn, [b]huangxm@seu.edu.cn, [c]101010035@seu.edu.cn

Keywords: CRCP, Hollow foundation, Concentrated vehicle load, Equivalence principle, Half-wave sine load, Load transfer.

Abstract. Based on the equivalence principle of bending deflection and torsional displacement, the concentrated vertical load which acts on the center of continuously reinforced concrete pavement (CRCP) is translated into the equivalent half-wave sine load by Fourier transform. On the basis of this transform and deformation harmony condition of crack, the equations of load transfer are established. According to the translation principle of the force, the equations of load transfer of adjacent slabs are worked out. With the small deflection theory of elastic thin slabs, the bending deflection and torsional displacement formulas of CRCP under the concentrated vertical load with hollow foundation are deduced, which is verified by the results of finite element(FE). The results show that the characteristic of CRCP after cracking is related to the rigidity factor which is proportional to the spacing of adjacent cracks and the width of CRCP.

Introduction

CRCP is a rigid pavement structure which is constructed with no preventive measures for transverse expansion or contraction joints. It is a form through which the weak links such as horizontal joints of cement concrete pavement expansion and contraction joints are avoided [1,2]. The superiority of CRCP is shown under some special conditions (such as overloaded traffic, heavy traffic, uneven settlement and poor hydrogeological conditions).

After construction, the early transverse cracks of slab are caused by the combined effect of temperature decreasing and dry shrinkage. As time goes by, the cracks become stable. The general crack spacing is within the range of 1 to 2.5 meters [3,4]. Under the repeated vehicle and environmental loads, the cracks become wider and the spalling of CRCP appear. The water entering through cracks will cause basal hollow and the load transfer efficiency (LTE) decreases. The crack LTE directly affects the service behavior of CRCP. For a long time, the phenomenon of hollow foundation is quite common. It has become one of the important factors that influence the usage life of cement concrete pavement [5,6]. So, the research of LTE of CRCP with hollow foundation has practical significance.

Recent study shows that the temperature of the CRCP has little influence on LTE of CRCP [7]. Therefore, the calculation model of longitudinal continuous elastic hinged slab is established according to practical situation of separated CRCP slabs under the concentrated vertical loads firstly. Secondly, the rules of LTE between slabs under concentrated vehicle loads are analyzed. Finally, the bending deflection and torsional displacement formulas of CRCP under the concentrated vertical load with hollow foundation are deduced.

Basic Theory and Differential Equations

Basic Theory. After construction, the early transverse cracks of the slab are caused by the combined effects of decreasing temperature and dryness shrinkage. Under the repeated vehicle and environmental loads, the cracks become wider and the spalling of CRCP appear. The water entering through cracks will cause basal hollow and the LTE decreases [8]. Compared with the cross-section area of the slab, the area of steel reinforcement is very small (0.6-0.8%) and the rigidity is rather low. Therefore, crack can be regarded as a hinge. As time goes by, the LTE decreases. The calculation model of CRCP can be regarded as a longitudinal continuous elastic hinged slab.

For a piece of CRCP slab under load P which is cracking because of combined effect of temperature contraction and shrinkage(Fig. 1(a)), when slab 1# is subjected to load P, in addition to its own deformation of transverse deflection, other slabs will also bend correspondingly(Fig. 1(b)). This is because of the load transferring action of internal forces that longitudinal reinforcements in each crack between slabs bear. In general case, internal forces induced by cracks include vertical shear $g(x)$, transverse moment $m(x)$, transverse shear $t(x)$ and normal force $n(x)$ (Fig. 1(c)). When CRCP slab is primarily applied vertical wheel load, the effect of transverse shear $t(x)$ is minimum when compared with normal force $n(x)$ and vertical shear $g(x)$. And the joint of crack can be usually regarded as a hinge approximately. Therefore, the effect of longitudinal moment to transferring load is little. It also can be left out. In this way, it is considered that the crack only transfers vertical shear $g(x)$ under vertical wheel load. This is the assumed premise of calculated theory of longitudinal continuous hinged slab.

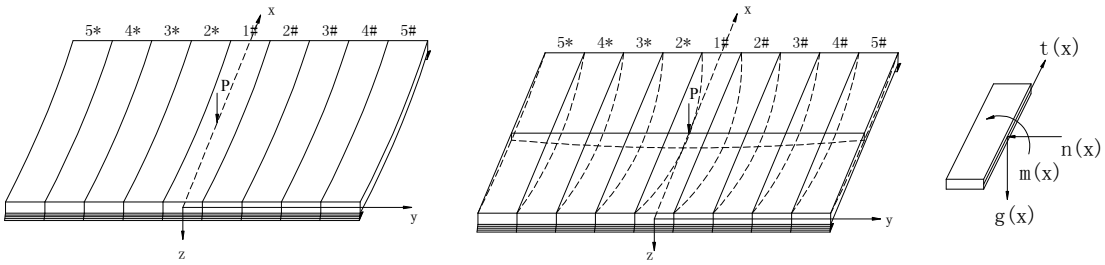

(a) Slab under the concentrated load (b) Deformation under the concentrated load (c) Internal forces in crack

Fig. 1 Continuously Elastic Thin Slab Subjected to Concentrated Vehicle Load

Equivalent Load Transform

The Methods of the Load Transform. With the Fourier transform, the concentrated vehicle load acting on the slab 1# is expanded as a half-wave sine load with peak load p_0.

$$p(x) = \frac{p_0}{l_d} \sin \frac{\pi x}{B}. \tag{1}$$

where p_0 is the maximum value of sine curve load, l_d is the distance between adjacent cracks, B is the slab width, x is the transverse distance from the edge of the slab($0 \leq x \leq B$). After the balanced load transform, the load pattern on the slab is shown in Fig. 2.

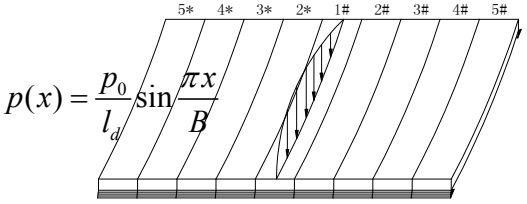

Fig. 2 Continuously Elastic Thin Slab Subjected to the equivalent Half-wave Sine Load

The Equivalency of Load Transform. As $0 \leq x \leq B$, Eq. 1 satisfies Dirichlet conditions [9]. Then, Eq. 1 is equal to P within $0 \leq x \leq B$.

Analysis of Longitudinal Load Translation

The Equation of the Longitudinal Load Translation.

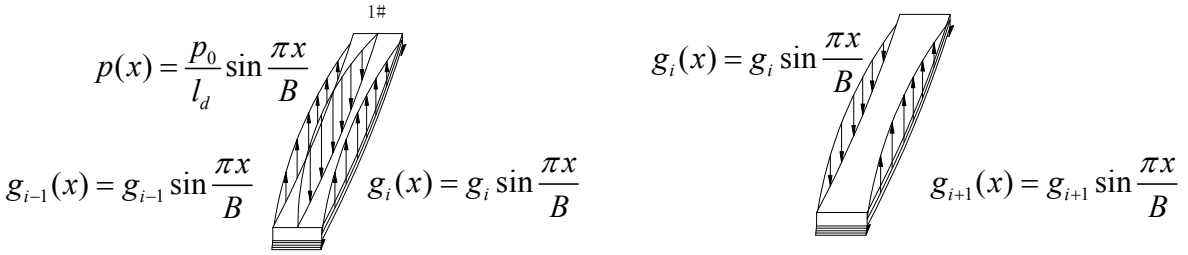

(a) Vertical Force of Slab with external load (b) Vertical Force of Slab without external load

Fig. 3 Vertical Force of Slab Subjected to the Half-wave Sine Load

Under the sinusoidal load $p(x)=(p_0/l_d)\sin(\pi x/B)$ (Fig. 3(a)), half-wave sine force $g_i(x)=g_i\sin(\pi x/B)$ is produced in each crack(Fig. 3(b)). In order to study relative rules of distributed load in each slab conveniently, unit length of cutting cross-section in the middle of slab is analyzed and the vertical force between adjacent slabs is represented by the peak of half-wave sine load.

Fig. 4(a) presents longitudinal section of continuous elastic hinged slab. When 1# slab is subjected to unit sinusoidal load on the axis, corresponding load is also produced in other slabs, as shown in Fig. 4(b).

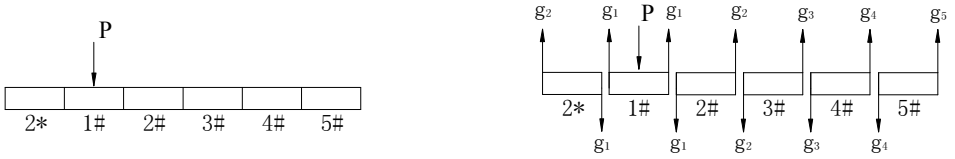

(a) concentrated load on the middle of 1# slab (b) load distributionofevery slab

Fig. 4 Calculation Model of Continuously Elastic Thin Slab

For m pieces of CRCP slab connected by (m-1) transverse cracks, a couple of half-wave sine loads which are opposite in direction and equal in magnitude is applied in each transverse crack. So, for m pieces of slab, there are (m-1) peaks of unknown vertical load g_i needed to be worked out. If each g_i is worked out, the peak of vertical load p_{i1} distributed in each slab can be obtained according to equilibrium principle of force. Considering that the sizes of the structure, load and boundary condition of CRCP are symmetric about 1# slab, we can analyze the load transfer using the half of the CRCP. As shown in Fig. 4(b). The load transfers between 1#、2#、3#、4# and 5# are written as:

$$\left.\begin{array}{l} 1\#\text{slab}\ \ p_{11}=1-2g_1 \\ 2\#\text{slab}\ \ p_{21}=g_1-g_2 \\ 3\#\text{slab}\ \ p_{31}=g_2-g_3 \\ 4\#\text{slab}\ \ p_{41}=g_3-g_4 \\ 5\#\text{slab}\ \ p_{51}=g_4-g_5 \end{array}\right\} \tag{2}$$

According to the principle of force method, the peak of half-wave sine load g_i can be worked out. Since 5# slab is relatively far from 1# slab, it can be assumed that g_5 is much less than g_1 and its effect can be ignored. Thus, the equation can be presented as follows:

$$\left.\begin{array}{l} 1\#\text{slab}\ \ p_{11}=1-2g_1 \\ 2\#\text{slab}\ \ p_{21}=g_1-g_2 \\ 3\#\text{slab}\ \ p_{31}=g_2-g_3 \\ 4\#\text{slab}\ \ p_{41}=g_3-g_4 \\ 5\#\text{slab}\ \ p_{51}=g_4 \end{array}\right\} \tag{3}$$

Eq. (3) is a statically indeterminate problem with (m-1) unknown vertical forces. Obviously, for (m-1) transverse cracks, each crack can be divided into a fundamental system. When taking advantage of deformation compatibility condition that vertical relative displacement of two adjacent slabs is zero at the place of transverse crack, all peaks of vertical force can be worked out. Thus, for the fundamental system in Fig. 4(b), four canonical equations are presented as follows:

$$\left.\begin{aligned}
&\delta_{11}g_1+\delta_{12}g_2+\delta_{13}g_3+\delta_{14}g_4+\delta_{1p}=0\\
&\delta_{21}g_1+\delta_{22}g_2+\delta_{23}g_3+\delta_{24}g_4+\delta_{2p}=0\\
&\delta_{31}g_1+\delta_{32}g_2+\delta_{33}g_3+\delta_{34}g_4+\delta_{3p}=0\\
&\delta_{41}g_1+\delta_{42}g_2+\delta_{43}g_3+\delta_{44}g_4+\delta_{4p}=0
\end{aligned}\right\} \tag{4}$$

Where δ_{ik} presents vertical displacement at the place of crack i caused by the unit sinusoidal vertical force in transverse crack k, δ_{ip} presents vertical displacement caused by external load p at the place of crack i.

Load Distribution Subjected to Single Load. In order to ascertain the constant coefficient δ_{ik} and δ_{ip} in canonical Eq. (4), we can study the typical circumstance that unit sinusoidal vertical force is applied on left crack of arbitrary slab as shown in Fig 5(a). Fig. 5(b) presents the unit length of cutting-cross section. For the slab whose transverse direction is approximately rigid, eccentric unit half-wave load can be decomposed into sinusoidal vertical load and sinusoidal torsion acting on centre according to load transferring principle[10]. Fig. 5(c) demonstrates relevant peak g_i and $m_1=l_d/2$ applying on span centre. If the deflection of span centre caused by unit central vertical load is w, angle of span centre caused by sinusoidal torsion is φ, and the overall deflection in left side of slab is $w+l_d\varphi/2$, the overall deflection in right side is $w - l_d\varphi/2$, as shown in Fig. 5(d).

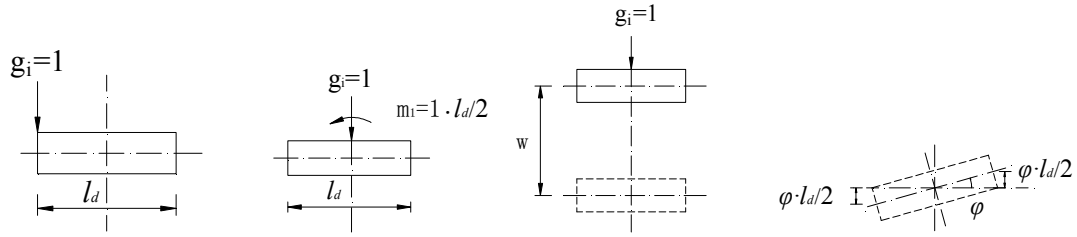

(a) unit half-wave sine load (b) the translation of load (c) the deflection affected by unit load (d) the tortion affected by unit load

Fig. 5 Deformation of Slab Subjected to the Half-wave Sine Load Acting on the Transverse Crack

As for this fundamental system shown as Fig. 5(b), all δ_{ik} and δ_{ip} can be presented by w and φ according to this typical deformation principle. The following stipulation of character should be obeyed: the positive is used when the transverse displacement is enlarged by the deflection and negative is used when the transverse displacement is reduced by the deflection. In other words, positive is used when the directions of δ_{ik} and δ_{ip} show no difference. According to the principle shown above, the constant coefficients of canonical Eq. (4) are written as:

$$\left.\begin{aligned}
&\delta_{11}=\delta_{22}=\delta_{33}=\delta_{44}=2(w+l_d\varphi/2)\\
&\delta_{12}=\delta_{23}=\delta_{34}=\delta_{21}=\delta_{32}=\delta_{43}=-(w-l_d\varphi/2)\\
&\delta_{13}=\delta_{14}=\delta_{24}=\delta_{31}=\delta_{41}=\delta_{42}=\delta_{2p}=\delta_{3p}=\delta_{4p}=0\\
&\delta_{1p}=-w
\end{aligned}\right\} \tag{5}$$

Substitute the coefficients above into Eq. (4) to make all equations divide by w, and assume the rigidity factor $\gamma=l_d\varphi/(2w)$, the canonical equation can be simplified written as:

$$\left.\begin{aligned} 2(1+\gamma)g_1 - (1-\gamma)g_2 &= 1 \\ -(1-\gamma)g_1 + 2(1+\gamma)g_2 - (1-\gamma)g_3 &= 0 \\ -(1-\gamma)g_2 + 2(1+\gamma)g_3 - (1-\gamma)g_4 &= 0 \\ -(1-\gamma)g_3 + 2(1+\gamma)g_4 &= 0 \end{aligned}\right\} \tag{6}$$

(M-1) simultaneous equations can be obtained when m slabs are considered. Its diagonal coefficients δ_{ii}/w are all 2(1+γ), minor coefficients δ_{ik}/w (k=$i\pm1$) are all -(1-γ), and others are all zero. Coefficient of items of load are -1 at the place of 1# slab, and others are zero. It is a typical sparse matrix, which can be solved by iterative method or cramer rule. The solution of Eq. (5) is obtained from:

$$\left.\begin{aligned} g_1 &= \frac{4\gamma^3+28\gamma^2+28\gamma+4}{5\gamma^4+60\gamma^3+126\gamma^2+60\gamma+5} \\ g_2 &= \frac{-3\gamma^3-7\gamma^2+7\gamma+3}{5\gamma^4+60\gamma^3+126\gamma^2+60\gamma+5} \\ g_3 &= \frac{2\gamma^3-2\gamma^2-2\gamma+2}{5\gamma^4+60\gamma^3+126\gamma^2+60\gamma+5} \\ g_4 &= \frac{-1}{5\gamma^7+45\gamma^6-39\gamma^5-143\gamma^4+143\gamma^3+39\gamma^2-45\gamma-5} \end{aligned}\right\} \tag{7}$$

Therefore, after the rigidity factor γ is confirmed, 4 peaks of unknown vertical forces g_i in the cracks of Eq. (6) can be solved. Then peaks of distributed vertical load in each slab subjected to vehicle load can be obtained from Eq. (3).

Calculation of deflection, torsional angle and rigidity factors

The Deflection.

The foundation of CRCP between adjacent cracks is hollow and other parts are coupling. According to the basic assumptions of elastic thin slab and the balance of internal forces and loads, the deflection differential equation of elastic thin slab is calculated as follows [1].

$$D_x\nabla^2\nabla^2 w = P(x)\,. \tag{8}$$

where w is the deflection of the slab, P is the concentrated load in the center of the slab, ∇^2 is Laplace operator, $\nabla^2 = \partial^2/\partial x^2 + \partial^2/\partial y^2$, D_x is transverse bending rigidity of the slab. $D_x = E_{csx}\, h^3/12(1-v_c^2)$, where E_{csx} is CRCP transverse elastic modulus [11], h is the thickness of the slab, v_c is Poisson's ratio of slab. The concentrated force in the slab is shown in Fig. 6.

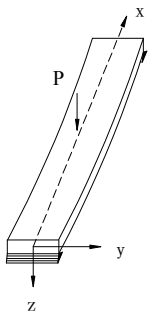

Fig. 6 Slab under the concentrated vehicle load

The moment and shearing force per unit width are given by

$$\begin{cases} M_x = -D_x(\dfrac{\partial^2 w}{\partial x^2} + v_c \dfrac{\partial^2 w}{\partial y^2}) \\ M_y = -D_x(\dfrac{\partial^2 w}{\partial y^2} + v_c \dfrac{\partial^2 w}{\partial x^2}) \\ M_{xy} = -D_x(1-v_c)\dfrac{\partial^2 w}{\partial x \partial y} \end{cases}. \tag{9}$$

Substituting the load transform of Eq. 1 into the elastic slab balance of Eq. 8, the new elastic thin slabs' differential equation of CRCP on a hollow foundation under the concentrated vehicle load is written as

$$D_x \nabla^2 \nabla^2 w = \frac{p_0}{l_d} \sin \frac{\pi x}{B}. \tag{10}$$

The right side item of the basic differential Eq. 10 is $p_0 sin(\pi x/B)/l_d$, and the left side item is $D_x(\partial^4 w/\partial x^4+2\partial^4 w/\partial x^2 \partial y^2+\partial^4 w/\partial y^4)$, which expresses the second-order and the fourth-order partial derivatives of w with respect to x and y. For the n-order derivative of $sinx$, When n is an even number($2k$,k=0,1,2……), $(sinx)^{(2k)}=(-1)^k sinx$. When n is an odd number($2k$+1, k=0,1,2……), $(sinx)^{(2k+1)}=(-1)^k cosx$ [12]. According to the character of these higher-order derivatives, w can be written as

$$w = (A_0 x^4 + A_1 x^3 y + A_2 x^2 y^2 + A_3 x y^3 + A_4 y^4 + A_5) \sin \frac{\pi x}{B}. \tag{11}$$

From the boundary conditions, when x=0, M_x=0, we have A_3=0. When x=0, M_{xy}=0, we have A_4=0. And when $y=l_d/2$, M_y=0, we have $A_0=A_1=A_2=0$. Where l_d is the distance of adjacent cracks.

Then putting A_0, A_1, A_2, A_3 and A_4 into Eq. 11, w can be simply written as

$$w = A_5 \sin \frac{\pi x}{B}. \tag{12}$$

Substituting the deflection of Eq. 12 into the elastic thin slabs differential Eq. 10, we have the following equation.

$$D_x w''''(x) = \frac{p_0}{l_d} \sin \frac{\pi x}{B}. \tag{13}$$

After the successive integration of Eq. 13, we can obtain the following equations.

$$D_x w''(x) = -\frac{p_0 B^2}{\pi^2 l_d} \sin \frac{\pi x}{B} + C_1 x + C_2. \tag{14}$$

$$D_x w(x) = \frac{p_0 B^4}{\pi^4 l_d} \sin \frac{\pi x}{B} + \frac{C_1 x^3}{6} + \frac{C_2 x^2}{2} + C_3 x + C_4. \tag{15}$$

According to the boundary conditions, we can obtain integral constants. As x=0, $w(x)$=0, we get C_4=0. As x=0, $w''(x)$=0, we get C_2=0. As $x=B$, $w(B)$=0, we have $C_1B^3/6+C_3B$=0, and with the condition $x=B$, $w''(B)$=0, we can simultaneously have C_1=0 and C_3=0.

By putting the coefficients $C_1=C_2=C_3=C_4$=0 into the Eq. 15, the deflection formula is written as

$$w(x) = \frac{p_0 B^4}{\pi^4 l_d D_x} \sin \frac{\pi x}{B}. \tag{16}$$

According to the equivalence of load transform, half-wave sine load will converge to P in the range $0 \leq x \leq B$. Calculating the definite integral of the half-wave sine load in this spacing, we have

$$P = \int_0^B \frac{p_0}{l_d} \sin \frac{\pi x}{B} dx = \frac{2B}{\pi l_d} p_0 . \tag{17}$$

$$p_0 = \frac{\pi P l_d}{2B} . \tag{18}$$

By putting Eq. 18 into Eq. 16, the slab deflection formula is written as

$$w(x) = \frac{PB^3}{2\pi^3 l_d D_x} \sin \frac{\pi x}{B} . \tag{19}$$

The Torsional Angle. According to the torsion theory of slab and the balance of internal forces and loads, the torsional differential equation of elastic thin slab is calculated as follows [13].

$$GI_T \varphi''(x) = -M_T(x) . \tag{20}$$

where G is the shear module of the slab, I_T is the moment of inertia of the slab, $I_T = l_d h^3/3$ [14], l_d is the spacing of adjacent cracks. φ is torsion angle of the slab. The torsion force in the slab is shown in Fig. 7.

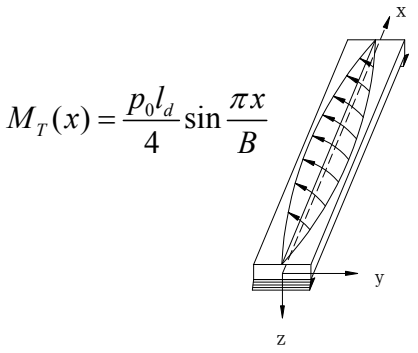

Fig. 7 Slab Subjected to Torsion Force Arousing by Half-wave Sine Load

The half-wave sine torsion force acting on the every slab is given by

$$M_T(x) = \frac{p_0 l_d}{4} \sin \frac{\pi x}{B} . \tag{21}$$

By putting Eq. 21 into Eq. 20, we have the slab torsional displacement formula under the concentrated vertical load.

$$GI_T \varphi''(x) = -M_T(x) = -\frac{p_0 l_d}{4} \sin \frac{\pi x}{B} . \tag{22}$$

After successive integral of Eq. 22, we can get equation as follows.

$$GI_T \varphi(x) = \frac{p_0 l_d}{4} \frac{B^2}{\pi^2} \sin \frac{\pi x}{B} + C_5 x + C_6 . \tag{23}$$

According to boundary conditions, we may obtain integral constants: ① as x=0, $\varphi(x)$=0, we may get C_6=0. ②as x=B,$\varphi(B)$=0, we may get C_5=0.

The equation of torsion angle is written as:

$$\varphi(x) = \frac{p_0 l_d B^2}{4\pi^2 GI_T} \sin \frac{\pi x}{B} = \frac{P l_d B}{8\pi GI_T} \sin \frac{\pi x}{B} . \tag{24}$$

Calculation of Rigidity Factors. Takinge advantage of Eq. 19 and Eq. 24, we have

$$\gamma = \frac{l_d}{2}\varphi / w = \frac{\pi^2 E_{csx}}{32G}(\frac{l_d}{B})^2. \tag{25}$$

As for a cement slab，when E_{csx}= E, G= 0.4E, and γ_c=0.2[15], we have

$$\gamma = \frac{l_d}{2}\varphi / w = \frac{\pi^2 E_{csx}}{32G}(\frac{l_d}{B})^2 \approx 0.771(\frac{l_d}{B})^2 \tag{26}$$

According to the method above, the all peaks g_i of known vertical forces acting on the crack can be solved when single load is applied on a slab after confirming the rigidity factor γ and quantity of slabs m. Then peaks P_{i1} of distributed vertical forces acting on each slab can be obtained from Eq. 3.

Rationality Verification of calculation results

Equivalence Verification of the Load Transform. For the same piece of the slab, the width B and bending rigidity D_x are constants. According to the nature of the derivative of trigonometric functions, the following formula is established.

$$\frac{w_1(x)}{w_2(x)} = \frac{\varphi_1(x)}{\varphi_2(x)} = \frac{P_1(x)}{P_2(x)} = \text{Constant}. \tag{27}$$

From Eq. 27, we can see that the rules for the change of loads, deflection and torsional displacement are consistent. It shows that the concentrated vehicle load on the slab can be replaced by the half-wave sine load through the Fourier transform. In this way, the analysis of the slab deflection, torsional displacement and rigidity factor is reasonable.

Rationality of assumption of solving equations. In order to solve equations conveniently, it can be assumed that vertical force is minor at the place of outboard of farthest slab, and it can be ignored. From the calculation result, we can see that the assumption is reasonable.

The comparative analysis between calculation results of equation and results of finite element. Using finite element software program of MIDAS CIVIL 2010 to analyze the deflection and torsion displacement, we can find that the result of equation calculation is a little larger than the result of finite element. The value of deflection is 5% bigger and the value of torsional displacement is 9% bigger. These two values are almost identical, and it demonstrates that the calculation result is reliable.

Conclusions

Based on the small deflection theory of elastic thin slab and the equivalence principle of deflection and stress, the concentrated vehicle load which acts on the center of CRCP can be translated into the equivalent half-wave sine load by the Fourier transform. On the basis of this transform, the CRCP load transfer formulas are put forward when subjected to a concentrated vehicle load with hollow foundation. The LTE of CRCP with hollow foundation after cracking is associated with rigidity factor. Rigidity factor is proportional to the square of crack distance. On the contrary, it is inversely proportional to the square of transverse width. The formulas and results given are reliable.

References

[1] X.J. Deng, X.M. Huang, in: Principles and Design Methods of Pavement, edited by Y.F. Liu, volume 7 of Design Method of Rigid pavement, chapter, 12, China Communications Publishers, Beijing, China (2007), p. 472-478(In Chinese).

[2] W. Huang, Z.D. Qian, in: Theory and Methodology of High-Class Concrete Pavement Design, volume 1 of Design of Continuously Reinforced Concrete Pavement, chapter, 4, China Communications Publishers, Beijing, China (2000), p.206-212(In Chinese).

[3] Ministry of Communications, in: Specification of Cement Concrete Pavement Design for Highway(JTG D40-2002), China Communication Press, Beijing, China (2003) (In Chinese).

[4] X.Y. Gu, Q. Dong and F.J. Ni: *Research on Crack Progression of Continuously Reinforced Concrete Pavement*, Journal of Highway and Transportation Research and Development, Vol. 6 (2007), p.37-40(In Chinese).

[5] AASHTO, in: Standard Specifications for Transportation Materials and Methods of Sampling and Testing, Washington DC: AASHTO(1989).

[6] M.I. Darter, J.M. Becker, M.B. Snyoer, et al. *Portland Cement Concrete Pavement Evaluation System(COPES)*, Washington DC: Transportation Research Board(1985).

[7] M. Won, C. Medina. In: Analysis of Continuously Reinforced Concrete Pavement Behavior Using Information in the Rigid Pavement Database. Austin, TX: Center for Transportation Research of the University of Texas at Austin(2008).

[8] Y.J. Jiang, X.Z. Dai, Z.D. Chen, et al. *Study on Mechanism of Cement Concrete Pavement Damage of Heavy—Duty Traffic Road and Countermeasures*, Journal of Highway and Transportation Research and Development, Vol. 7 (2005), p.31-35(In Chinese).

[9] Department of Mathematics of Tongji University, in: Higher Mathematics(Volume II), edited by S. Guo, volume 7 of Fourier Series, chapter, 11, Higher Education Press, Beijing, China (1996), p.293-309(In Chinese).

[10] Y.Z. Guo, Z.H. Zhou, in: Theoretical Mechanics, Tsinghua University Press, Beijing, China (2005), p. 12-15(In Chinese).

[11] X.Y. Wang, J.Y. Xiao, Y.Z. Tang et al, in: Mechanics Analysis and Design of Composites, edited by Q. Luo, volume 4 of Micromechanics of Composite Materials, chapter, 4, National University of Defense Technology Press, Changsha, China (1999), p.100-118(In Chinese).

[12] Department of Mathematics of Tongji University, in: Higher Mathematics(Volume I), edited by S. Guo, volume 5 of Higher Order Derivatives, chapter, 2, Higher Education Press, Beijing, China (1996), p.124(In Chinese).

[13] X.F. Sun, X.S. Fang and L.T. Guan, in: Mechanics of Materials, volume 7 of Stress and Deformation of Straight Bar with Uniform Cross Section Under Free Torsion, chapter, 3, Higher Education Press, Beijing, China (1990), p.132-133(In Chinese).

[14] M.Z. Wang, W. Wang and J.K. Wu, in: Theory of Elastic Mechanics, edited by S.Q. Qiu, volume 9 of Torsion of Rectangular Cross Section, chapter, 6, Peking University Press, Beijing, China (2002), p.146-150(In Chinese).

[15] Ministry of Communications, in: Code for Design Highway Reinforced Concrete and Prestressed Concrete Bridges and Culverts(JTG D62-2004), China Communication Press, Beijing, China (2004) (In Chinese).

Applied Mechanics and Materials Vols. 97-98 (2011) pp 69-72

doi:10.4028/www.scientific.net/AMM.97-98.69

The analysis and solvement of some geotechnical topics in post-disaster reconstruction highway

Hejun Chai [1, a], Changlin Zhang[1, b], Yunwei Meng [1, c] and Haiping Li [1, d]

[1] China Merchants Chongqing Communications Research & Design Institute Co., Ltd., Chongqing, 400067, China

[a]chaihejun@ccrdi.cmhk.com, [b]zhangchanglin@ccrdi.cmhk.com, [c]mengyunwei@ccrdi.cmhk.com, [d]lihaiping@ccrdi.cmhk.com

Keywords: Geotechnical Problems, Reconstruction, Landslide, Filling, Gabion Retaining Wall.

Abstract. The highway in earthquake region suffered serious damage during Wenchuan's Earthquake in 2008. In all projects of post-disaster reconstruction, the reconstruction of highway and making highway work once again are prerequisite. There are a plenty of rock fall, dangerous rock, landslide, and debris flow sections along the highway between epicenter areas Wenchuan County to Li County. Among the post-disaster reconstruction of the highway, efficiently solvement of these disaster or potential disaster is one of geotechnical engineering topics. Phyllite rock occurs in large number along the highway but is defective fillings. This kind of material if not made full used, it will be able to lead to filling shortage and environmental disruption. How to treat it as a resource for roadbed fillings is the second of the important geotechnical engineering topics in the highway reconstruction. There are many narrow sections along the highway, and Inside Mountain is not stable. Common anti-skating retaining wall is not fit the severe condition because of its basement dug being harmful for mountain slope steady. How to pass this kind of sections is also bottle neck technique. The above technical problems are analyzed and the relevant solutions are proposed. So the troubles are solved efficiently and the highway is open to traffic on schedule. The terms of settlement provide reference for similar highway reconstruction projects.

Introduction

Wenchuan earthquake of 512 brought a large-scale people and infrastructure in disaster area. In the disaster area transportation infrastructure construction extremities[1,2,3]. Wenchuan to Maerkang highway of National highway 317 is one of the most important channels in disaster areas, and the reconstruction of the quality after disasters will bring great influence on economic recovery. Among the highway, the section of Wenchuan to Li County will face a lot of problems because of the limit of complicated terrain, geological condition, hydrological conditions and local building materials. The geological disaster's understanding and reasonable avoid and control along the highway, a lot of phyllite rock defective fillings' use, narrow road unstable slope processing technology are main technical problems, will affect the traffic, roadbed quality and project cost. Therefore the above questions are studied by the numbers, and the corresponding technical measures are provided. This schedule of the road reconstruction project design provides the basis and guarantees the smooth progress of the highway reconstruction and open to traffic on time.

Understanding and management of geological disaster along the highway

The highway section of Wenchuan to Li County is typical mountainous area sitting near the hill and river. There are shallow metamorphic phyllite rock, schist rock and slate rock. Structure development and rock mass brokering because of structure influence. The highway is an area where geological hazards are widely distributed.

Before the earthquake, the geological disasters along the highway had been surveyed and evaluated detailed in two stages design. It shows in the investigation report that the landslides distributed in large area, which included 25 sections of unstable slopes as follows: 6 places super large-sized landslide, 8 places large-sized landslide, 7 places middle-sized landslide, 4 small-sized landslide,13

places debris flows, 25 places collapse(dangerous rock, rockfall, rock flake), 43 places roadbed subsidence and sink resulting from scouring rivers. After the earthquake of 512, new geological disaster occurred took a turn for the worse of existing disasters bodies because of it's located in epicentral area. It shows after earthquake that custom disasters bodies occurred as follows: 28 places slope collapse, 28 places slope fragment flow, 29 places slide and dangerous rock, 4 places debris flows and 1 induced landslide.

One of the difficult problems in design of the highway is how to recognize large-scale landslide, including landslide boundary condition, the design and calculation parameters of geotechnical engineering, the stability of the present situation, the suitability of route through, the stability of engineering construction disturbance and the suitable prevention and control of engineering.

In the study, it insisted that the engineering geological mapping, exploration, laboratory and field experiment and test, theoretical analysis and calculations, the combination of engineering experience, on the basis of understanding the mechanism of selection of appropriate models and methods of stability analysis, the scene of geological phenomena, test means and method of calculating the values of safety factor closely linked. Through the above studies it suggested that, the landslide along the highway has the characteristics of traction destroy. Excavation led to the crack in front of the local mountain, sliding surface, thereby cause the trailing edge cracking of the larger mountain range, and under the rainfall and infiltration of irrigation water from farmland and orchards, cause the formation of slope instability hazards, and even into the deep push landslide, threaten the safety of construction and operation of highway construction.

Based on the above understanding of landslide hazards sections, it takes three programs: (1) undisturbed or less disturbed of landslide: fine-tuning and relocation of near-river section, reserve heap space to avoid hazards caused by direct touch; (2) bypassing: bypassing or crossing by setting bridge or tunnel; (3) appropriate control project: in the condition of the terrain and economic constraints, the above two programs can not solve the serious disease point, it would choose hangar tunnel, open cut tunnel, or pre-reinforced slope (landslide) treatment technology.

One of the large-scale landslides is shown in Fig. 1, limited by the terrain, the route must through along the front by the landslide, and the landslide will be disturbed and the landslide must be treated.

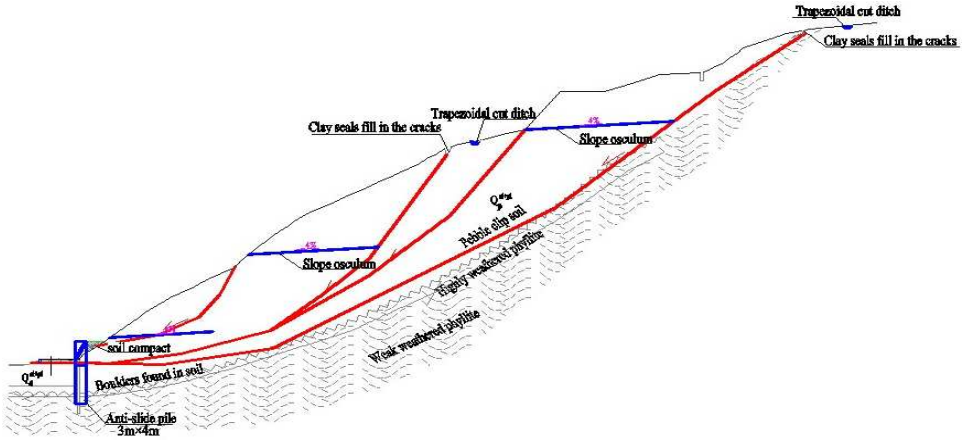

Fig.1 The design calculations and disposal sketch map of trail-type landslide

The landslide is traction mode from analysis. With the first crack face, shear parameters are obtained by parametric inversion, and the second cracking stage is the range of stability calculation. The calculation shows that slope safety margin is not enough, and need reinforcement. Set sliding pile before the foot of the slope and take back pressure 5m in height before the pile excavation. The excavation of sliding pile is by job-hopping. At present the treatment of the landslide has been completed. There are several landslides along the highway with a similar treatment methods and techniques to achieve the desired effect.

Through the application of the above understanding and results, cost-effective solutions are used to the disaster in Wenchuan to Li County landslide disasters.

The road performance and use technology of phyllite as filling

The main rock is phyllite, slate and schist, phyllite to the majority along the road. Tunnel excavation whole residue, a large number of earthquakes collapse talus slope excavation and a huge amount of disposable side exit in the area, while good filling along the road is not enough. If phyllite can be used as roadbed filler, the project can save a lot of engineering investment, and can bring considerable economic, social and environmental benefits; but phyllite is typical low-grade filler, rarely used at home and abroad as a subgrade filling. The reason is water stability and less wind resistance capabilities of phyllite, easily to soften after soaking, if used as subgrade, roadbed prone to uneven settlement, or settlement is too large and other diseases. Therefore, this study of phyllite road performance studies, according to the local topography, climate and geological conditions, proposed use of phyllite techniques and methods.

According to “soil test standards for highway”, sample from site was obtained and the heavy compaction test was performed, and the relation of dry density with moisture content variation was analyzed, and then the compaction properties of phyllite was studied.

It can be found from the compaction test results phyllite is similar to other soft rock, and phyllite is more sensitive to the moisture content. In low moisture content, particle surface water film is thin, friction large and difficult to compact. If the moisture content increased to the appropriate range, the particle surface water film thickness, lubrication effect, the friction decreases, making it easy to compaction. This feature is the same characteristics of soil compaction, and there exists an optimal moisture content and maximum dry density. As Fig. 2shows, the maximum compacted dry density is 2.19g/cm^3, optimum moisture content is 8%, and void ratio is small, so it shows phyllite has good compaction properties.

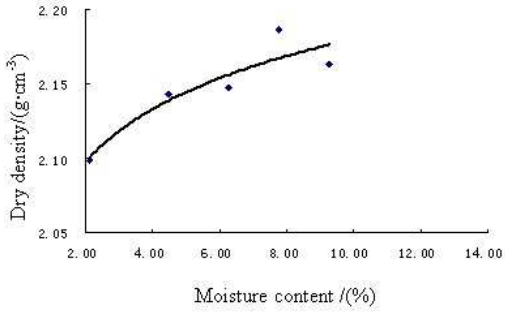

Fig. 2 The compaction test results of phyllite

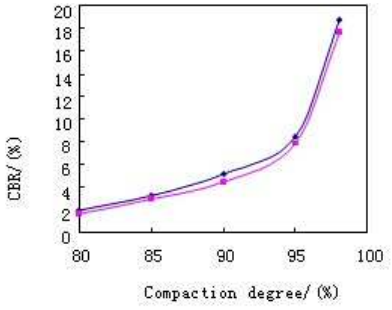

Fig. 3 The relation of compaction degree with

According to indoor compaction test results of phyllite, the specimens is prepared using the optimum moisture content and the capacity bearing ratio (CBR) test is performed. The material test results when penetration capacity is 5.0mm is shown as Table 1.

Table 1 The test results of CBR

Sample NO.	Dry density /g·cm^3	*CBR*	Swell increment/mm	Degree of free swelling /%	Compaction times
1	2.190	3.6	-	-	98
2	2.183	2.4	33.4	27.8	98
3	2.105	2.4	47.2	39.3	98
4	2.101	1.4	43.2	36.0	50
5	2.124	1.4	40.6	33.8	50

2 group specimens are collected from different levels of compaction, and the CBR test is performed. The curve of CBR results is obtained as shown in Fig. 3. CBR value increases with the increase of the degree of compaction.

As shown in Table 1, phyllite can not meet the filler strength requirements of 2nd more road bed, but meet the standard of "embankment under the CBR value of not less than 2%" of the requirement, which indicates that below 1.5m the top surface of the road bed phyllite embankment is available. In addition, CBR test results show that the CBR value of phyllite is generally low, although the embankment of the CBR value is met its close to the minimum specification value, indicating poor water stability of phyllite. If phyllite filling embankment is used, drainage must be strengthen.

The use of gabion retaining wall

There are a large accumulation of loose bodies and smaller less stable slopes along the road after the earthquake. Loose slopes are thick, and the roadbed in these areas is easily to touch the slope, which will slump and it needs to take engineering measures to reinforce. If the traditional sliding or weight-type retaining wall is used, the larger and deeper excavation pit be chosen to make the base is located in the high strength of the rock body, but which will be a wider range of slopes and even lead to instability . Therefore, the gabion retaining wall is used as these parts of the retaining structure. Gabions has many advantages compared with other structures, such as flexible, low bearing capacity of the foundation, uneven settlement of coordination ability and so on. This section has dry climate. The gabion retaining wall is piled up with phyllite stones. The gabion retaining wall is coordinated with the natural environment and beautiful appearance. At present, the construction of gabion retaining along the road has completed. A variety of diseases is solved and achieved good economic results.

Conclusions

The corresponding theoretical and applied physical engineering technology is obtained by analysis of some typical geotechnical problems along Wenchuan to Li County road. The technical problems are solved and reach the following conclusions.

The key of dealing with geological disasters in highway projects understands of the laws, which is based on field research, the phenomenon of deformation and failure, and the comparative analysis of prototype with similar projects or the natural one.

Poor filling material can be used under some special conditions. In the premise of full awareness of its road performance and the impact factor, its deterioration factors can be eliminated. The poor filling can be used for filling certain parts of the embankment to reduce the debit and abandoned volume, protect the environment and save project cost.

Gabion retaining wall has advantages such as adaptability, uniformity of bearing capacity and low demand from local materials, etc. it can be in widely used in mountain road slope protection and retaining engineering.

References

[1] Hongming Wang, Wei Wu: Investigation and Analysis of Road Traffic Accidents after"5.12"Wenchuan Earthquake [J]. Journal of Chongqing Jiaotong University (Natural Science), 2010, 29(3): 433-436. (in Chinese)

[2] Runqiu Huang, Weile Li: Research on Development and Distribution Rules of Geohazards Induced by Wenchuan Earthquake on 12th May, 2008[J]. Chinese Journal of Rock Mechanics and Engineering, 2008, 27(12): 2585-2592. (in Chinese)

[3] Heping Xie, Jianhui Deng, Jiajia Tai, et al: Wenchuan Large Earthquake and Post-earthquake Reconstruction-related Geotechnical Problems [J]. Chinese Journal of Rock Mechanics and Engineering, 2008, 27(9): 1781-1791. (in Chinese)

Applied Mechanics and Materials Vols. 97-98 (2011) pp 73-77

doi:10.4028/www.scientific.net/AMM.97-98.73

Numerical Simulation Study on Superposed Combined Exterior Protected Structure

Xiao-xin Yan[a], Zong-ming Li[b], Yue-hua Chu[c]

North China University of Water Conservancy and Electric Power, Zhengzhou 450045, China

[a] yanxiaoxin@ncwu.edu.cn [b]lizongming@ncwu.edu.cn [c]Angel5301@163.com

Keywords: the underground diaphragm wall; horizontal displacement; monitor; superposed combined exterior protected structure; a flexible spring support system.

Abstract: In this article, the waterproof curtain, the underground diaphragm wall and the soil between them are regarded as superposed combined exterior protected structure, then build a flexible spring support system. When using senior ANSYS finite element analysis program to simulate the strained condition and displacement of the underground diaphragm wall, we will combine with the monitoring result and the result of traditional comouting method. After contrasting, we can get a conclusion: the strained condition and displacement of the wall of this simulation method are more coincident with practical projects, and can reduce unnecessary waste.

Introduction

As these factors that influence the deformation of diaphragm wall have much indeterminacy, the calculation result of diaphragm wall also has much indeterminacy. By campareing the calculation result of trandational software with monitoring results in practical engineering, it can be seen that trandational software is always too conservative and this leads to a lot waste. In order to induce cost of construction and avoid unnecessary input, in this article, ANSYS, senior finite element program, is used to optimize methods of calculating and put forward a new simulation method which is more practical, by comparing with monitoring deformation results in practical engineering and results of trandational methods.

General situation of the projict

The proposed building has a super high-rise buildings of 36 floors and a podiums of 4 floors. The super high-rise building of 36 floors is a frame-tube structure. There are three layers of the basement, about 15.2m deep. As the surrounding environment and ground are complex, many structures need to be protected, and the excavation is deep, so the degree of protection of the foundation pit is one.

According to the working drawings, we select a typical section. Through this section, we can see that there are three internal supports, the first 1.6m away from the ground, the second 8m. the third 13.6m.

A brief introduction of ANSYS

ANSYS, senior finite element program, by modeling, meshing, loading, solving, post processing and other steps, scatter the whole into a system of equal value, build several equilibrium equations, then combine them together, import boundary conditions, and finally get the solution at the discrete points of quondam structure[1]. In this article, we use ANSYS, senior finite element

program, to imitate and analyse the way in which the underground diaphragm wall and the soil word together, to calculate the displacement of the diaphragm wall under soil pressure and upper loads. Then compare the result with monitoring deformation results, in order to study about new method to imitate and calculate diaphragm wall.

3. Imitating and calculating of ANSYS and comparin

3.1 Calculating model and important parameter

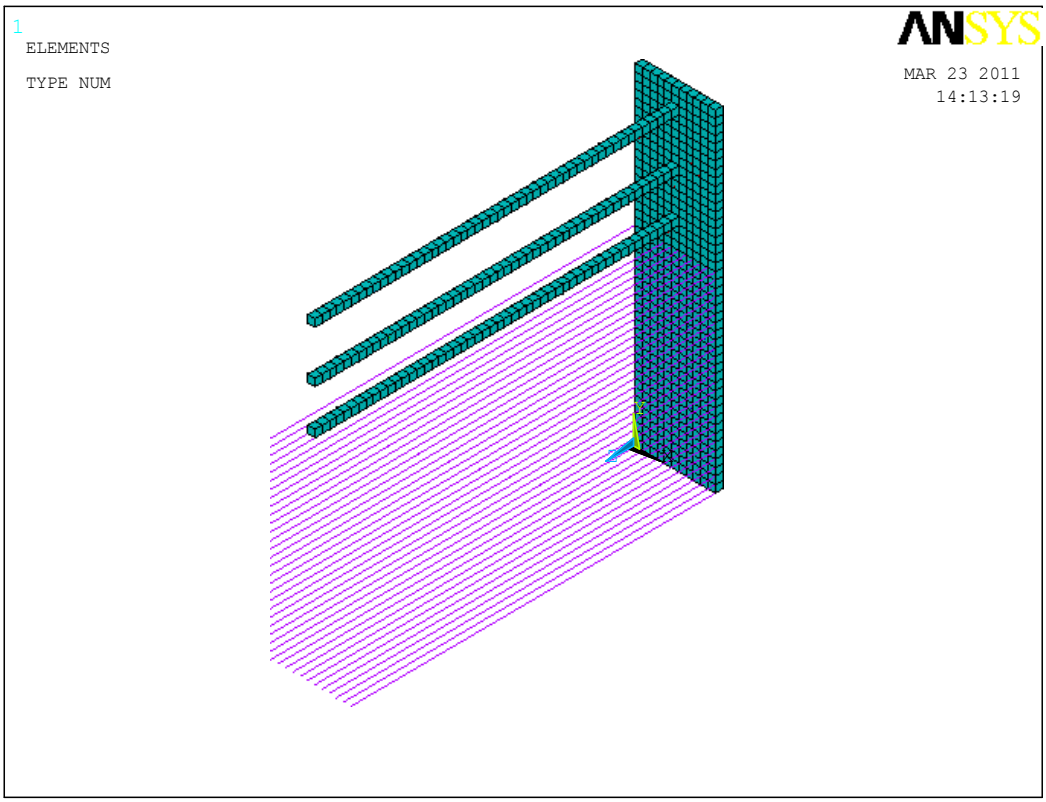

Photograph 3-1 Calculating model of diaphragm wall of ANSYS

According to the practical condition of the project, to simplify the model, we select a half structure to model. The diaphragm wall is 36m deep, 0.8m thick, and is imitated by element solid 45. Three internal supports are imitated by element solid45 too. Solid inside are imitated by element combin14. Rigidity of the springs[2] can be got by the formula below：

$$k = \frac{bE_0}{(1-\lambda^2)\omega} \tag{1}$$

In the formula, b stands for space between springs, ω is a coefficient concerned with shape, and when $b/d = 1.0$ (d is the width of foundation beam), ω =0.88. E_0 is the modulus of deformation of soil, and λ is Poisson's Ratio.

3.2 Cloud picture of horizontal displacement and analysis of diaphragm wall.(photograph 3-2 to 3-6)

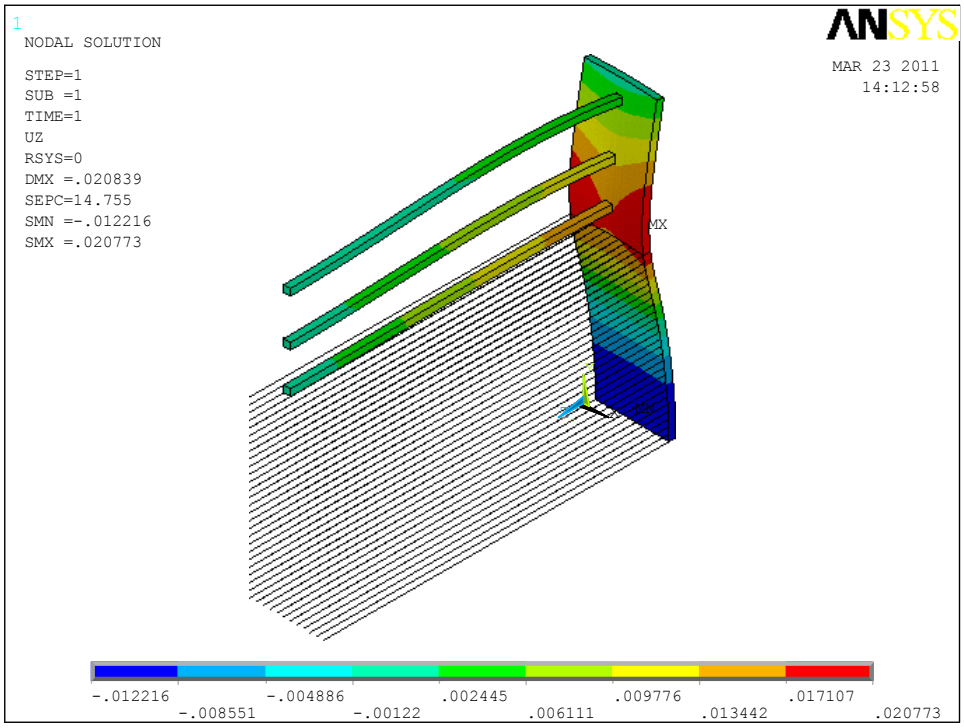

Photograph 3-2 Could picture 1 of horizontal displacement of diaphragm wall

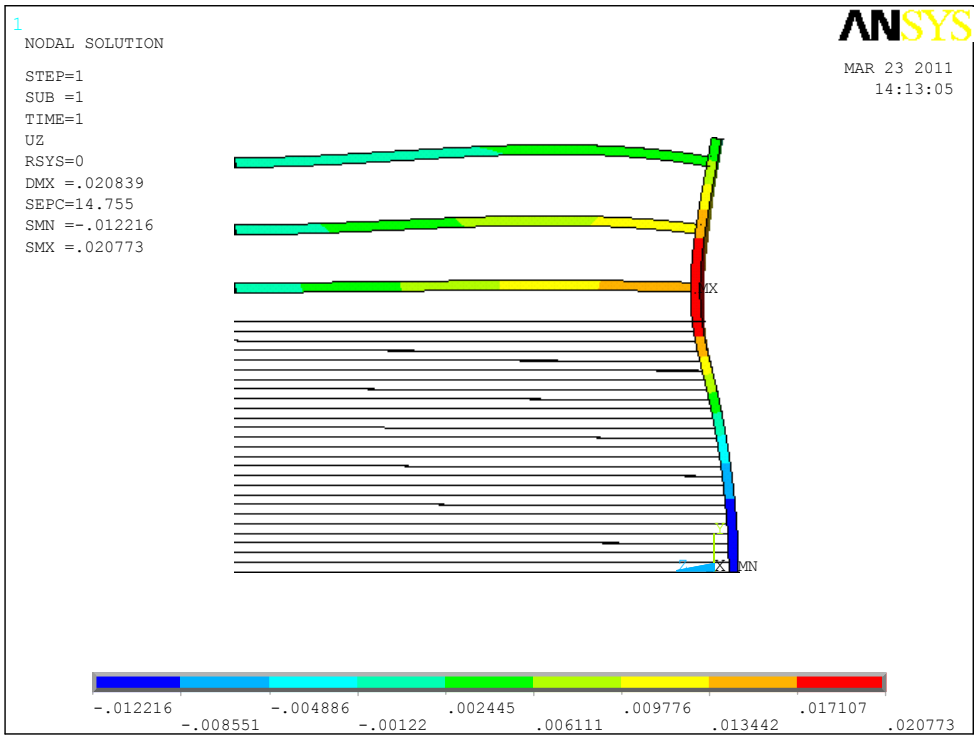

Photograph 3-3 Could picture 2 of horizontal displacement of diaphragm wall

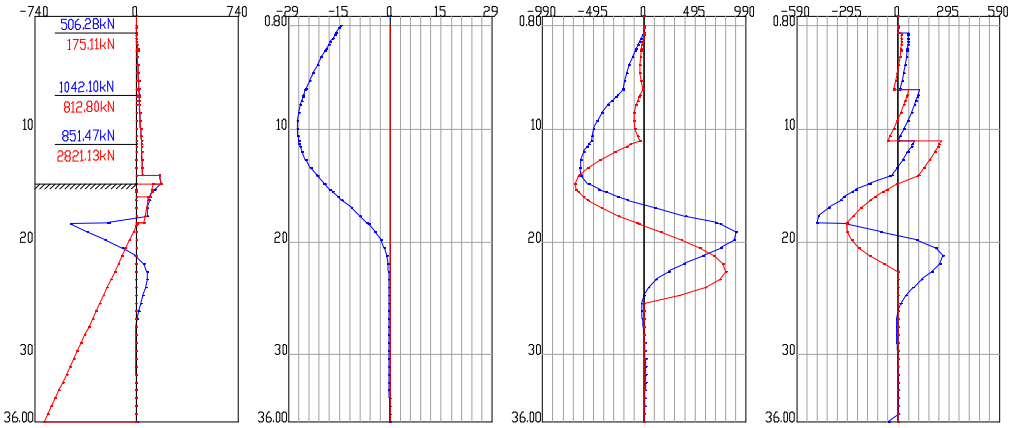

Photograph 3-4 Horizontal displacement of diaphragm wall of traditional method

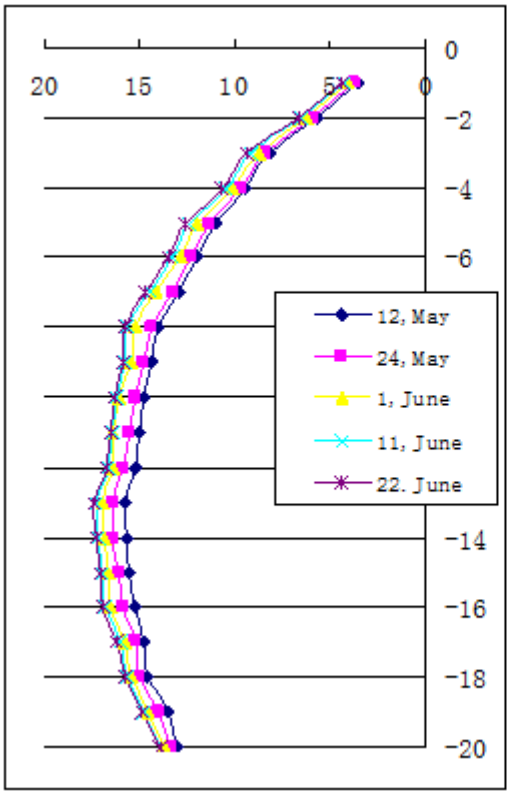

Photograph 3-5 Monitoring values of horizontal displacement of diaphragm wall

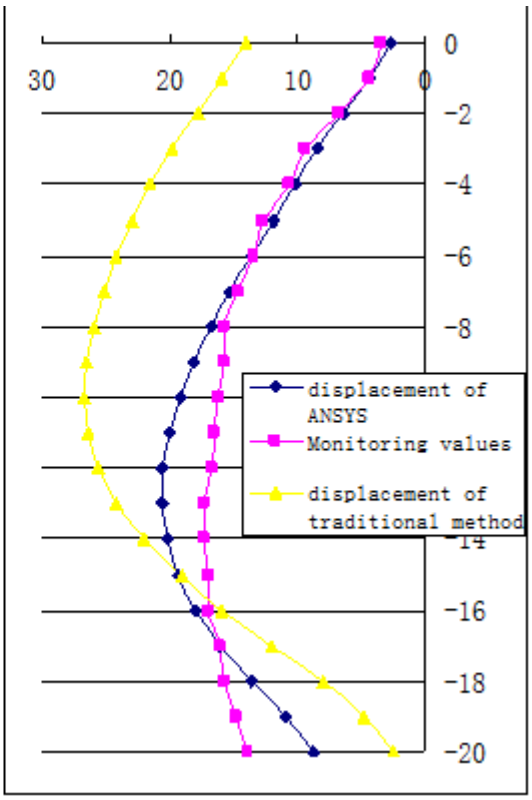

Photograph 3-6 Comparison of horizontal displacement of diaphragm wall

According to the monitoring values of different times, we can get a photograph as 3-5. Then we compare the monitoring values at June 22 with results of traditional method and of ANSYS. The results are in photograph 3-6.

From photograph 3-2,3-3 we can know that, when adopting ANSYS, senior finite element program, the maximum displacement of the diaphragm wall is 20.73mm, deformation towards internal foundation pit, at the point of 13m underground; when adopting traditional method, the maximum is 26.76mm, at the point of 10m underground; actually, it's 17.39mm at 13m undergroud. And from photograph 3-6, we can see that it's much more approximate with actual monitoring values when adopting ANSYS to imitate and calculate.

Conclusion

When using traditional motheds to design and calculate the displacement of diaphragm wall, the results is always too bigger than actual monitoring values. This leads to much unnecessary waste. ANSYS senior finite element program can imitate the project and the stress of diaphragm wall better. The diaphragm、the water protecting curtains and the soil between them are seen as a integral flexibility structure. At the ame time, soil spring element has approximate properties with soil, and according to formula 1, we can get different spring rigidityies of different soil layer. These make ANSYS a better way to imitate displacement of diaphregm wall. The results including maximum and regular pattern are more approximate than traditional mothed. By this way, we can save investment as much as possible.

References

[1] Xu Fengnian,Chen Shenghong. Development and existing problems in reinforce technology of geotechnical prestress anchor rod Water Conservancy and Hydroelectric Power News 2001, 22(10).

[2] Lu Shen. Study of support technique for deep excavation in subway station of substep excavation and support. Zhejiang University 2005

Applied Mechanics and Materials Vols. 97-98 (2011) pp 78-84

doi:10.4028/www.scientific.net/AMM.97-98.78

Study on Stability of High Embankment with Strong Weathering Filling under Complicated Stress Conditions

Shengchuan Liu

Research Institute of Highway Ministry of Transport, Beijing 100088, China

liushengchuan@126.com

Keywords: strong weathering filling; high fill embankment; stability; three-dimensional finite element; strength reduction method

Abstract: Strength reduction elasto-plastic finite element analysis defines the reduction factor when slope has been destroyed as the slope stability factor of safety, which combines with strength reduction technique, the limit equilibrium theory and the principle of elastic-plastic finite element. Three-dimensional finite element analysis should be used in stability analysis of slope because it can overcome the short advantages of two-dimensional finite element and can simulate the complex topographic and geological conditions. Based on the large-scale triaxial shear test, the modified Duncan-Chang model is established. Based on strength reduction elasto-plastic finite element, stability of high fill embankment was studied with three-dimensional finite element method considering the complex terrain conditions. Study results suggest that plastic strain and displacement mutant of slip surface node can be a sign of slope instability as a whole. At the same time calculation of three-dimensional finite element also does not converge. Therefore, it can be slope instability criterion calculate whether the finite element static analysis converges or not. On the other hand, stability safety factor of high fill embankment under three-dimensional conditions is larger than that of two-dimensional conditions, which shows that boundary conditions of high fill embankment enhance its stability.

Introduction

Compared to the traditional limit equilibrium method, finite element method not only satisfies the force equilibrium conditions but also considers the material stress-strain relationship. The calculation does not need to make any assumptions so that it can automatically obtain the critical slip surface and the corresponding minimum safety factor, which also can reflect the slope instability and the plastic zone. Therefore its application in slope stability analysis gets attention. Strength Reduction Elasto-plastic finite element is a method that combined with the strength reduction technique, the limit equilibrium theory and the principle of elastic-plastic finite element, which firstly determine the stress, strain or displacement field of slope for a given strength reduction factor. Then it takes numerical calculations to get distribution of stress, strain or displacement and characteristics of finite element calculation through increasing the discount factor until the analysis shows that these characteristics of unstable failure occur based on the results. And the reduction factor is defined as the slope stability safety factor.

Many scholars have done a lot of work. Ugai (1989) assumed that the soil is ideal elastic-plastic material and used strength reduction finite element method to make more systematic study on the stability of vertical slope, inclined slope, non-homogeneous slope and complex slope with pore water pressure[2]. He thought that elastic strength reduction finite element method has strong adaptability. Ugai and Leshchinsky (1995) took the strength reduction technology into the elastic-plastic finite element method for the stability analysis of three-dimensional slope [3]. And

they also made more comprehensively comparative study with the results of limit equilibrium calculations. Although both the theoretical basis and achieving means were completely different, the results of strength reduction plastic finite element method were still close to that of the limit equilibrium method with the astonishing same effect which implied that the strength reduction finite element method is credible. Domestic scholars Song Erxiang (1997) used strength reduction method for the slope stability analysis and determined the displacement of certain slope part as the convergence indicator [8].

Large-scale triaxial shear test

Since the triaxial apparatus can be static and dynamic loading, the control specimen drainage conditions, the stress in the specimen is relatively clear, the energy measure pore water pressure, etc., it is widely used, is the most important geotechnical laboratory testing instruments. Most used in engineering practice in the constitutive model, the model parameters are determined from the triaxial tests. For particle size larger coarse-grained soil, the test must be carried on in a large triaxial apparatus.

Triaxial test apparatus is the SJ-70 large-scale high-pressure triaxial apparatus, where the axial maximum output is 250T and the maximum confining pressure is 7MPa. Sample diameter is 300mm and its height is 700mm which dry density is 1.75 g/cm^3.

The relation curve of the main stress difference $(\sigma_1-\sigma_3)$ with the axial strain ε_1 is shown in Fig.1.

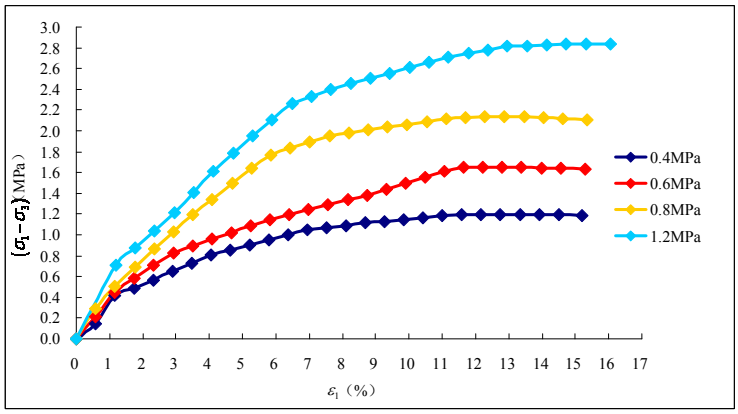

Fig.1 Relation curve of the main stress difference $(\sigma_1-\sigma_3)$ with the axial strain ε_1

Failure stress test results are obtained as shown in Table 1.

Table 1 Failure stress test results of different confining pressures

confining pressures（MPa）	0.4	0.6	0.8	1.2
failure stress（MPa）	1.197	1.653	2.14	2.838

By the Eq.1:

$$\varphi=\sin^{-1}\left(\frac{\sigma_1-\sigma_3}{\sigma_1+\sigma_3}\right) \quad (1)$$

Non-linear strength index φ of the samples are calculated as follows: 36.8°, 35.4°, 34.9°, 32.8°.

Then: φ_0=41.8°, $\Delta\varphi$=8.1°.

Then the linear intensity indicators are obtained as follows: c=0.119, φ=30.5°.

It can be seen that the material shear strength parameters φ gradually reduces with increasing confining pressure.

Constitutive model of embankment filling

According to large-scale triaxial test results, it is possible to describe soil deviatoric stress-strain relationship using Duncan-Chang model approach. But it needs to make appropriate amendments in description of soil volume change for further analysis. So it is more reasonable that the relationship between the volume change and axial strain is established.

According to $\varepsilon_3 - \varepsilon_1$ relation curve, ε_3 is described by the quadratic equation of ε_1. Therefore it is linear relationship of the tangent Poisson's ratio μ_t with axial strain ε_1, namely:

$$\mu_t = \mu_i + D\varepsilon_1 \tag{2}$$

Where, μ_i is the initial tangent Poisson's ratio and D is a model constant. And the relationship of μ_i with confining pressure σ_3 can be expressed as Eq.3:

$$\mu_i = M - N\lg\left(\frac{\sigma_3}{p_a}\right) \tag{3}$$

Where, M and N are model parameters.

Based on the above results, the improved Duncan-Chang model is expressed as follows:

Stress-strain relationship: $\sigma_1 - \sigma_3 = \dfrac{\varepsilon_1}{a + b\varepsilon_1}$

Initial tangent modulus: $E_i = Kp_a\left(\dfrac{\sigma_3}{p_a}\right)^n$

Tangent bulk modulus: $B = K_b p_a\left(\dfrac{\sigma_3}{p_a}\right)^m$

Tangent elastic modulus: $E_t = \left[1 - \dfrac{R_f(1-\sin\varphi)}{2c\cos\varphi + 2\sigma_3\sin\varphi}(\sigma_1 - \sigma_3)\right]^2 Kp_a\left(\dfrac{\sigma_3}{p_a}\right)^n$

Where, internal friction angle φ is expressed as Eq.4:

$$\varphi = \varphi_0 - \Delta\varphi\lg\left(\frac{\sigma_3}{p_a}\right)^n \tag{4}$$

Tangent Poisson's ratio: $\mu_t = \mu_i + D\varepsilon_1$, where, $\mu_i = M - N\lg\left(\dfrac{\sigma_3}{p_a}\right)$

where, φ_0, $\Delta\varphi$, R_f, K_b and m are model parameters and p_a is the standard atmospheric pressure.

3D finite element analysis of high fill embankment stability

4.1 Definition of safety factor

In the limit equilibrium stability analysis, soil shear strength can be obtained using the definition of safety factor F_s and the Mohr-Coulomb criterion:

$$\tau_m = \tau = \frac{\tau_f}{F_s} = \left(\frac{c'}{F_s}\right) + \sigma'\left(\frac{\tan\varphi'}{F_s}\right) = c_m + \sigma'\tan\varphi_m \tag{2}$$

Where,

$$c_m = \frac{c'}{F_s}, \quad \tan\varphi_m = \frac{\tan\varphi'}{F_s}$$

Then it takes elastic-plastic finite element using the method and corresponding strength reduction factor is overall safety factor of slope when reaching the limit equilibrium state with instability criterion.

4.2 Calculation model and mechanical parameters

According to the design and measured data, the calculation models are shown in Fig.2～Fig.7.

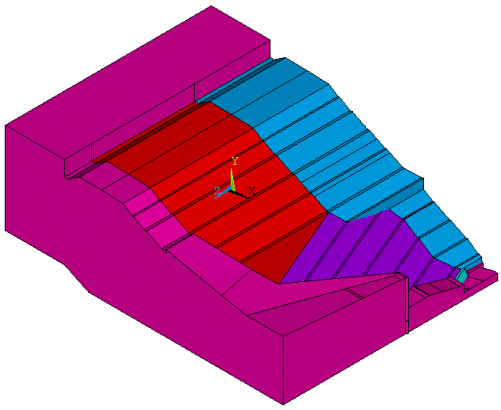

Fig.2 Overall geometry model

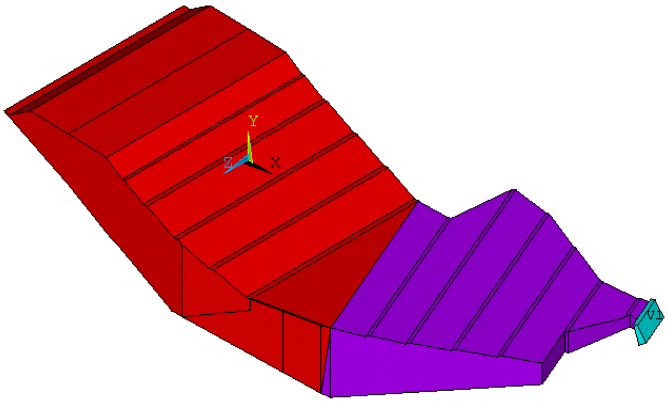

Fig.3 Geometric model of high fill Embankment

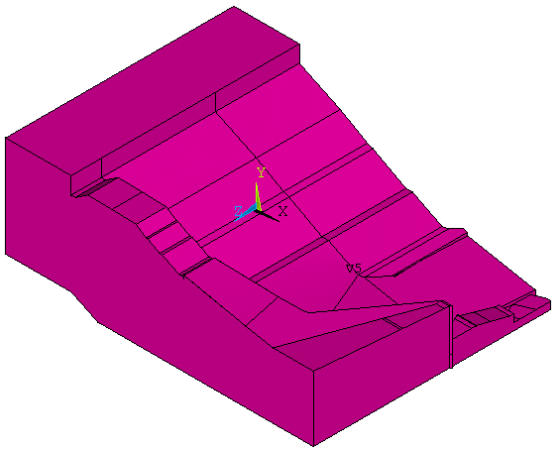

Fig.4 Geometric model of the ground

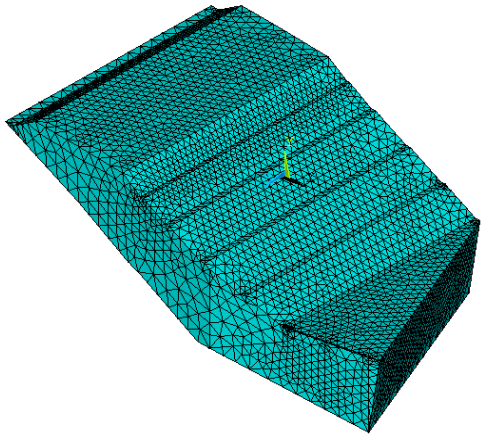

Fig.5 Main line high fill embankment grid model

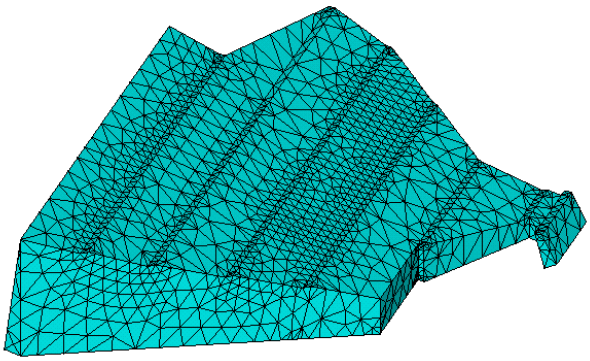

Fig.6 Mesh model of under high fill embankment and retaining wall

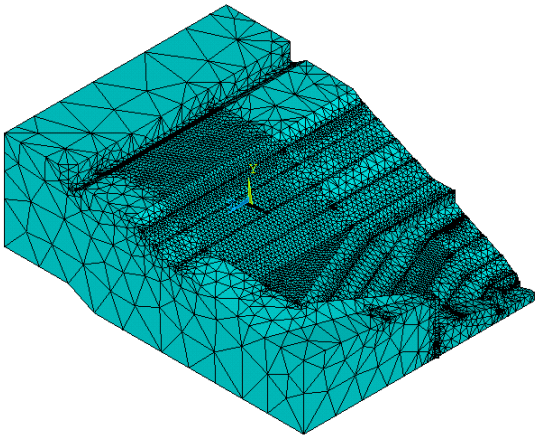

Fig.7 Mesh model of whole high fill embankment

The strength parameters of embankment corresponding to different strength reduction factors are shown in Table 2.

Table 2 Strength parameters of embankment corresponding to different strength reduction factors

Strength reduction factors F	Above embankment		Lower embankment	
	Cohesion c/Pa	Internal friction angle $\varphi/^\circ$	Cohesion c/Pa	Internal friction angle $\varphi/^\circ$
1.2	99.2	26.2	0	30.3
1.4	85	22.8	0	26.6
1.6	74.4	20.2	0	23.6
1.8	66.1	18.1	0	21.3
2	59.5	16.4	0	17.5

Improved Duncan-Chang model is adopted as constitutive model of embankment and the parameters of the model are shown in Table 3 and Table 4.

Table 3 Material parameters of embankment

ρ（kg/m^3）	c (kPa)	$\varphi(^\circ)$	R_f	n	K_f	k_b	m
2.2×10^3	0.119	30.5	0.9	0.4	65	100	0.3

Table 4 Material parameters of ground

ρ （kg/m^3）	c (kPa)	$\varphi(^\circ)$	E（kPa）	n
2.23×10^3	0	38	2e6	0.5

4.3 Calculating results

The results of embankment in initial state are shown in Fig.8～Fig.11. And plastic deformation has not occurred from the displacement changes maps.

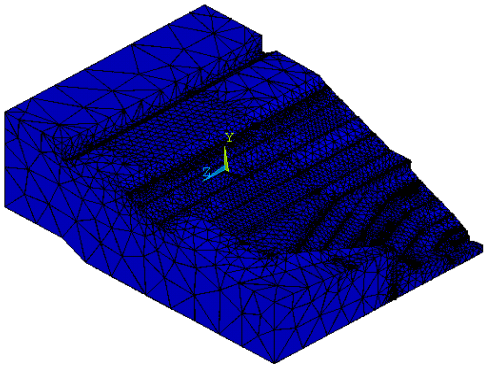

Fig.8 Whole model deformation

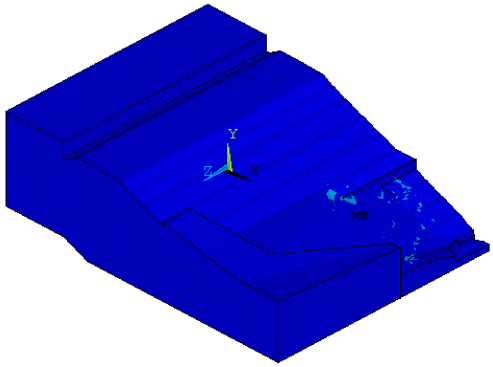

Fig.9 Lateral displacement field in the initial state

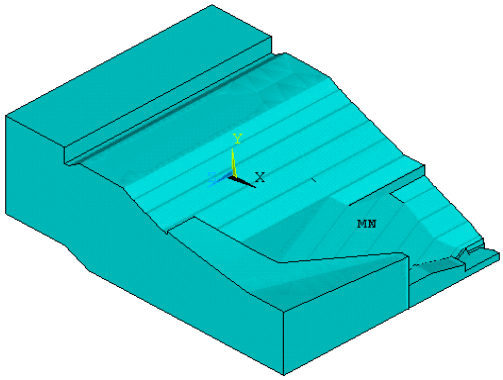

Fig.10 Vertical displacement field in the initial state

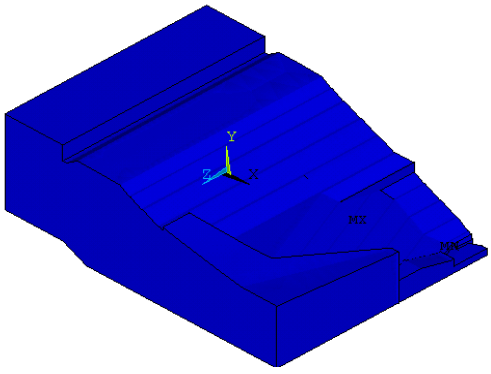

Fig.11 Displacement vector in the initial state

The results of embankment when F =1.8 are shown in Fig.12～Fig.14. And plastic deformation has not occurred from the displacement changes maps. Maximum lateral displacement is 116mm and maximum vertical displacement is 96mm.

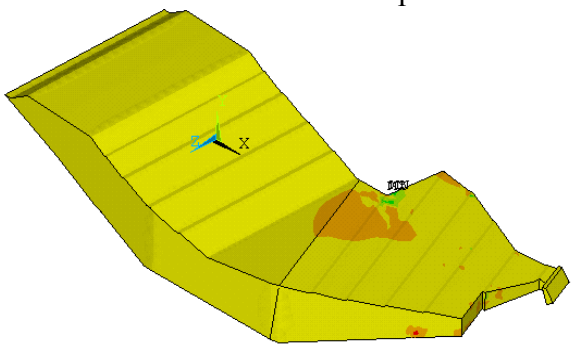

Fig.12 Lateral displacement field when F =1.8

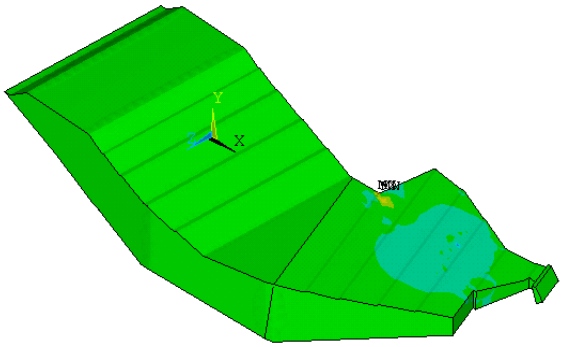

Fig.13 Vertical displacement field when F =1.8

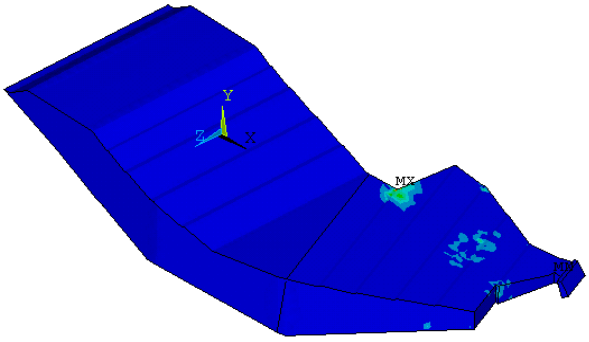

Fig.14 Displacement vector field when F =1.8

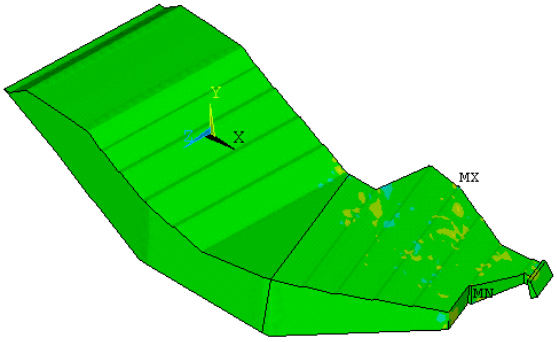

Fig.15 Lateral displacement field when F =2.0

The results of embankment when F =2.0 are shown in Fig.15～Fig.17. And plastic deformation has occurred. Maximum lateral displacement is 188mm and maximum vertical displacement is 413mm. the calculation does not converge and embankment has so larger deformation that tends to reach instability. So the stability safety factor of high fill embankment is between 1.8 and 2.0.

Fig.16 Vertical displacement field when F =2.0

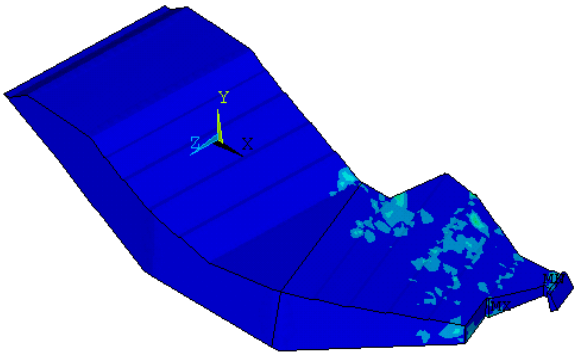

Fig.17 Displacement vector field when F =2.0

Conclusions

Through 3D finite element analysis of high fill embankment stability under complex terrain conditions, conclusions are made as follows:

(1) The modified Duncan-Chang model is established considering the relationship between the volume change and axial strain.

(2) Based on strength reduction elasto-plastic finite element, stability of high fill embankment was studied with three-dimensional finite element method considering the complex terrain conditions.

(3) Study results suggest that it can be slope instability criterion calculate whether the finite element static analysis converges or not.

(4) Stability safety factor of high fill embankment under three-dimensional conditions is larger than that of two-dimensional conditions, which shows that boundary conditions of high fill embankment enhance its stability.

References:

[1]. Zienkiewicz O C,Humpheson C and Lewis R W.Associated and non-associated visco-plasticity and plasticity in soil mechanics[J]. Geotechnique,1975,25(4):671～689.
[2]. Ugai K. A method of calculation of total factor of safety of slope by elasto-plastic FEM[J]. Soils and Foundations,1989,29(2):190～195.
[3]. Ugai K,Leshchinsky D. Three-dimensional limit equilibrium and finite element analysis[J]. Soils and Foundations,1995,35(4):1～7.
[4]. Griffiths D V. Finite element analyses of walls,footings and slopes[D]. Department of Engineering,University of Manchester,1980.
[5]. Jiang G L, Magnan J P. Stability analysis of embankments: comparison of limit analysis with method of slices[J]. Geotechnique,1997,47(4):857～872.
[6]. Dawson E M, Roth W H, Drescher A. Slope stability analysis by strength reduction[J]. Geotechnique, 1999,49(6):835～840.
[7]. Manzari M T, Nour M A. Significance of soil dilatancy in slope stability analysis [J]. Journal of Geotechnical and Geoenvironmental Engineering, ASCE,2000,126(1),75～80.
[8]. Song Erxiang. Finite element computation of safety factor of geotechnical structural [J]. Journal of Geotechnical Engineering, 1997,19 (2): 1～7. (In Chinese)

Applied Mechanics and Materials Vols. 97-98 (2011) pp 85-90

doi:10.4028/www.scientific.net/AMM.97-98.85

The Relationship between Deflection and Maximum Stress Distributed on The Layer Bottom in The Typical Semi-rigid Bituminous Pavement Structure

Zhizhong Zhao[1, 2,a],Kui Li[2,b],Ning zhang[3,c]

[1]Department of Transportation Engineering,Tongji University;Shanghai,China;

[2]Department of Civil Engineering,Shandong Jiaotong University;Jinan,China;

[3]Dezhou Highway Administration ;Dezhou,China;

[a]11asc@163.com [b]zyjsxy8698@163.com [c]zhangning78@126.com

Key word: Semi-rigid Bituminous pavement Structure Deflection Maximum stress Correlation formula

Abstract: This article carries on the test to materials of the roadbed and the pavement in the room, and obtains mechanics computation parameter; Considered the road overload situation, we carries on the modeling computation to the typical semi-rigid bituminous pavement structure through using the finite element software; Carrying on the analysis, we obtains the correlation formula between the road deflection and various structures level maximum stress .it can provide the theory basis and the instruction experience for the highway pavement structure design, the examination and the construction control.

Deflection and maximum tensile stress are two important controlling indexes in the design of highway pavement structure. Deflection of the surface is simple and easy to measure while it is time-consuming and strenuous to test the tensile stress distributed on the level bottom, making it a difficult and inaccurate job. In addition, since design with the assumption of each level to be completely continuous has already satisfied the requirements of the deflection and maximum stress, deflection thus becomes the only index used to control the whole quality of the pavement structure in the process of design and construction whereas the tensile stress index appears to be useless. But in the failure modes of pavement, aside from some early-age water damages, most of them are structural failures and characterized by ruptures in the structural layers. Fracture of base course appears before the deflection of pavement structure exceeds the limits, which shows that the decisive factor for the failure of the bituminous pavement with semi-rigid base course is really the maximum tensile stress distributed on the structural level bottom ,leading to the necessity to test the maximum stress of each pavement structure level. In order to make full use of the deflection that is simple and easy to measure to reflect the maximum tensile stress distributed on level bottom ,the FEM analysis is applied to discover the good correlation between deflection and maximum stress and the formulas of a typical pavement structure are also developed in this paper. This way the maximum tensile stress distributed on level bottom is obtained and controlled through testing the deflection value .

Technical Thoughts

Models are set up for the typical semi-rigid bituminous pavement structure and FEM software utilized to calculate the stress and displacement. Considering characteristics of the typical semi-rigid bituminous pavement structure and the existing problems, assumptions for conditions of subgrade , layer contact and the circumstance of overloading shown are as follows :

1).Subgrade Conditions : In order to comply with the untreated subgrade and the upper modulus and rigidity , 60cm are divided into three layers with each of 20cm .Content of lime of each layer from the top to the bottom is :12%,5% and 3% respectively .

2).Layer Contact Conditions : upon completion of the expressway, continuous state is sustained among each layer due to the existence of the sticky course .After being open to traffic for one or two years ,under the action of heavy loadings especially the existence of the semi-rigid base course ,the continuous state among each layer changes gradually to the state of semi-sliding and semi-continuous under the action of kneading .Based on the practical circumstance ,it is assumed completely continuous among each layer without any relative displacement in the simulation of new-built freeway ; in the simulation of expressway being open to traffic for two or three years ,it is assumed completely continuous among three bituminous courses ,and semi-sliding and semi-continuous between the surface and the base course ,the base course and the sub-base course ,and the sub-base course and the subgrade .

3).Vehicle Loading Conditions : Overloading is currently very serious on China's expressways. The number of vehicles with heavy loadings ,especially overloading with large margin grows remarkably ,axial weight increasing from the limited 100kN to more than 200kN ,tyre pressure increasing from the limited 0.7MPa to 1.0MPa ,even 1.4 MPa—this has already been very common .For simulating the real situation o overloading, tyre pressure is set to be 0.7 MPa for the standard value , 0.85 MPa, 1.0 MPa, 1.2 MPa for the overloading and 1.4 MPa for the serious overloading.

Material parameters

By conducting tests on asphalt concrete of the surface ,cement stabilized macadam of the base course ,lime-fly ash soil of the subbase course and the lime soil of subgrade treatment , its elasticity of modulus ,the density and the Poisson ratio can be determined . Silty clays of different compaction are tested to determine its modulus ,density , Poison's ratio and value of c, φ, offering parameters for finite element calculation .The needed values are shown in Table-1 as follows :

Table-1 Calculating parameter values of material in each level

Pavement level	Materials	Thickness (cm)	Modulus (MPa)	Density (Kg/m^3)	Poisson's ratio	Cohesion force （KPa）	Angle of friction(^{o})
Surface	Fine-grained asphalt concrete	4	1400	2400	0.25	—	—
	Medium-grained asphalt concrete	6	1200	2400	0.25	—	—
	Coarse-grained asphalt concrete	8	1100	2400	0.25	—	—
Base course	Cement stabilized macadam	32	1500	2300	0.25	—	—
Subbase course	Lime flyash soil	18	750	1700	0.27	—	—
Subgrade	Lime soil（12%）	20（0）	500	1750	0.27	—	—
	Lime soil（5%）	20（0）	250	1800	0.3	—	—
	Lime soil（3%）	20（0）	100	1850	0.3	—	—
	Roadbed 96 zone	80	63.57	1899	0.35	50.5	35.5
	Upper embankment 94 zone	70	58.91	1860	0.35	40	34.9
	Down embankment 90 zone	190	57.53	1800	0.35	29	33

Note: （0）represents zero thickness, i.e. subgrade not treated with lime .

3.Relationship between the deflection and maximum stress distributed on the structural level bottom in a typical structure

3.1 The relationship between deflection of the surface and maximum tensile stress distributed on the structural level bottom prior to subgrade treatment

After calculation ,the relationship between the deflection and maximum stress is shown in Table 2 ,Table 3 and Figure 1 ,Figure 2 .

Table 2 The relationship between the deflection of the surface and the maximum tensile stress distributed on the structural level bottom before subgrade treatment

Interface conditions	Tyre pressure (MPa)	Deflection of surface tyre bottom (10^{-2}mm)	Deflection of surface tyre space (10^{-2}mm)	Stress of surface (Pa)	Stress of base course (Pa)	Stress of subbase course (Pa)	Stress of the top subgrade (Pa)
Continuous interface	0.7	20.33	15.45	−4.62E+04	3.63E+04	1.98E+04	−3.07E+04
	1	46.99	37.9	−1.07E+05	9.61E+04	5.90E+04	−5.81E+04
	1.2	72.96	61.15	−1.79E+05	1.56E+05	1.86E+04	−8.57E+04
	1.4	106.12	90.5	−2.84E+05	2.24E+05	1.45E+05	−1.21E+05
Semi-sliding interface	0.7	26.92	22.49	1.17E+05	1.23E+05	2.87E+04	−4.50E+04
	1	67.01	59	2.34E+05	3.20E+05	6.85E+04	−9.37E+04
	1.2	106.48	96.04	3.05E+05	5.02E+05	1.09E+05	−1.42E+05
	1.4	157.36	144.07	3.91E+05	7.41E+05	1.67E+05	−2.03E+05

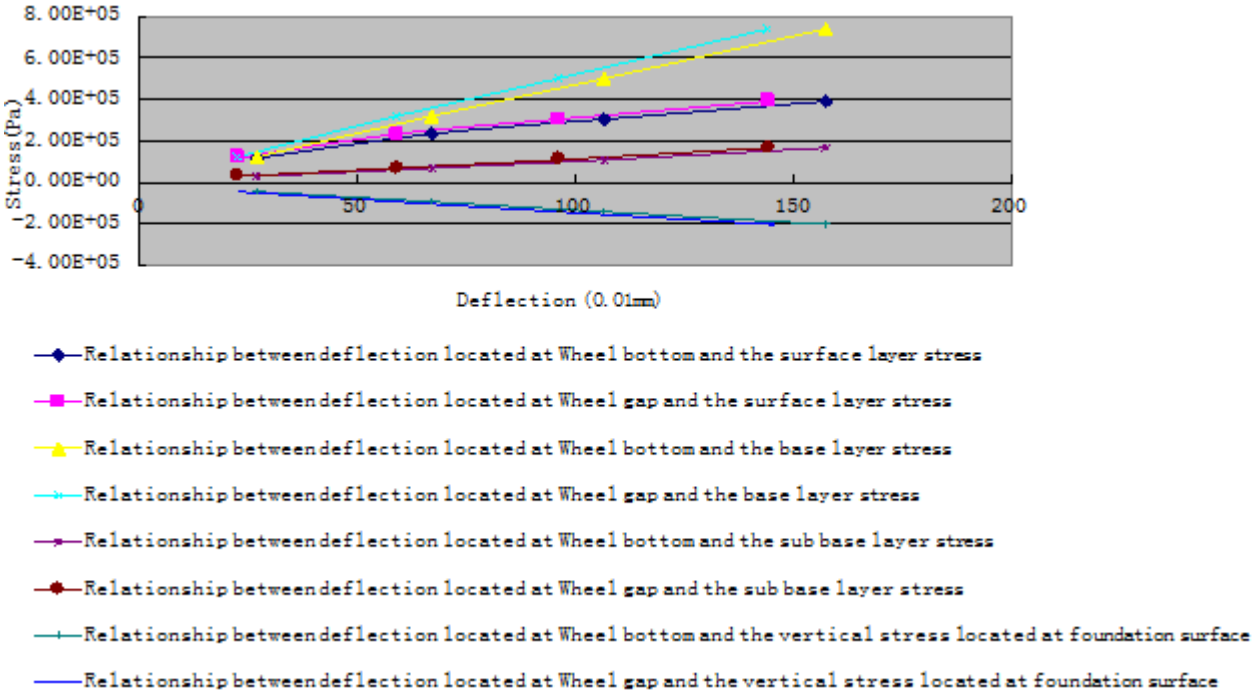

Figure 1 Relationship between the deflection and structural level stress prior to subgrade treatment with semi-sliding interface

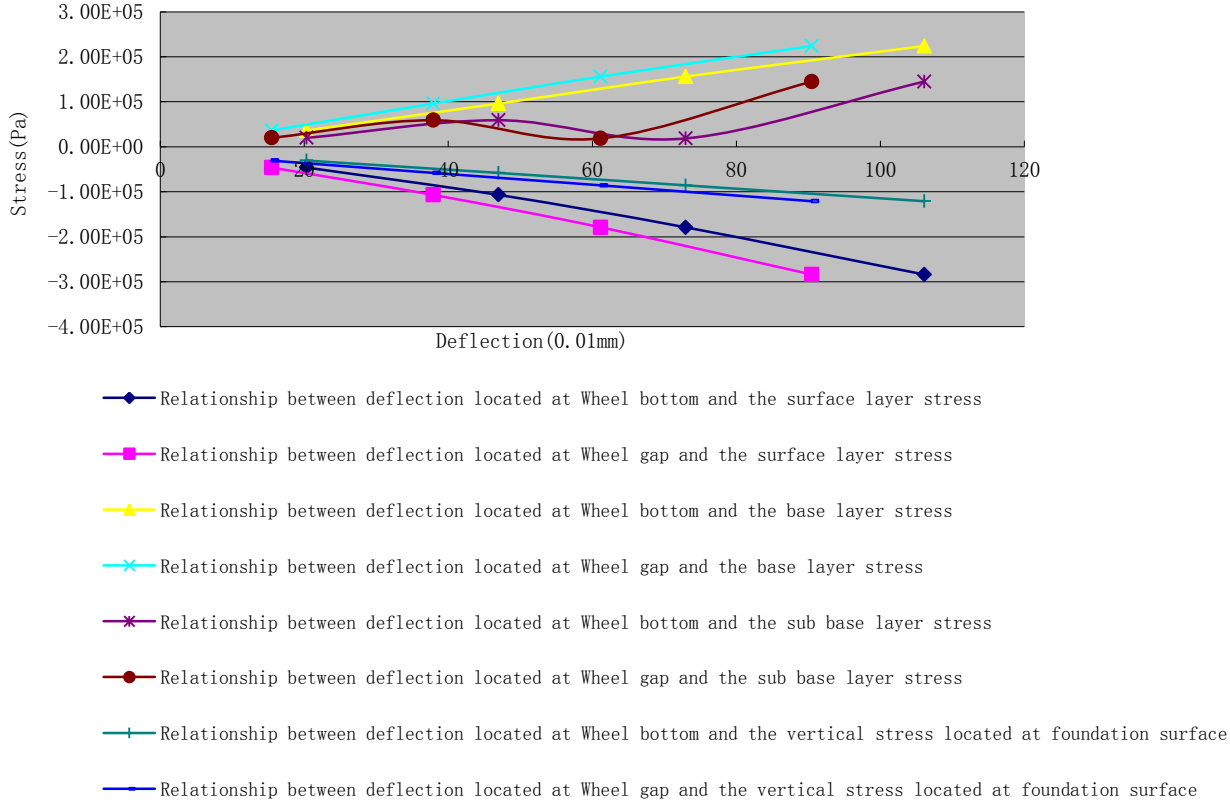

Figure 2 Relationship between the deflection and structural level stress prior to subgrade treatment with continuous interface

It can be seen from Figure 1 and Figure 2 that the deflection of surface has good correlation with the maximum tensile stress distributed on each level bottom , the formula of which can be obtained by data regression .

Table 3 Correlation formula between the deflection of surface and maximum tensile stress distributed on the structural level bottom prior to subgrade treatment

Stress of pavement structure	Continuous interface	Semi-sliding interface
With the maximum tensile stress of surface level bottom	$y=-8.8701x^2-2227.8x-9705.3$ R2=1	$y=-8.2329x^2+3587.6x+43218$ R2=0.9971
With the maximum tensile stress of base course level bottom	$y=-3.6567x^2+2892.9x-7723.5$ R2=1	y=5062.9x+14446 R2=0.9996
With the maximum tensile stress of subbase course level bottom	————	$y=0.7957x^2+1002x+5985.1$ R2=0.9999
With the maximum tensile stress Of top subgrade level bottom	$y=0.137x^2-1216.2x-12011$ R2=1	$y=0.4022x^2-1366.5x-14471$ R2=1

3.2 Relationship between the deflection of surface and maximum stress of structural level after subgrade treatment

After calculation ,the relationship between the deflection and maximum stress is shown in Table 4 ,Table 5 and Figure 3 ,Figure 4 .

Table 4 The relationship between the deflection of the surface and maximum tensile stress distributed on the structural level bottom after subgrade treatment

Interface condition	Tyre pressure (MPa)	Deflection of surface tyre bottom (10^{-2}mm)	Deflection of surface tyre space (10^{-2}mm)	Stress of surface (Pa)	Stress of base course (Pa)	Stress of subbase course (Pa)	Stress of top subgrade (Pa)
Continuous interface	0.7	18.69	13.43	-39200	25800	11500	-35100
	1	42.67	33.5	-102000	66400	36100	-68000
	1.2	65.17	51.57	-177000	96500	56800	-99300
	1.4	95.29	78.97	-272000	153000	94000	-141000
Semi-sliding interface	0.7	24.6	20.17	13800	102000	13800	-50100
	1	63.6	55.21	210000	284000	52100	-108000
	1.2	103.76	93.26	285000	458000	90700	-165000
	1.4	155.06	141.71	359000	671000	133000	-234000

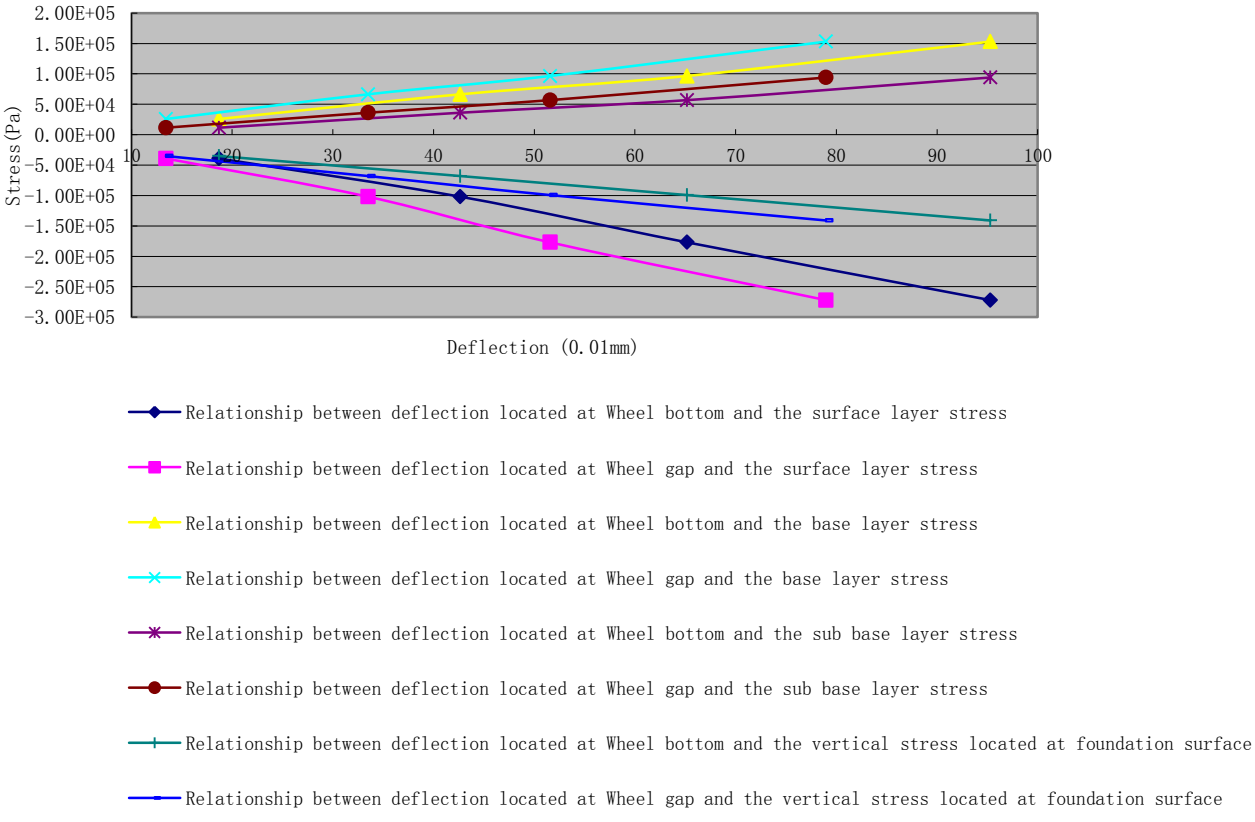

Figure 3 Relationship between the deflection of surface and stress of structural level after subgrade treatment with continuous interface

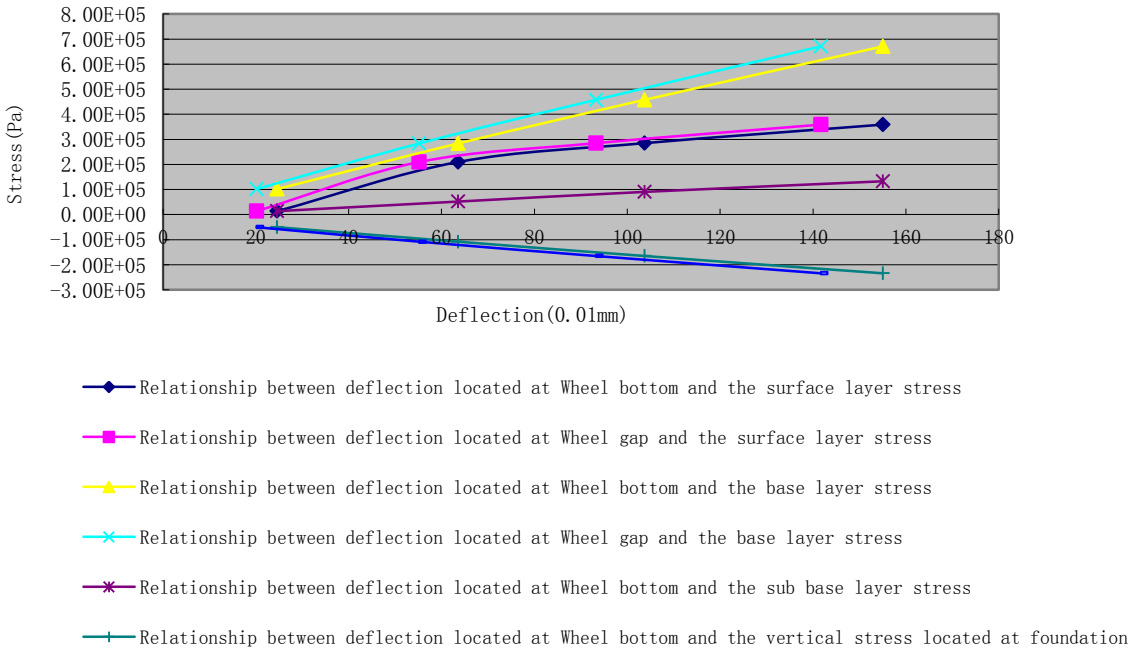

Figure 4 Relationship between the deflection of surface and stress of structural level after subgrade treatment with sliding interface

Table 5 Correlation formula between the deflection of surface tyre space and stress of the structural level after subgrade treatment

Structural stress of pavement	Continuous interface		Semi-sliding interface	
With stress of surface	$y=-2.269x^2-3386.9x+8504.9$	$R^2=0.9981$	$y=176110\mathrm{Ln}(x)-509702$	$R^2=0.9964$
With stress base course	$y=1.2354x^2+1807.4x+2086.4$	$R^2=0.9987$	$y=-4.6638x^2+5420.9x-4260.7$	$R^2=0.9999$
With stress of subbase course	$y=1.8655x^2+1079.2x-3037.2$	$R^2=0.9996$	$y=-1.4074x^2+1209.9x-10134$	$R^2=1$
With stress of top subgrade	$y=1.7034x^2-1780.7x-11187$	$R^2=0.9997$	$y=1.3649x^2-1731x-15972$	$R^2=1$

Conclusion

The previous analysis has indicated that the deflection value possesses a good correlation with the maximum tensile stress distributed on the structural level bottom .A correlation formula between the two factors in a typical semi-rigid bituminous pavement structure has also been produced. With the application of these formulas , control over the maximum stress distributed on the structural level bottom can be achieved by testing the deflection value of surface in the construction sites , which will offer a simple and quick method for testing the stress of level bottom and meanwhile will offer the basis for unifying the deflection and the maximum stress index in design .

References :

[1] Code for Highway Bituminous Pavement Design (JTJ 014-2006),Ministry of Communications of China .

[2]Sha Qinglin .Semi-rigid base course bituminous pavement of high grade highways [M].Beijing : People's Communications Press,1999.

[3] Long Yuqiu .Concept of finite element method .Beijing : Higher Education Press,1991,10

[4] Gao Yingdeng .Stress analysis of bituminous pavement under traffic overloading [J].Highway Communication Science and Technology . 2001，18（6）：25-27

Applied Mechanics and Materials Vols. 97-98 (2011) pp 91-94

doi:10.4028/www.scientific.net/AMM.97-98.91

Nonlinear Finite Element Research for the Rutting of Asphalt Pavement Base on Shear Stress Analysis

Yi Dong [1,a], Miaojuan Peng [2,b], Yongqi Ma [1,c], Wei Feng [1,d]

[1] Shanghai Institute of Applied Mathematics and Mechanics, Shanghai University, Shanghai 200072, China

[2] Department of Civil Engineering, Shanghai University, Shanghai 200072, China

[a] dymayi@gmail.com, [b] mjpeng@shu.edu.cn, [c] mayq@staff.shu.edu.cn, [d] wfeng@sh163.net

Key words: rutting; shear stress; load of vehicles; middle course; visco-elastic-plasticity theory;

Abstract: In this paper, visco-elastic-plasticity theory is employed to establish a nonlinear finite element model of the asphalt mixture pavement. The influence of pavement structure, the ability of rutting resistance of middle layer and traffic load on shear stress distribution for asphalt pavement are discussed. The numerical results show that shear stress analysis can be used to analyze the rutting of asphalt pavement. The asphalt materials of middle layer have a great impact on rutting and shear stress. Modified asphalt is a useful middle layer material to decrease the rutting, and the hard asphalt is also an economical material to reduce rutting. Overload and overpressure easily cause pavement rutting damage. Pavement longitudinal grade is not the main reason leading to rutting at the long slope, but brake frequently in the long slope is the real cause of rutting.

Introduction

As one of the major causes for the damage of asphalt pavements, the rutting and the related problems have been paid more and more attention.

In recent years, the finite element method becomes a useful tool in the research of asphalt pavement rutting. Hua [1] employed a nonlinear viscoelastic model to analyze a three layers asphalt pavement. Hau [2] employed the elastoplasticity model to research the influence of road structure on rutting deformation. Peng and Xu [3] deduced a new nonlinear constitutive relationship basing on the Maxwell viscoelastic model and employed this new model to estimate rutting deformation. Su [4] analyzed the traffic road influence on the rutting deformation and shear stress using elastic finite element method.

The mechanism of rutting is shear flow deformation [5]. So the shear stress distribution in asphalt pavement impact the rutting deformation. so the shear stress analysis more conveniently finds the point at which the most rutting deformation happen and researches the stress or rutting distribution in pavement than deformation analysis. But the previous research paid more attention to estimate the rutting deformation and the shear stress has been rarely analyzed.

In this paper, visco-elastic-plasticity theory is employed to establish a nonlinear finite element model of the asphalt pavement. Besides, the effect factors of the rutting have been deeply discussed base on shear stress analysis.

Finite Model and Pavement Parameters

In order to investigate the rutting deformation of asphalt pavement when the traffic loads act on it, the author designed one high-class three-layer asphalt concrete road (Fig. 1a). And the ABAQUS which is finite element software was used to generate a 3D finite model (Fig. 1b). In this model, the vertical deformation of undersurface, X directions deformation of the right and left set of model are restricted. And all of elements are C3D8R element

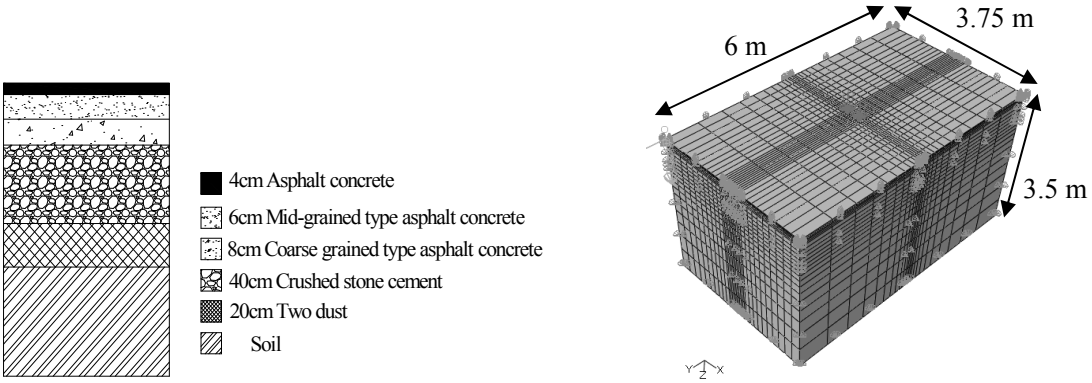

(a) (b)

Fig. 1 Pavement structure and Finite model

Because overload vehicles are the main reason to form rutting, the 11.00-20 type towards pattern tie which is one of main type tie used on overload vehicles has been researched by Sun [6]. In this article, Sun's experimental results are used to be the load conditions.

Since asphalt concrete is a kind of time, stress and temperature dependent material in the high temperature condition, The Drucker-Prager creep theory has been employed to simulate the visco-elastic-plasticity behavior of asphalt. And the creep law using time hardening model (Eq. 1)

$$\dot{\bar{\varepsilon}}^{cr} = A(\bar{\sigma}^{cr})^n t^m \tag{1}$$

where $\dot{\bar{\varepsilon}}^{cr}$ is creep strain rate, $\bar{\sigma}^{cr}$ is creep stress， A,m,n is creep parameters which is temperature dependent. And the asphalt concrete parameters are shown in Table 1.

Table 1 Asphalt concrete parameters

Asphalt concrete	A	n	m
Normal asphalt	6.802×10^{-6}	0.803	-0.532
Hard asphalt	4.361×10^{-8}	0.773	-0.522
Modified asphalt	3.150×10^{-8}	0.384	-0.502

The rutting deformation mainly happens in asphalt layer, so the elasticity theory has been employed to simulate the base behavior. The modulus of crushed stone cement is 1200Mpa and Poisson's ratio is 0.2. The elastic modulus of two dusts is 800Mpa and Poisson's ratio is 0.3. The modulus of soil is 45Mpa and Poisson's ratio is 0.4

Result Analysis of Numerical Simulation

The numerical simulation approach is used to calculate rutting deformation during the traffic load acting on it. With respect to three cases of middle layer material, the rutting deformations along distance to road surface under the standard tire pressure (600kPa) and standard load (25kN) are shown in Fig. 2(a). Because the mechanism of rutting is shear flow deformation, the shear stress distribution in asphalt pavement impact on the rutting deformation. In order to research the shear stress distribution in asphalt pavement and the interrelation between shear stress and rutting, shear stresses along distance to road surface are shown in Fig. 2(b).

It is readily apparent that the area of biggest deformation occurs in middle layer whatever material has been used to be asphalt middle layer. And the behavior of middle layer material has greater impact on the rutting. It is easy to draw the conclusion that the shear stress distribution along distance to road surface consist with rutting when we contrast Fig. 2(a) and Fig. 2(b). And maximum rutting deformation occurs near the maximum shear stress. This conclusion complies with the experimental result by reference [5].

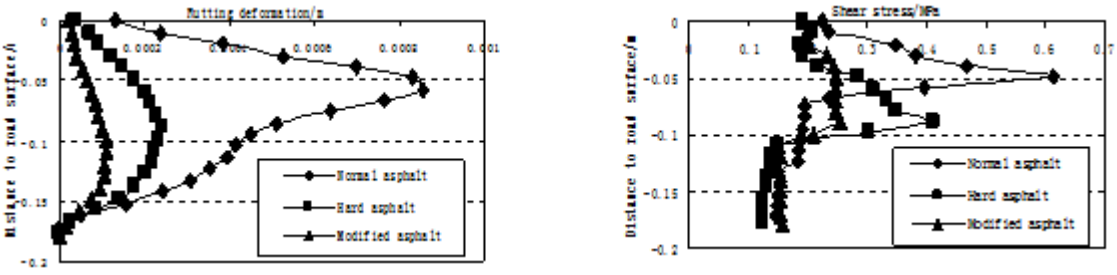

(a) (b)

Fig. 2 Rutting deformation and shear stress along distance to road surface

Fig. 2(b) shows that the maximum shear stress is the least when the modified asphalt is applied to middle layer and the largest when the normal asphalt is used. So the modified asphalt is effective material to eliminate the rutting. Because of the high price, modified asphalt is not economical. The rutting of hard asphalt is less than modified asphalt, but it is much cheaper. Taking into account the economic elements, the hard asphalt is a useful material to eliminate the rutting.

Rutting deformation is considered to be shearing deformation under traffic load. So traffic load greatly impacts on rutting and shear stress in the pavement. In order to investigate the influence of traffic load on shear stress in pavement, the pressure (as shown in reference [6]) was input into the finite element model and the maximum shear stress in pavement have been calculated under different tie pressure and traffic load (Fig. 3)

Fig. 3 illustrates that the different tie pressures and traffic loads have huge influence on shear stress. Especially, when the overload and the overpressure always cause bigger shear stress in the pavement than standard load and pressure, i.e. the shear stress is only 0.242MPa when the load is 25kN and the tie pressure is 600kPa. When the load increases by 50% or when the tie pressure increases to 810kPa, the shear stress increase. Accordingly, the overload and overpressure easily cause pavement to happen rutting damage. When the tie pressure and load are 1050kPa and 25kN, the maximum shear stress in pavement is 0.35MPa and is bigger than the standard tie and overload (i.e. In the case of 600kPa/37.5kN, the maximum shear stress is only 0.29MPa). So it illustrates that the overpressure is great influence on rutting than overload.

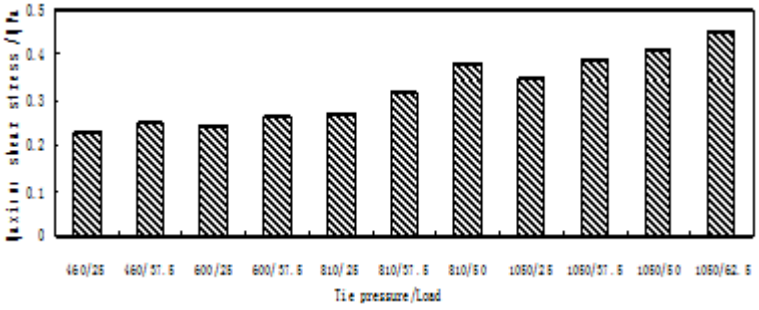

Fig. 3 The maximum shear stress under different tie pressures and loads

On the other hand, when the tie pressure is 460KPa which is lower than standard pressure, the maximum shear stress is 0.251MPa. So the low pressure intensifies the rutting damage.

Previous investigations show that the rutting at long slope is deeper than at flat. That is because horizontal force acts on pavement and shear stress in pavement changes. In order to research the main reason leading to rutting soared at long slope, we analyze the shear stress changes with the road ramp and coefficient of friction when the vehicle brake, as shown in Fig. 4(a) and Fig. 4(b).

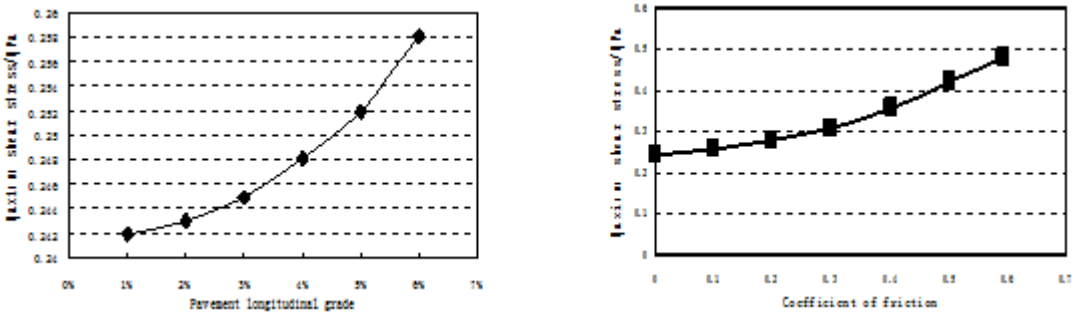

(a) (b)

Fig. 4 Maximum shear stress with pavement longitudinal grade and coefficient of friction

Fig. 4 shows that the maximum shear stress increases with the horizontal force and coefficient of friction increasing. Comparing Fig. 4(a) and Fig. 4(b), we can easily draw the conclusion that the influence of braking on shear stress is much greater than pavement longitudinal grade. Accordingly, pavement longitudinal grade is not the main reason leading to rutting at the long slope. And it is the real cause of rutting that people brake frequently at the long slope.

Conclusions

In this study, the reason that leads to rutting has been researched and the influences of pavement material and traffic load have been discussed deeply. To investigate the cause of rutting, a series of models have been studied. The results of the calculation lead to the following conclusion.

(1). Shear stress analysis is a useful method to analyze asphalt pavement rutting. Compared with deformation analysis, it can better explain rutting changes under different circumstances.

(2). The asphalt material of middle layer has a great impact on rutting and shear stress in pavement. The hard asphalt also be an economical material to reduce rutting.

(3). Overload and overpressure easily cause pavement to witness rutting damage.

(4). Pavement longitudinal grade is not the main reason leading to rutting at the long slope. And it is the real cause of rutting that people brake frequently at the long slope.

Reference

[1]. Hua J. Finite Element Modeling and Analysis of Accelerated Pavement Testing Devices and Phenomenon. Master Dissertation, West Lafayette: Purdue University(2000)

[2]. Hau K M，McDowell G R. Evaluating Permissible Subgrade Rut Depth in Pavement Design. Proceedings of the Institution of Civil Engineers: Geotechnical Engineering,Vol.158 (2005),p.45-46

[3]. Peng Miaojuan,Xu Zhihong. Research on Nonlinear Constitutive Relationship of Permanent Deformation in Asphalt Pavements. Science in China Ser. G: Physics, Mechanics and Astronomy, 2006, 49(6): 671-682

[4]. SU Kai. SUN Lijun. WANG Yongxin. Mechanics Analysis of Loads and Pavement Structure Type to Asphalt Pavement Rutting By 3D Finite Element Method. Journal of Tong Ji university(Natureal Sicence), Vol.35(2007),p.87-192 In Chinese

[5]. Paterson W D O. Road Deterioration and Maintenance Effect: Models for Planning and Management Standard Series, The Highway Design and Maintenance Standard Series. Baltimore: Published for the World Bank, The John Hopkins University Press(1987)

[6]. SUN Lijun.The asphalt pavement structure behavior theory. Tongji University Publishing House(2006) In Chinese

Applied Mechanics and Materials Vols. 97-98 (2011) pp 95-99

doi:10.4028/www.scientific.net/AMM.97-98.95

Effects of Ramp Spacing on Freeway Mainline Crashes

Yongqing Guo

University of Utah, Salt Lake City, Utah, US

yongqing.guo@utah.edu

Keywords: Ramp spacing, freeway safety, accident modification factor.

Abstract. This research applies Negative Binomial (NB) regression models to investigate safety effects of ramp spacing. Data for model estimation was collected in 112 freeway segments where each entrance ramp is followed by an exit ramp. Three years (2005-2007) of freeway crash data were examined by the NB model in this study. The modeling results suggest that the frequencies of total crashes, fatal-plus-injury crashes, single-vehicle crashes and multiple-vehicle crashes increase as ramp spacing decreases, and the frequencies of total crashes and multiple-vehicle crashes increase at significant rates. The modeling result has been geared into the development of accident modification factors (AMFs) for ramp spacing that can be used safety prediction of freeways.

Introduction

Recent researches indicate a high crash risk of the through lanes in sections between closely spaced entrance ramps and exit ramps on freeway. However, when constructing new freeways with interchanges or adding interchanges to existing freeways especially in urban area, two or more ramp terminals are often located in close succession to carry large traffic volumes. Although the AASHTO *Green Book* has recommended minimum ramp terminal spacing for various ramp pair combinations, such recommendations are acknowledged to be based on operational experience and are lack of solid theoretical foundation. The objective of this study is to investigate the relationship of ramp spacing and highway safety, which provides theoretical foundation for the optimal design of ramp spacing to decrease freeway accidents.

Related Research

Three studies took a direct look at the relationship between ramp or interchange spacing and safety [*1, 2, and 3*]. In all three, the lengths of freeway segment and ramp spacing were considered equal, but it can be not certain that the effect of ramp spacing is fully captured in the segment length definition. Several other studies explored safety effects of a ramp or interchange count or density on a freeway segment of length through multivariate regression models [*4, 5, 6 and 7*]. This technique focuses more on corridor-level safety analyses of interchange spacing. Hadi et al. [*4*], Anastasopoulos et al. [*6*] and Park et al. [*7*] showed that the expected accident rates increase as the interchange and ramp count or density increase. However, Milton [*5*] showed an opposite tendency, lower accident severities for segments with increased interchange density. Overall, little is known regarding the effects of ramp spacing on accident frequency.

Data Collection

The study area is on I-5 in the Washington State, US. We used the following four steps in data collection process:

1. Gathering ramp locations and ramp-related features in both directions of freeway travel.
2. Defining freeway segments for safety analysis. Our study focuses on the ramp combination where each entrance ramp followed by an exit ramp. Ramp spacing is defined as the distance from the physical entrance gore to the successive physical exit gore. Freeway segment is defined as the distance from cross street associated with entrance ramp to cross street associated with exit ramp. The complete dataset for analyses in this study consists of 112 freeway segments.

3. Collecting traffic and geometric data for defined freeway segments.
4. Determining crash frequencies and severities on each defined freeway segments. The number of crashes occurred on each segment in the year 2005-2007 was counted. The crash counts were made by total crash, fatal-plus-injury crash, multiple-vehicle crash and single-vehicle crash.

Model Approach

The relationship between ramp spacing and safety has been explored using the NB regression modeling approach. In the model functional form (equation 1), segment length is included as an offset variable for the linear increase in expected crash frequency with an increase in segment length. Traffic volume has been commonly used as a key variable for transportation safety analysis. Ramp spacing is the primary variable in the model. However, a number of other traffic and geometric variables are also included to decrease unexplained variation in expected crash frequency and minimize omitted variable bias. Given accident type *i* or severity *j*, Equation 1 is used to estimate the expected number of accidents:

$$E(Y) = L^{1.0} ADT^{\beta 1} ADT_{EN}^{\beta 2} ADT_{EX}^{\beta 3} \exp(\alpha + \beta_4 \frac{1}{S} + BX) \quad (1)$$

Where, E(Y) = expected number of accidents of type *i* or severity *j*, L = segment length (miles), ADT = freeway ADT (average daily traffic) just upstream of entrance ramp, ADT_{EN} = ADT on entrance ramp, ADT_{EX} = ADT on exit ramp, S = physical gore-to-physical gore spacing (miles), X = matrix of other geometric variables, B, β, α = parameters estimated with maximum likelihood. Stata software is used for estimating model parameters. Model fit is evaluated using the McFadden Pseudo R-squared (R^2), and higher values indicate better model fit.

Model Results and Interpretation

Four models have been applied to estimate different types of accidents, including all crashes (Total), fatal-plus-injury crashes (FplusI), single-vehicle crashes (Sveh) and multiple-vehicle crashes (Mveh). The modeling results are given in Table 1, along with the goodness-of-fit measures. The asterisked variables in Table 1 are other geometric variables used in this study to mitigate unexplained variation of crash frequency and minimize omitted variable bias. The model for multiple-vehicle crashes demonstrates relatively good model fit. The proportion of explained variation by single-vehicle crash model is the smallest, which may indicate that the model is missing major variables and has dispersion-parameter estimation problem by the low sample mean. Preliminary results indicate that the parameter of ramp spacing has a significant effect on crash frequency. The parameters for ramp spacing are positive for all crash types, but their parameter magnitudes are different. In order to better understand the effect of ramp spacing, Figure 1 is constructed to illustrate the modeling result.

The expected numbers of accidents are normalized distance between ramps, shown in Figure 1. The resulting rate is with units of accidents per feet per 3 year. The greater or lower tendencies of different crash frequency models as ramp spacing decreases are illustrated in the figure:

- Figure 1 shows an increase in the frequency of all crash types with decreasing ramp spacing. It can also be seen that, as ramp spacing decreases, the expected frequencies of total crashes and multiple-vehicle crashes increase at significant increasing rates, and the expected frequency of fatal-plus-injury crashes and single-vehicle crashes increase at small increasing rates.
- In general, the curves for total and multiple-vehicle crashes are roughly parallel over the selected distance, and the curve for single-vehicle crashes is approximately horizontal. This implies that the increase of total accidents is mainly attributed to the increase of multiple-vehicle accidents, and the proportion of multiple-vehicle crashes increases.

- In detail, when ramp spacing is less than 2000ft, the increasing rate of multiple-vehicle crash frequency tends to be slightly greater than total crash. It may indicate a significant likelihood of the occurring of a multiple-vehicle crash over the distance range. When the ramp spacing is greater than 10000ft, the expected numbers of different types of accident tend to keep similar. It may indicate that the effect of ramp spacing on crash frequency is not significant.
- When the ramp spacing is greater than 10000ft, the opportunities of fatal-plus-injury crashes involving one vehicle or multiple-vehicle may be not significantly different. As the ramp spacing decreases, a larger likelihood of a fatal-plus-injury crash involving multiple-vehicle appears, and especially when the spacing is less than 2000ft, the likelihood is more significant.

Table 1 Summary of Model Estimate Results for Parameter Estimate

Variable	Definition	Total	FplusI	Sveh	Mveh
Invspai	Inverse of ramp spacing	*595.400*	*178.719*	*136.746*	*775.691*
LogADT	Natural logarithm of ADT upstream of entrance ramp	1.253	1.467	0.240	1.999
LogADTen	Natural logarithm of ADT on entrance ramp	0.160	0.142	0.065	0.235
LogADTex	Natural logarithm of ADT on exit ramp	0.026	-0.018	0.058	0.019
Auxln*	Presence of an auxiliary lane between an entrance & exit ramp (1 if auxiliary lane present; 0 if no)	-0.387	-0.312	-0.163	-0.523
Perbarrl*	Barrier length adjacent to median shoulder divided by segment length	0.278	0.446	-0.033	0.405
Perbarrr*	Barrier length adjacent to right shoulder divided by segment length	0.060	0.149	0.088	0.105
Mainen*	Vertical relationship between cross street for entrance ramp and mainline (1 if mainline over cross street; 0 if mainline under cross)	-0.037	-0.024	-0.015	0.015
Mainex*	Vertical relationship between cross street for exit ramp and mainline (1 if mainline over cross street; 0 if mainline under cross)	-0.052	0.054	-0.043	-0.066
Noln2*	Number of directional through lanes on the freeway segment (1 if two lanes; 0 if three or four lanes)	0.050	0.185	-0.185	0.309
Hcur*	Horizontal curvature change	0.027	0.040	0.015	0.028
Vgra*	Vertical grade change	0.011	0.008	0.003	0.018
Urbru*	Functional classification (1 if urban; 0 if rural)	-0.009	0.081	-0.129	0.118
Constant		-12.083	-15.077	-1.465	-21.428
LogLen	Nature logarithm of segment length	1	1	1	1
R^2	R-squared	0.153	0.162	0.032	0.206

The above modeling results and analysis support the follows:

- In closely spaced ramps, mutual interaction of vehicles exiting or entering the freeway may cause a great decrease of average speed for vehicles on through lane. It can be estimated that the average density may also greatly increase as speed decreases based on speed-density relationship. Vehicles with high density along with frequently lane-change tend to result in an increase of multiple-vehicle crashes. Meanwhile, multiple-vehicle collisions at a relatively fast speed are likely to cause serious injuries or even death.
- There is a slight increase of single-vehicle crash as ramp spacing decreases. One reason may be like that most single-vehicle accidents occur at low volumes. Under this condition, the effect of ramp spacing on the accident is not significant. Another reason might be like that after single-vehicle crash occurs, the following vehicles are difficult to avoid because of the close space and fast speed, which shifts a single-vehicle crash to multiple-vehicle crash.
- It is referred above that the expected frequencies of total crashes and multiple-vehicle crashes increase at significant increasing rates in closely spaced ramps. Crashes would occur frequently at location of merge section, diverge section, and weaving section of a freeway segment. Especially, when a merge area is closely followed by a diverge area, or both areas are overlap, which appear in short spaced ramps, the number of crashes tend to multiply increase.

- If the ramp spacing is long enough, the merge and diverge areas can have their own independent effect on traffic safety. The crash increases due to ramp exit can be minimized. So the expected crash frequency just tends to slightly decrease although the ramp spacing increases.

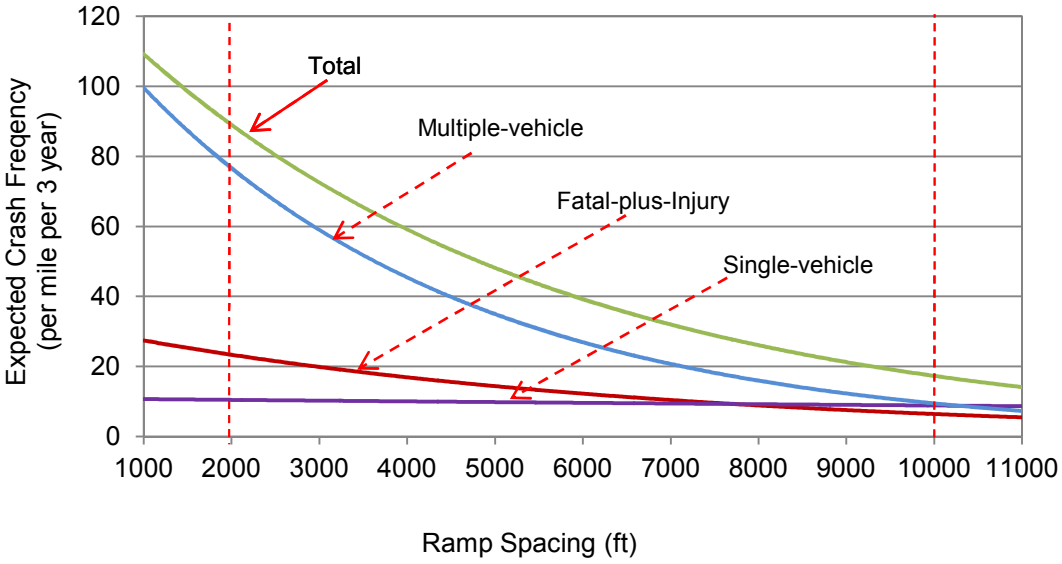

Figure 1. Summary of freeway model with results normalized for ramp spacing

Implementation of Model Results

An AMF represents the relative change that occurs in crash frequency when a particular geometric design component is added or removed, or when a design element is changed in size [*8*]. An objective of this research is to develop an accident modification factor for ramp spacing. Ramp spacing of 2000ft is used as a base condition.

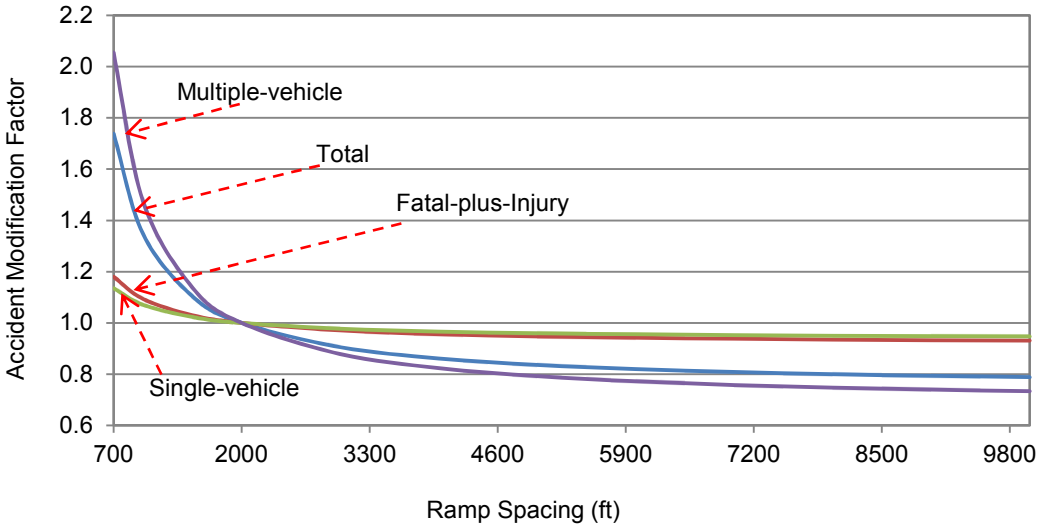

Figure 2**.** Accident Modification Factor of ramp spacing

The AMFs for four different types of crashes are recommended as the follows:

$$AMF_{TOT} = e^{-0.2977+ (595.400/S)} \qquad AMF_{FI} = e^{-0.0894+ (178.719/S)}$$
$$AMF_{MV} = e^{-0.0684+ (136.746/S)} \qquad AMF_{SV} = e^{-0.3883+ (775.691/S)} \qquad (2)$$

Where: AMF_{TOT} = AMF of ramp spacing for total crashes, AMF_{FI} = AMF of ramp spacing for fatal-plus-injury crashes, AMF_{MV} = AMF of ramp spacing for multiple-vehicle crashes, AMF_{SV} = AMF of ramp spacing for single-vehicle crashes, S = ramp spacing (ft). The AMF functions for four different types of crashes are plotted in Figure 2. AMF set to 1.0 for ramp spacing of 2000feet. The results show that all types of crashes increase as ramp spacing decreases. For example, a ramp spacing of 700 feet compared to a ramp spacing of 2000 feet, approximately 70 percent more total crashes and 18 percent more fatal-plus-injury crashes are expected.

Conclusion and Future Work

This paper mainly explores the safety effects of ramp spacing on the frequencies of freeway crashes. It quantifies the effects of ramp spacing on different accident types and explains the causes and effects. The implementation of model results is to develop accident modification factor function of ramp spacing to estimate the safety change when the ramp spacing changes in size. This paper presents some preliminary work of our research. Future work includes refining the models and applying the models to a larger set of real world crash data and different types of freeway crashes.

References

[1] Bared, J.G., P.K. Edara and T. Kim. *Safety Impact of Interchange Spacing on Urban Freeway.* In TRB 85th Annual Meeting Compendium of Paper. CD-ROM. Transportation Research Board of the National Academics, Washington, D.C., 2006.

[2] Cirillo, J. A. *The relationship of Accidents to Length of Speed-Change Lanes and Weaving Areas on Interstate Highway.* In highway Research Record, Journal of the Highway Research Board, No. 312, Highway Research Board of the National Academies, Washington, D.C., 1970, pp 17-32.

[3] Pilko, P., J. G. Bared, P. K. Edara and T. Kim. *TRCHBRIEF: Safety Assessment of Interchange Spacing on Urban Freeway.* Publication FHWA-HRT-07-031. FHWA, U.S. Department of Transportation, 2007.

[4] Hadi, M.A., J. Aruldhas, L-F Chow, and J.A. Wattleworth. *Estimating Safety Effects of Cross-Section Design for Various Highway Types Using Negative Binomial Regression.* Transportation Research Record, Washington, D.C. 1995, No. 1500, pp169-177.

[5] Milton, J. C., V.N. Shankar and F.L. Mannering. Highway Accident Severities and the Mixed Logit Mode: An Exploratory Empirical Analysis. In Accident Analysis and Prevention, Vol. 40, 2008, pp 260-266.

[6] Anastasopoulos, P.C., A.P. Tarko and F.L. Mannering. *Tobit Analysis of Vehicle Accident Rates on Interstate Highways.* In Accident Analysis and Prevention, Vol. 40, 2008, pp 765-775.

[7] Park, B-j, Fitzpatrick, K. and Lord, D. *Evaluating the Effects of Freeway Design Elements on Safety.* CD-ROM .Transportation Research Record, Washington, D.C., 2010.

[8] Bonneson and K. Zimmerman. *Procedure for Using Accident Modification Factors in the Highway Design Process.* Report 0-4703-P5, Texas Transportation Institute.

Applied Mechanics and Materials Vols. 97-98 (2011) pp 100-107

doi:10.4028/www.scientific.net/AMM.97-98.100

Design Optimization and Safety Evaluation Of Cross-sea Bridge Barrier

Lei Fang[1,a], Liang Zhang[2,b], Shuming Yan[3,c], Ning Jia[3,d], Min Jing[3,e] and Liang Ma[3,f]

[1]South China University of Technology School of Civil and Transportation Engineering, guangzhou guangdong 510641, China

[2]CCCC Highway Consultants Co., Ltd, Beijing 100088, China

[3]Beijing Zhongluan Traffic Technology Co.,Ltd, Beijing 100071,China

[a]fl@hzmbo.com, [b]xmhkgzd2006@163.com, [c]shumingyan@sina.com, [d]jn790109@sohu.com,[e]jingmin618@126.com, [f]mlpyjmwr@163.com

Keywords: Bridge Barrier, Impact Condition, Evaluation Specification, Full-Scale Impact Test

Abstract. By comprehensive analysis and design optimization of barrier structure parameters, a new type of beam-and-post steel barrier was invented according to impact test condition and acceptance criteria of cross-sea bridge barrier. Full-scale impact tests and finite elements analysis were conducted to do safty evalution of the barrier. The results show that, ASI value is 1.62 for test and that is 1.67 for FEA, THIV is 30.7km/h for test and that is 31.2km/h for FEA. Working width is 0.88m for test and that is 0.62m for FEA. Occupant risk evaluation index can meet the requirements of level B and the working width can meet the requirements of level W3. Both of tracking and posture of vehicles are well. The study results above show that safety performance of cross-sea bridge barrier can meet or exceed the acceptance criteria. FEA results are consistent with Full-scale impact test, which validate the reliability of FEA. cross-sea bridge barrier can meet the highest test level for beam-and-post steel barrier, which can defend the out-of-control vehicles effectively and help to ensure the bridge safety.

Introduction

Cross-sea bridge provides us with a convenient road access, however because it located in the sea area, traffic accidents could become an important factor in operational efficiency. Bridge barrier is the last line of defense to protect the accident vehicle safety and reduce the severity of the accident. If barrier is poorly designed,in the event of the accident that vehicle impact barrier, then the vehicle will be easy to fall off the bridge, which will cause serious damage to the vehicle and serious injury to passengers. It also may cause secondary accidents that the falling vehicle smash hit the ships at sea.

It proposed impact conditions and evaluation specification of bridge barrier, and designed a new type of beam-and-post steel barrier, at last do safty evalution by the method of full-scale impact tests and finite elements analysis to test whether its ability to meet the impact resistance of the relevant standards.

Impact Conditions and Evaluation Specification

Impact Conditions. Generally, the designed speed of cross-sea bridge is 80km/h~120km/h, the vechile rushing out of the bridge will cause secondary accidents or even worse. So determine the crash rating of the barrier to be SS level which is the highest level of specification in china[1], the impact energy is 520kJ.

Table 1 shows the impact conditions.

Tab.1 Impact Test Condition

Test Vehicle	Vehicle Weight[t]	Impact Velocity[km/h]	Impact Angle[degree]	Impact Energy[kJ]
Car	1.5	100	20	—
Bus	18	80	20	520

Note: Hight of car CG point is 0.53±0.05m, and that of bus is 1.3±0.1m.

Evaluation Specification. By comparison of the domestic and foreign relevant norms[3~5], from the safety, reliability, operability point of view, do evaluation of the safety performance of the barrier by evaluation specification of European EN1317.

The evaluation indicators include:

1) Protective performance of barrier: Barrier can stop and direct the vehicle, but not allowed to be washed off. The main part of the barrier mustn't fall from it, and the lost parts must not penetrate the passenger compartment or injure passengers.

2) Vehicle's trajectory: The center of the test vehicle can not cross the center line of deformed barrier, test vehicle during and after impact sholud maintain normal driving state, and moderate swing, pitch, deflection are all acceptable. Trajectory should not cross the line F in Fig. 1, A=E＋width＋length×0.16, for small passenger car, E = 2.2m, B = 10m, and for other vehicles, E = 4.4m, B = 20m.

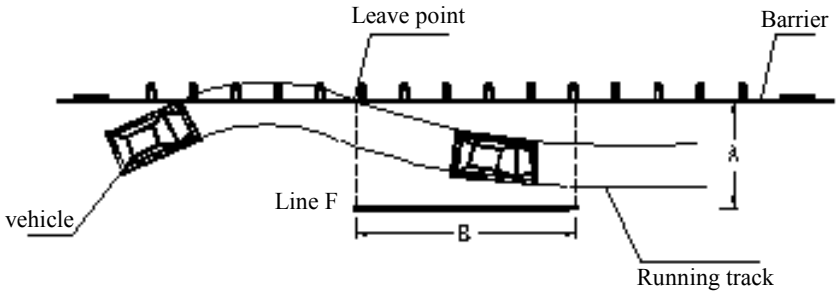

Fig. 1 Tracking Requirements of Vehicle Impact

3) Occupant risk: Acceleration Severity Index (ASI), calculated by the acceleration of mass center and yaw rate of test vechile, and theoretical head impact velocity(THIV) should be at least C-level requirements in table 2.

Tab.2 Occupant Risk Evaluation Index

Level	Index value		
A	ASI≤1.0		
B	1.0＜ASI≤1.4	and	THIV≤33km/h
C	1.4＜ASI≤1.9		

4) Barrier deformation: The work width of barrier should be at least W4 grade (W ≤ 1.3m).

Design and Optimization of Barrier

Barrier Structure. Barriers which are used for bridges mainly can be classified into reinforced concrete wall, combination and beam-and-post steel types. Concrete barrier protective effect is good, and easy to achieve particularly high crash rating, but the landscape is less effective. Through matching the bottom structure of concrete wall and upper structure of metal beams, combined barrier is easier to achieve high crash rating, but the landscape is less transparent, and it with greater weight. Beam-and-post steel barrier is more transparent, can effectively reduce wind loads. And it with lighter weight, which benefits the main structure of the bridge,Although the cost of it is higher.

By analysis, use beam-and-post steel barrier as cross-sea bridge barrier.

Barrier Height. Height is an important parameter in the design process of barrier. Barrier with much height has a stronger impact resistance, but it has some influence on the landscape. Barrier with low height, not conducive to the protection of large vehicles, it is difficult to achieve a higher crash rating.

Reference to domestic and international norms to determine barrier height of 1.5m[1,2].

Beam of Barrier. The form of barrier's beam can be classified into circular tube, special tube and rectangular tube. Special tube processing is difficult, and the connection of post and round tube is not convenient. Beam of beam-and-post steel barrier with high crash rating requires a strong flexural capacity, rectangular tube has a stronger flexural capacity with the same amount of material, therefore chosen rectangular tube as beam.

After matching analysis of the overall structure, select the section 160mm×120mm rectangular tube as a beam structure, height from centers of the beams to the ground are: 435mm, 770mm, 1105mm and 1440mm. Established the finite element model of vehicle impact barrier, after several iterative calculation, determine the thickness of two upper beams is 8mm, which are strong beams can provide protection for large vehicles, and the thickness of two bottom beams is 4mm, which are weak beams can provide buffer protection to small cars.

Post of Barrier. Barrier post structures are mainly classified into H-type, square tubes, U-type and special tubes. Special tubes are difficult to process, U-type tubes have poor landscaping and square tubes are inconvenient to connect with post, so H-type posts shall be selected. The post provides fixed support to the beam, and it's spacing of SS-level in domain specification is 1.5m, but from renderings, we found that post spacing of 1.5m will affect transparent performance of barrier.

The H-type post, thickness of flange is 12mm and thickness of connection plan is 10mm, can meet the requirements for protecting, after calculating by finite element simulation[6~11], will benefit transparent performance of barrier.

Beam and Post Connections. Beams and posts are mainly bloted connection, the choice of connections are shown in Fig. 2.

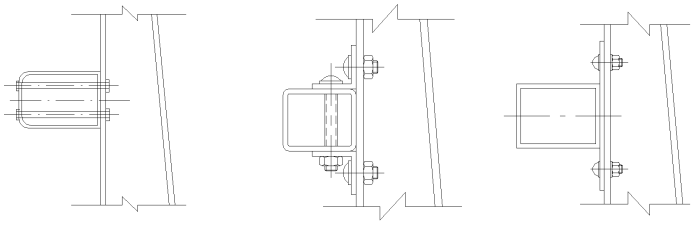

(a) the 1st sketch (b) the 2nd sketch (c) the 3rd sketch

Fig. 2 Methods of Beam and Post Connection

Fig. 3 shows the results of a large-scale vehicle crash the barrier of the first sketch, the connection has the following questions: the beam is squeezed flat, the bolt head break out the beam surface, easy to virtually scratch vehicles. If the bolt is too weak, it may be cut off, which will affect the overall protection performance of the barrier. If the bolt is too strong, there will be some security risks of stumbling blocking vehicles.

(a)Simulation results (b)Test results

Fig. 3 Impact Results of the 1st Skectch Connection

Fig. 4 shows the results of a large-scale vehicle impact the barrier of the second sketch. The bolts are in a non-impcat side, which can be an effective solution to the security risks of stumbling blocking vehicles.

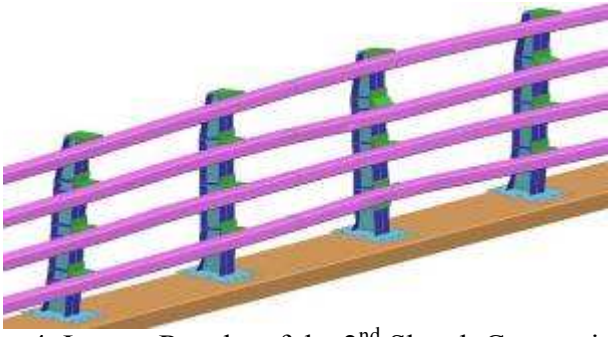

Fig. 4 Impact Results of the 2nd Skecth Connection

Fig. 5 shows the results of a large-scale vehicle impact the barrier of the third sketch. Posts and beams with short bolt connection, not only can be an effective solution to the security risks of stumbling blocking vehicles, but also reduce the cost and with good landscape.

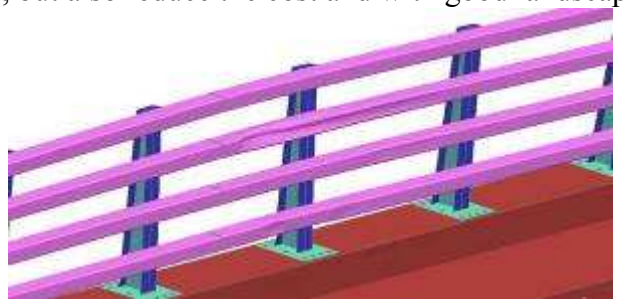

Fig. 5 Impact Results of the 3rd Sketch Connection

By the analysis, the third sketch of connections is selected, which is a optimization of security, landscape and construction cost.

Height of Kerbstone. Setting kerbstone can improve strength of barrier foundation, but it's height may affect risk indicators of occupants in the cars. Do special analysis on the height of the kerbstone,by simulating passenger car impact barrier[6~11]. As shown in Fig. 6, when the kerbstone is too high, the vehicle may climb up it. The deformation and damage of vehicle body at impact side and wheel is serious, evaluation of occupant risk index does not meet the standard requirements.

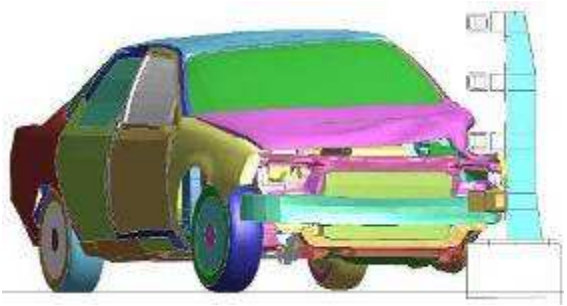

Fig. 6 Posture of Car Impact（Kerbstone Height is 250mm）

Through multiple optimization study to determine the height of kerbstone to 150mm, that ensure occupant risk index meet the evaluation standard requirements, and barrier foundation intensity meet stress requirements.

Barrier Structural Projects. Through the optimization analysis, determine the final structure of barrier as shown in Fig. 7.

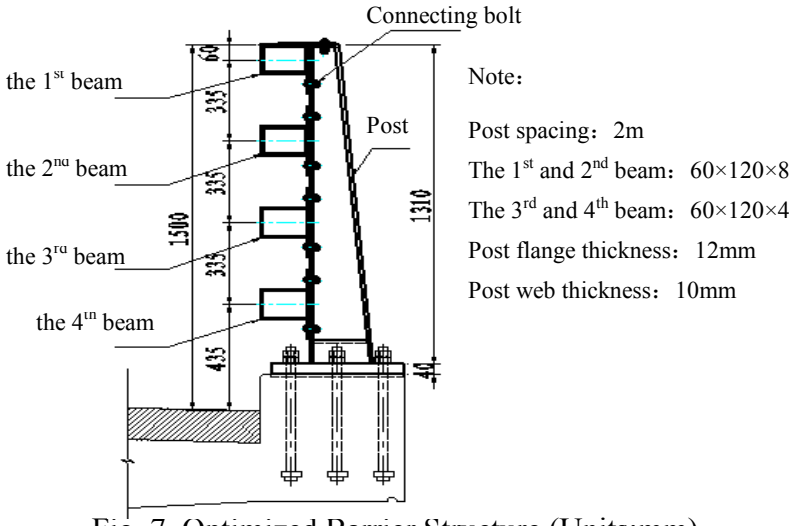

Fig. 7 Optimized Barrier Structure (Units:mm)

Safety Performance Validation

By the method of combination of full-scale impact tests and finite elements analysis[6~11], verify whether the barrier structure of the program evaluation criteria to meet the requirements, according to impact test conditions in Table 1.

Car Impact. Test vehicles and barrier shown in Fig. 8.

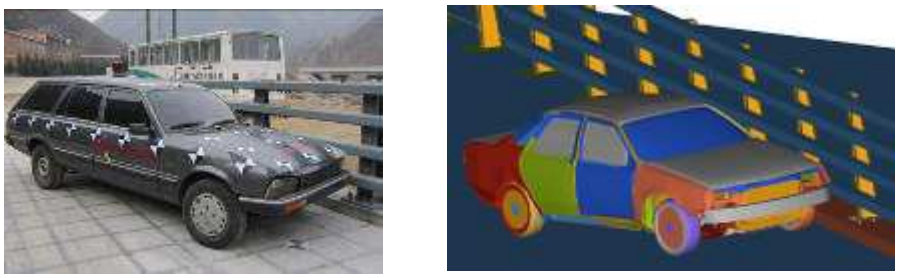

Fig. 8 Impact Car and Barrier

After car impact barrier, the barrier hasn't been broken, and the main components didn't fall off, structural distortion is less than 5cm. There are scratches in the impact region only and a few part appear depression. Protection function of the barrier meet the requirements of evaluation criteria. Fig. 9 shows the running track of car impact barrier, obviously the car driving leave barrier smoothly after impact, and returned to normal driving posture without horizontal turned, switching and overturned. It meets the requirements of evaluation criteria.

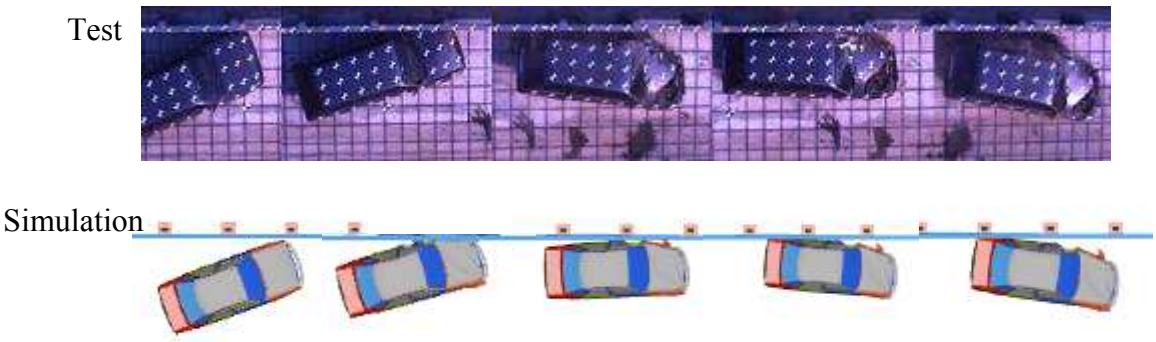

Fig. 9 Tracking of Car Impact

Fig. 10 shows the running track of test car. After impact,the test car didn't run across the line F. It meets the requirements of evaluation criteria.

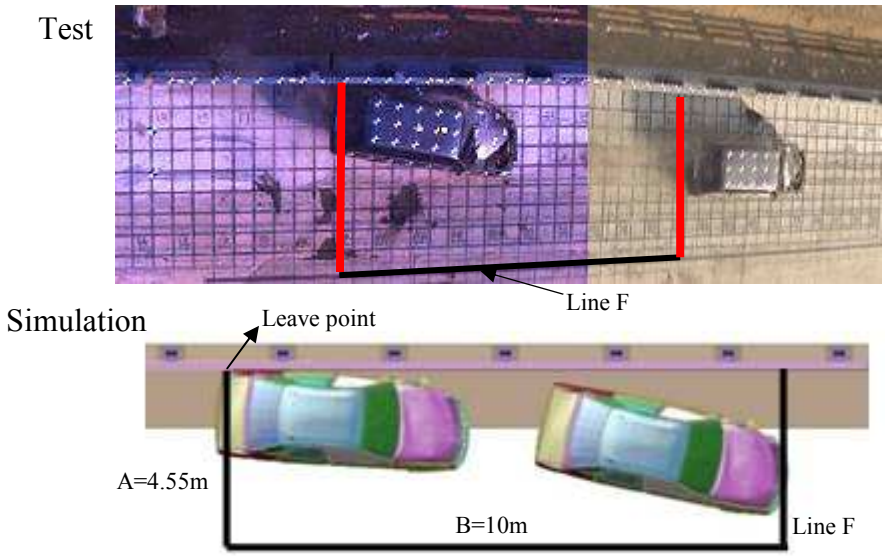

Fig. 10 Car Exit Box

As the value of passenger car occupants' risk evaluation index in impact shown in Table 3, which meets the requirements of B-level in evaluation criteria, beyonds the C-level. The barrier provides good protection to occupants.

Tab.3 Occupant Risk Evaluation Result

Program	ASI	THIV (km/h)
Test Results	1.62	30.7
Simulation Results	1.67	31.2

In summary, the results of passenger car impact barrier meet the requirements of evaluation criteria.

Bus Impact. Test vehicles and barrier are shown in Fig. 11.

Fig. 11 Impact Bus and Barrier

As shown in Fig. 12, after bus impact barrier, the barrier structure hasn't been broken, and the main components didn't fall off. There are scratches in the impact region only and a few part appear depression. Protection function of the barrier meets the requirements of evaluation criteria.

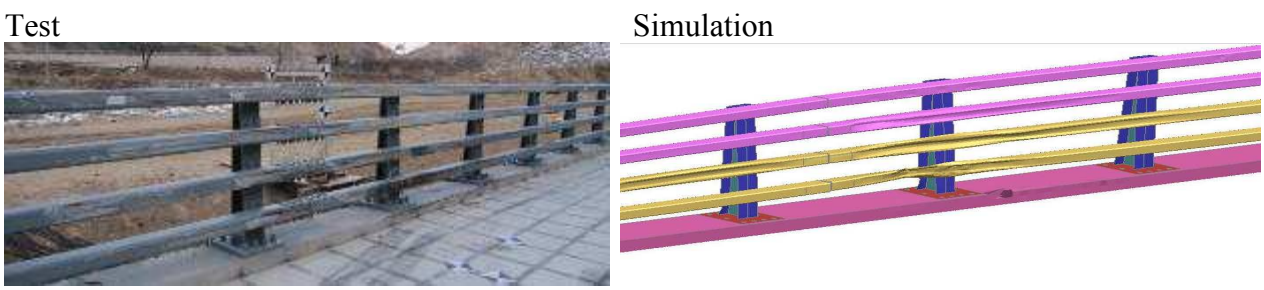

Fig. 12 Barrier Distortion and Shatter after Bus Impact